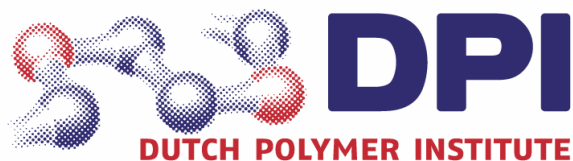


**LOW SURFACE ENERGY RUBBER MATERIALS: RELATIONSHIP BETWEEN NETWORK
ARCHITECTURE AND TACK OF SILICONE RUBBERS**



The studies described in this thesis are part of the Research programme of the Dutch Polymer Institute (DPI), PO Box 902, 5600AX Eindhoven, The Netherlands, project nr. #317.

Low Surface Energy Rubber Materials: Relationship Between Network Architecture and Tack of Silicone Rubbers

By M. Mikrut

PhD Thesis, University of Twente, Enschede, the Netherlands, 2007
With references – With summary in English and Dutch

Copyright © M.Mikrut, 2007.
All rights reserved.

Cover design by Marek Mikrut.
Front cover illustration: The separation of two pieces of rubber during a tack test.

Printed by Print Partners Ipskamp, P.O. Box 333, 7500 AH, Enschede, the Netherlands.

ISBN: 978-90-365-2565-7

**LOW SURFACE ENERGY RUBBER MATERIALS:
RELATIONSHIP BETWEEN NETWORK ARCHITECTURE
AND TACK OF SILICONE RUBBERS**

DISSERTATION

to obtain
the degree of doctor at the University of Twente,
on the authority of the rector magnificus,
prof. dr.W.H.M. Zijm,
on account of the decision of the graduation committee,
to be publicly defended
on Thursday the 25th of October 2007 at 13.15

by

Marek Mikrut

born on the 23rd of July 1976
in Szerzyny, Poland

This dissertation has been approved by:

Promotor: prof. dr. ir. J.W.M. Noordermeer

If you try and take a cat apart to see how it works, the first thing you have on your hands is a non-working cat. Life is a level of complexity that almost lies outside our vision (...).

As quoted in Richard Dawkins' Eulogy for Douglas Adams

Rodzicom oraz bratu

Table of contents

Chapter 1	Introduction: The Importance of Adhesion	1
Chapter 2	Literature Survey: Theories and Models of Elastomer Adhesion	5
Chapter 3	Silicone Elastomers: Properties and Characterization	27
Chapter 4	Development of the Tack Testing Device	43
Chapter 5	Silicone Rubber Tack in Relation to Network Structure	59
Chapter 6	The Time-dependent Autohesion for Symmetric Rubber-Rubber Contacts of Silicone Rubbers	79
Chapter 7	Adhesion of Dissimilar Rubber-Rubber and Rubber-Steel Contacts of Silicone Rubber	99
Chapter 8	The Influence of Loose and Semi-anchored Siloxane Polymer Chains on the Tack of Crosslinked Silicone Rubber	113
Chapter 9	Summary and Final Remarks	127
Samenvatting en laatste opmerkingen		131
Symbols and Abbreviations		135
Bibliography		141
Curriculum Vitae		143
Acknowledgements		145

Chapter 1

Introduction:

The importance of Adhesion

"Begin at the beginning,' the King said gravely, 'and go on till you come to the end: then stop."

Lewis Carroll, in *"Alice's Adventures in Wonderland"*

This chapter provides an introduction into the research described in this thesis by giving a general view of rubber adhesion (tack) and its importance for a great many applications.

1.1 GENERAL INTRODUCTION

Anyone who has once touched a pressure sensitive adhesive tape has an intuitive idea about the phenomenon of tack. The application of adhesives is as old as humanity. The first adhesives were natural gums and other plant resins. Archaeologists have found 6000-year-old ceramic vessels that had broken and been repaired using plant resins. Most early adhesives were animal glues, made by processing animal parts such as hooves. During the times of Babylonia, tar-like glue was used for gluing statues. Also ancient Egypt was one of the most prominent users of adhesives, which the Egyptians used to glue furniture, ivory and papyrus. The Mongols used adhesives to make their short bows. Native Americans in what is now the eastern United States used a mixture of spruce gum and fat as adhesive and as caulk to waterproof seams in their birchbark canoes. In Europe in the Middle Ages, egg white was used to decorate parchments with gold leaves. In the 1700s, the first glue factory was founded in Holland, which manufactured hide glue. Later, in the 1750s, the British introduced fish glue¹.

The adhesion of rubber, apart from its scientific interest, is important in a great many industrial processes. Good adhesion of uncrosslinked rubber compounds is essential in tyre manufacturing to assemble tyre components before curing. Uncrosslinked, elastomeric materials, are used in the pressure sensitive adhesives². The performance of tyres depends on strong and durable adhesion between rubber and the steel wires formed during curing process^{3,4}. Furthermore, many rubber articles are composed of the intimately adhered

rubber/steel, rubber/thermoplastic and other combinations, which have to withstand most severe temperatures and environmental loadings without any risk of failure: e.g. steel/rubber engine mounts for vibration damping, rocket and satellite seals, etc.

The problem of the mechanism behind tack formation has been a controversy for many years. There are two main mechanisms that are quoted as responsible for tack: bond formation via polymer chains diffusion through the interface and subsequent entanglements⁵ on either side, and contact area formation via wetting and viscous flow⁶. Although mass transfer through the interface is not questioned, the problem lies in relevant timescales. The discussion, which mechanism is dominant, still exists and there is no definite answer yet to this question.

Elastomer tack is a very complex phenomenon, mainly because the large amount of variables affecting it, namely: contact time and pressure, rate of pull testing, material viscosity and degree of crosslinking, etc. Thus, accurate tack testing is a complicated task, since the detailed testing conditions significantly influence the values obtained. The ways of testing vary from already standardized peel tests², to somewhat microscale testing, like the JKR method⁷.

In this thesis a tensile method of measuring tack is employed for silicone rubber tack testing. In order to achieve this, a custom device is built, based on the Tel-Tak principle⁸. The aim of the study is to gain insight into mechanisms that influence poly(dimethyl)siloxane (PDMS) rubber tack. This includes a study of the influence of network structure, polymer molecular weight, addition of loose chains and type of contact on PDMS tack and tack-time dependence.

1.2 STRUCTURE OF THE THESIS

Chapter 2 provides an introduction into the subject of elastomer tack, as well as the mechanisms behind tack creation and molecular models used to describe it. Special attention is devoted to the diffusion-based tack theory of Wool, derived from the reptation model of deGennes. A very brief overview of the Hertz and Johnson, Kendall and Roberts (JKR) theories of elastic contact is given at the end of the chapter.

The first part of **Chapter 3** gives a description of the synthesis and properties of siloxane polymers. Then the methods of crosslinking are described, with special attention paid to the hydrosilylation reaction, as the method widely used in this thesis. The second part describes the NMR methods, which are used for polymer characterization with respect to the average number of crosslinkable sites per polymer molecule.

Chapter 4 provides a general introduction into methods of tack testing in the first part. The second part provides details about the construction of the custom tack testing device used in the research described in this thesis. The device is capable of accurately recording separation forces in the range of milli-Newtons,

which is very important since PDMS rubber inherently exhibits very low tack values. All technical features of this device are explained in detail.

In **Chapter 5** the influence of polymer molecular weight, crosslink density and crosslinker functionality on PDMS rubber-rubber tack is described. These factors heavily influence the amount of loose chains, as well as their ability to entangle. The telechelic PDMS, containing crosslinking sites only on the chain ends, is a very good substrate for preparation of well-defined networks. With this, the changes in tack can be relatively easily related to network morphology. The larger the ability of the polymer chains to entangle, the higher the tack of the PDMS rubber. The crosslinker functionality does strongly reduce tack, since crosslinkers with higher functionality are more able to couple with the polymer chains.

In **Chapter 6** the time-dependence of the autohesive behavior of loosely crosslinked PDMS rubber is described. The autohesion data are gathered for PDMS with different molecular weights, and the influence of molecular weight of the polymer is found to be very pronounced. The data are interpreted on basis of the Wool-deGennes reptation theory, and the application of first order kinetics of wetting is also tested. The reptation model describes well the autohesion data for high molecular weight polymers, while Voyutskii's viscoelastic wetting model is more appropriate for the description of the autohesion of low molecular weight PDMS.

Chapter 7 focuses on the tack of dissimilar substrates. The effects of steel versus PDMS, with varying molecular weights and crosslink densities, as dissimilar contact substrates on tack are described. The tack heavily depends on the type of contact, thus the range of observed behaviors is large. Rubber-steel tack is generally lower than the rubber-rubber autohesive tack, due to inability of chains to cross the interface by reptation. Dissimilar rubber-rubber tack of PDMS networks based on different molecular weights and crosslink densities, depends strongly on the crosslinking levels of the contacting sides.

In **Chapter 8** the influence of addition of non-reactive silicone oil on tack is described. This additive can be considered either as a tackifier or as so-called "connector molecules", and as such should be able to cross the interface and entangle, promoting tack. This is true only to a certain extent, since the thermodynamic incompatibility causes the silicone oil to migrate to the surface of the samples, actually causing the tack to decrease.

¹ From Wikipedia, <http://en.wikipedia.org/wiki/Adhesive>

² Gent A.N., Hamed G.R., *Elastomer Technology – Special Topics*, ACS Rubber Division, Akron Ohio, 2003.

³ van Ooij W.J., *Rubb. Chem. Technol.*, **57**, 421, 1984.

⁴ van der Aar, N., *PhD Thesis*, University of Twente, 1998.

⁵ Wool R.P. *Fundamentals of Adhesion*, L.H. Lee (Ed.), Plenum Press: New York, 1991.

⁶ Hamed G.R., *Rubb. Chem. Technol.*, **54**, 576, 1981.

⁷ Johnson K. L., Kendall K., Roberts A. D., *Proc R. Soc. Lond. A.*, **324**, 301, 1971.

⁸ Beatty J.R., *Rubb. Chem. Technol.*, **42**, 1040, 1969.

Chapter 2

Introduction: Theories and Models of Elastomer Adhesion

“A man who knows how little he knows is well, a man who knows how much he knows is sick.”

Witter Bynner, in *“The Way of Life”* (1944)

In this chapter the phenomena of polymer adhesion and autohesion, as well as the molecular models describing them on a molecular level are introduced. The most important theories are: the adsorption theory, followed by the reptation theory of DeGennes and the crack healing model of Wool. Then the opposing viscoelastic contact theories are introduced. Finally, a brief overview of the Hertz and JKR elastic contact theories is given.

2.1 INTRODUCTION

It is important to define some terminology at the beginning of this chapter to avoid possible confusion. In polymeric materials, *adhesion* or *tack* is the ability to resist separation after bringing separate surfaces together into contact for a short time under light pressure¹. If both materials have the same chemical composition, then the phenomenon is called *autohesion*.

The thermodynamic *work of adhesion* is the work needed to break the bonds formed across the interface, being the sum of all molecular interactions^{2,3}. However, it has been proved many times, that the actual work needed to separate polymer surfaces is much higher than in theory: there is no simple relation between macroscopic adhesion and microscopic thermodynamic work of adhesion².

2.2 ADSORPTION THEORIES

Adsorption theories attribute the formation of autohesive bonds to the intermolecular forces of attraction or van der Waal's forces between surface molecules. It was proposed by Fowkes, that the work of adhesion is the sum of components coming from various types of bonds⁴:

$$g = g^d + g^p + g^h \quad (2 - 1)$$

where γ is the surface tension or surface free energy, and with contributions coming from dispersive, polar and hydrogen bonds, respectively. For a solid-liquid contact Young⁵ derived an equation, which is now written in the following form:

$$g_{sv} = g_{sl} + g_{lv} \cos q \quad (2 - 2)$$

where the subscripts sv, sl and lv refer to the solid-vapor, solid-liquid and liquid vapor interface, respectively, and q is the contact angle as shown in Figure 2-1:

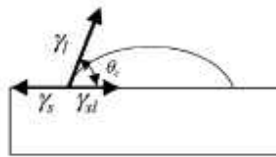


Figure 2-1. Balance of the forces on the three-phase line of the drop of liquid on the solid body.

There is one special condition, which fulfills Young's equation:

$$\text{If } g_{sv} - g_{sl} > g_{lv} \text{ then } \cos q = 1 \quad (2 - 3)$$

Historically, the next development was due to Dupré⁶, who introduced the concepts of work of adhesion (W^a) and work of cohesion (W^c). The work of adhesion is the work required to separate two bodies of heterogenic nature, as depicted in Figure 2-2.

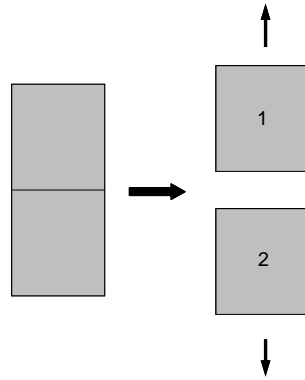


Figure 2-2. Illustration of thermodynamic adhesion process.

When two dissimilar bodies are reversibly brought together, the free energy change per unit area ΔG^c is the free energy of adhesion, the negative of the work of adhesion W_{12}^a :

$$\Delta G^c = -W_{12}^a = g_{12} - g_1 - g_2 \quad (2 - 4)$$

It is important to note, that the surface free energies γ_1 and γ_2 are those of pure substances. The g_{12} term, the interfacial tension, corresponds to the additional energy needed to create the interface. For identical substances this term equals zero, and equation (2 - 4) is reduced to a form:

$$\Delta G^c = -W^c = -2g \quad (2 - 5)$$

where ΔG^c represents the free energy change per unit area of contact, and W_c represents the work of adhesion upon contact. Combining equations (2 - 4) and (2 - 2), the Young-Dupré equation⁷ is obtained:

$$\Delta G_{sl}^a = -g_{lv}(1 + \cos q) \quad (2 - 6)$$

The Young-Dupré equation is valid only if adsorption of either component at the solid-vapor or the liquid-vapor interface can be neglected.

As already mentioned, Fowkes⁸ in a theoretical consideration of attractive forces at interfaces suggested, that the total free energy on the surface is the sum of contributions from different intermolecular forces. From Young's equation, Fowkes derived an expression for the contact angle of a liquid spreading on a solid in terms of the dispersion force contributions of each:

$$1 + \cos q = 2\sqrt{g_s^d} \left(\frac{\sqrt{g_l^d}}{g_{lv}} \right) \quad (2 - 7)$$

where the g_s^d and g_l^d are the dispersive contributions to the surface energies of solid and liquid, respectively. It is possible to approximate the value of g_s^d from the single measurement of q , because values of g_l^d have been published for many liquids⁹. The precondition is that only dispersion forces operate: i.e. the liquid or solid is nonpolar.

The interfacial tension g_{12} , can be also approximated using the Good-Girifalco parameter F , which is expressed as¹⁰:

$$\Phi = \frac{g_1 + g_2 - g_{12}}{2\sqrt{g_1 g_2}} \quad (2 - 8)$$

from which the interfacial tension becomes:

$$g_{12} = g_1 + g_2 - 2\Phi\sqrt{g_1 g_2} \quad (2 - 9)$$

It should be noted, that the Good-Girifalco parameter depends on the type of interactions (polar, dispersive, etc.), as well as on mutual configurations of the interacting molecules¹¹.

Another type of thermodynamic approach was made by Wu¹². He suggested a spreading coefficient to be the driving force for wetting. This coefficient was defined as:

$$I_{12} = W_A - W_C = g_2 - g_1 - g_{12} \quad (2 - 10)$$

where W_A and W_C are the thermodynamic work of adhesion and cohesion, respectively. On the basis on the concept of energy additivity it is assumed, that surface and interfacial energies can be resolved into dispersion and polar components. Wu has shown, that I_{12} has a maximum when the mutual polarities of both components are equal. In such case adhesion will be favoured. Wu reported qualitative correlations between I_{12} and adhesive strength¹².

The final remark about the adsorption theory is, that the work of detachment is actually much higher than the theoretically expected value of ΔG^a , and only a small fraction of it can be regained when the surfaces are joined again. Detaching and adhering is a highly irreversible process. Taking into account only molecular interactions on the interface, is not a good way to estimate strength of an adhesive joint¹³.

2.3 DIFFUSION THEORIES

Diffusion theories state that autohesive bonding takes place as a result of self-diffusion of polymer molecules across the polymer-polymer interface and subsequent entanglement of the migrated chain ends with their new neighbors. If the two contacted polymer layers are uncrosslinked, the interface will eventually disappear and the strength of the junction, the autohesive bond, will become identical to the cohesive strength in the bulk of the material.

2.3.1 THE REPTATION MODEL

Historically, the first systematic studies on the subject were undertaken by the group of Voyutskii¹⁴. He postulated, that due to diffusion of segments of macromolecules, a sufficiently strong bond can be obtained, which results in a high adhesive strength, as depicted in Figure 2-3:

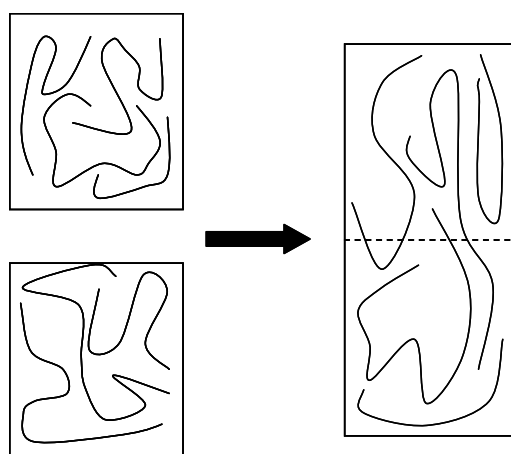


Figure 2-3. The diffusion model of polymer-polymer interface healing.

The situation before contact is shown on the left. The chains are prevented from extending through the polymer-air interface for energetic reasons. After contact has been established, configurational relaxation takes place, leading to an increase in number in junctions crossing the interface. The mechanical strength of the joint reflects the number of intersections of polymer chains.

The problem of motion of individual chains in the polymer bulk has been investigated by many researchers. Rouse¹⁵ and Zimm¹⁶ derived models for the 3-dimensional movement of chains dissolved in a solvent of low molecular weight. On the basis of these models deGennes developed a reptation theory of the movement of polymer chains in a one-dimensional manner within a strongly crosslinked polymer gel¹⁷. Only this theory and its further extensions for polymer tackiness and self-healing will be discussed in this chapter in details. For more information reference is made to other texts^{18,19} on the subject of polymer chain dynamics.

In the model of de Gennes, a polymer chain is confined to a tube having a similar shape as the chain conformation. The tube represents topological constraints from neighboring chains, which restrict the motion of monomers to that along the tube. Because of thermal motions, the chain wriggles around in its tube. These wriggling motions are small in magnitude but occur rapidly, and over a large time-scale, the chain moves back and forth along the center line of its tube with a certain diffusion constant. For a change in its conformation, the chain has to 'escape' from the tube that was defined earlier. Disengagement occurs when one of the chain ends moves out of the tube, and chooses its direction randomly. The whole process is shown on the Figure 2-4. At $t = 0$ the chain is in its initial tube. The chain ends are free to pick any random direction, at times t_1 and $t_2 > t_1$ the memory of the initial tube is gradually lost and parts of the chain (called minor chains) already escaped. After the relaxation time for reptation t_r , usually only the middle part of the chain still retains its initial position.

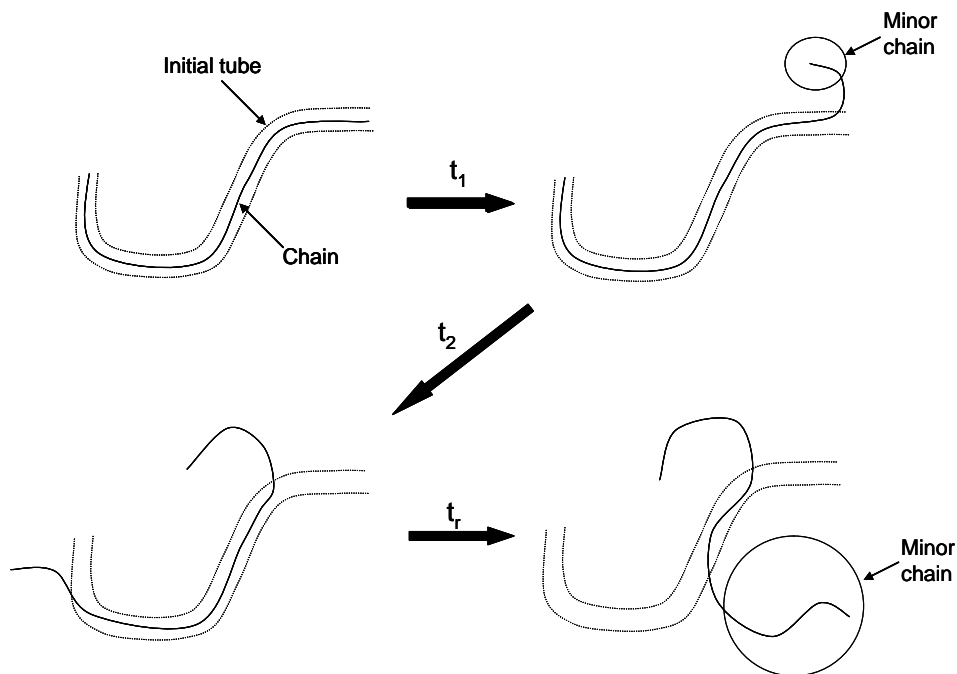


Figure 2-4. The reptation model for a random-coil chain.

2.3.2 THE MODEL THEORY OF CRACK HEALING

Wool applied de Gennes' model for the development of a theory of crack healing at a polymer-polymer interface^{20,21}. On a microscopic scale, the minor chain of length l escaping from the tube is also a random coil and obeys Gaussian statistics. From the reptation model there are some relations summarizing the description of a linear polymer chain movement in an entangled melt. The mean-square length of an escaped minor chain $\langle l^2 \rangle$ is:

$$\langle l^2 \rangle = 16D_1 \frac{t}{p} \quad (2 - 11)$$

where the one-dimensional curvilinear diffusion coefficient, D_1 :

$$D_1 \approx M^{-1} \quad (2 - 12)$$

with M being the molecular mass of the full-length chain. The mean-square monomer displacement of the minor chains is:

$$\langle X^2 \rangle \approx \langle l^2 \rangle^{1/2} \quad (2 - 13)$$

The mean-square center of mass diffusion distance:

$$\langle X_{cm}^2 \rangle \approx 2Dt \quad (2 - 14)$$

with the center of mass self-diffusion coefficient D :

$$D \approx M^{-2} \quad (2 - 15)$$

And the reptation time (time needed for a chain to fully escape its original conformation) t_∞ :

$$t_\infty \approx M^3 \quad (2 - 16)$$

The above relations form the basis for the evaluation of the process of polymer-polymer interface healing.

The foregoing considerations were applicable for only one chain, but interface healing is a process involving reptation and entangling of many polymer chains, as depicted in Figure 2-5.

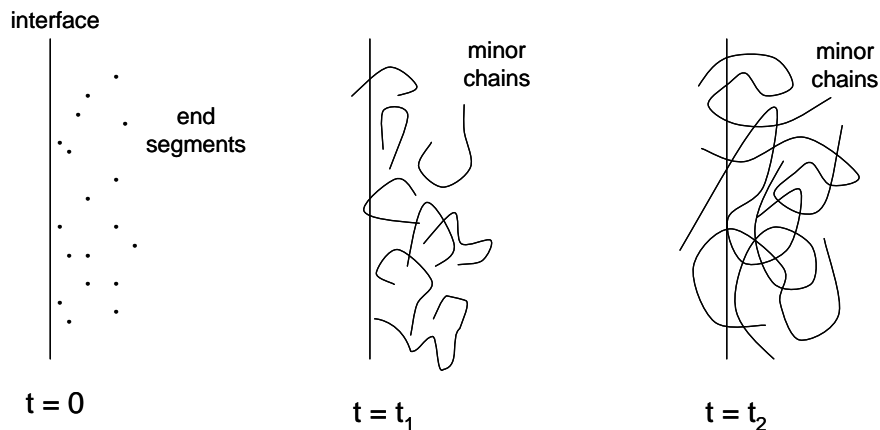


Figure 2-5. The interdiffusion process on the polymer-polymer interface.

$$0 < t_1 < t_2 < t_\infty$$

It is assumed that at $t = 0$, instantaneous complete molecular contact between the surfaces occurs i.e. the wetting stage is instantaneous or immediately complete. The minor chains are responsible for mass transfer: since they do not encounter any obstacles at the interface, their growth to random conformations constitutes the interdiffusion of chains across the interface. As $t \rightarrow t_\infty$, the interface is said to be healed, since all initial conformations will completely be replaced by new (Gaussian) ones of the now fully escaped minor chains. For times $0 < t < t_\infty$, partial healing will already have occurred, accompanied by a measurable resistance to separation of the two surfaces; in other words an autohesive bond has begun to develop.

From this model many molecular aspects of the interpenetration process can be determined²²:

Number of chains intersecting the interface, $n(t)$ – the number of random coils penetrating the interface as a function of time and molecular weight:

$$n(t) \sim t^{1/4} M^{-5/4} \quad (t \leq t_\infty) \quad (2 - 17a)$$

$$n_\infty \sim M^{-1/2} \quad (t \geq t_\infty) \quad (2 - 17b)$$

The term $t \leq t_\infty$ represents the healing period, and $t \geq t_\infty$ means that the healing process is complete and the interface is again in its virgin state. For the fully healed interface, time dependence disappears and only the polymer molecular weight dependence remains.

Number of bridges intersecting the interface, $p(t)$ – an interpenetrating chain has to cross the interface back and forth to create a molecular bridge. The number of bridges behaves with time as:

$$p(t) \sim t^{1/2} M^{-3/2} \quad (2 - 18a)$$

$$p_\infty \sim M^0 \quad (2 - 18b)$$

It is interesting, that the number of bridges for the healed interface does not depend on the molecular weight.

Average interpenetration length $l(t)$ – the average length of chain segments diffused through the interface:

$$l(t) \sim t^{1/2} M^{-1/2} \quad (2 - 19a)$$

$$l_\infty \sim M^{-3/2} \quad (2 - 19b)$$

Average interpenetration depth, $X(t)$ – the average interpenetration depth of the diffused monomer segments behaves as:

$$X(t) \sim t^{1/4} M^{-1/4} \quad (2 - 20a)$$

$$X_{\infty} \sim M^{1/2} \sim l^{1/2} \quad (2 - 20b)$$

Average length of a molecular bridge $l_p(t)$ – the average length of a molecular bridge across the interface is given by:

$$l_p(t) \sim t^{1/4} M^{-1/4} \quad (2 - 21a)$$

$$l_{p\infty} \sim M^{1/2} \quad (2 - 21b)$$

Note, that this scales identically as the average interpenetration depth.

2.3.3 MICROSTRUCTURAL FRACTURE CRITERIA

In order to model the macroscopic interfacial bonding (or fracture) strength, Wool adopted a strain energy fracture approach, which considered both chain pull-out and chain fracture mechanisms.

Consider a volume element containing a small area of interface. A uniaxial stress σ is acting normal to the interface such that the strain energy density U of the volume element is given in the linear elastic approach as:

$$U = \frac{\sigma^2}{2E} \quad (2 - 22)$$

where E is the tensile Young's modulus of the volume element. It can be shown experimentally and theoretically that:

$$E \sim t^0 M^0 \quad (2 - 23)$$

so that E remains constant during tack bond development.

The number of polymer chains per unit volume N_V is

$$N_V = \frac{rN_A}{M} \quad (2 - 24)$$

with r being the density of the volume element and N_A Avogadro's number. When equations (2 - 22) and (2 - 24) are combined, the strain energy density per chain U_C can be written as:

$$U_c = \frac{U}{N_V} = \frac{s^2 M}{2ErN_A} \quad (2 - 25)$$

For polymer chains $l \sim M$, so that the strain energy of a (segment of) chain with length l is associated with:

$$U_c \sim s^2 l \quad (2 - 26)$$

If the stored strain energy in the chain is used to pull it out across the interface, a fraction criterion for the interphase can be written as:

$$U_c \geq U_p \quad (2 - 27)$$

where U_p is the energy required to pull a chain out of its tube by a force f and velocity $\frac{dl}{dt}$.

The pullout force can be given by:

$$f = \frac{\mu \cdot dl}{dt} \quad (2 - 28)$$

where m is the friction coefficient for the chain segment of length l . The friction coefficient is related to the monomer friction coefficient m_0 via $\mu = m_0 \cdot l$, such that the force can be written as:

$$f = \frac{\mu_0 \cdot l \cdot dl}{dt} \quad (2 - 29)$$

U_p can be derived from the integral of $f \cdot dl$:

$$U_p = \int f \cdot dl = \int_{l=0}^{l=l} \mu_0 \cdot l \cdot \left(\frac{dl}{dt} \right) \cdot dl \quad (2 - 30)$$

with solution:

$$U_p = \frac{1}{2} \cdot \mu_0 \cdot \left(\frac{dl}{dt} \right) \cdot l^2 \quad (2 - 31)$$

or:

$$U_p \sim l^2 \quad (2 - 32)$$

From (2 - 26), (2 - 27) and (2 - 31) it now follows that:

$$\sigma \sim t^{1/2} \quad (2 - 33)$$

And because $X_{\infty} \sim t^{1/2}$, finally:

$$\sigma \sim X_{\infty} \quad (2 - 34)$$

Since $X(t) \sim t^{1/4} \sim \sigma$, this model regards the average monomer interpenetration depth as the controlling factor for σ , the macroscopic interfacial bonding stress.

As already said, the aforementioned model takes into account chain fracture and chain pull-out mechanisms. Chain fracture is favored by low temperatures, high polymer molecular weight and high testing rate, as well as by long compression times. In most cases, however, both mechanisms chain fracture and chain pull-out coexist.

2.3.4 EFFECTIVE CROSSINGS DENSITY

A polymer chain is considered with a molecular weight M greater than $2M_e$, with M_e the molecular weight between two neighboring entanglements of the chain with other chains²³. The polymer chain is partitioned into m segments between entanglements:

$$m = \frac{M}{M_e} \quad (2 - 35)$$

It is assumed that an entanglement is found at the end of each segment, excluding the final one. Consequently, there are $m-1$ entanglements along a m -segment chain. Polymer segments that can support stresses are those being confined between two entanglements. Consequently, a chain segment crossing the interface is considered effective in terms of stress support only, if the two adjacent entanglements are not located at the same side of the interface. If two adjacent entanglements are located at the different sides of the interface, the number of *effective* crossings is one, but not the *actual* number of crossings of the particular segment (see Figure 2-6).

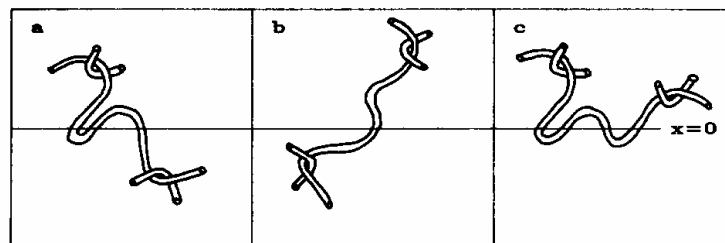


Figure 2-6. The effective (a, b) and not effective (c) chain crossings.

Thus this puts a limitation on the effectiveness of chains crossing the interface, in being able to support bonding stress. Only those chains or chain segments are effective, which after crossing are able to hook into entanglements, at least one on each side. This may be considered a modification of Wool's model described before in the sense, that a minimum molecular weight of the reptating polymer is required to be able to span the distance across the interface and to reach two effective entanglements, one at either side. Below a certain minimum molecular weight the load bearing bonding strength will not develop. The bonding strength model developed before represents an ideal case as if all polymer molecules are equally effective. The alternate approach can be summarized as follows:

$$\frac{\sigma(t_c)}{\sigma_\infty} = \frac{n(t, M_w, M_e)}{n(t_\infty, M_w, M_e)} \quad (2 - 36)$$

where $n(t_c, M_w, M_e)$ is the number of effective crossings per unit area as a function of contact time t , molecular weight M_w , and molecular weight between entanglements M_e . The denominator is the number of effective crossings per unit area of the interface after equilibrium conditions have been reached.

The total number of effective crossings per unit crossing area, n_{eff} , is however also predicted^{24,25} to scale with $t^{1/4}$, and claimed to be determinant for the time-dependence of autohesive bonding.

2.4 VISCOELASTIC WETTING THEORIES

2.4.1 VISCOELASTIC CONTACT FORMATION

The above described models assumed that the dominant process in a time-dependent autohesion is diffusion, and that the interface creation is an instantaneous process. However, on a microscale, most surfaces have a rough topography. Therefore, initially contact will only occur at the areas in which the asperities and craters of one surface meet those of the other, as depicted in Figure 2-7.

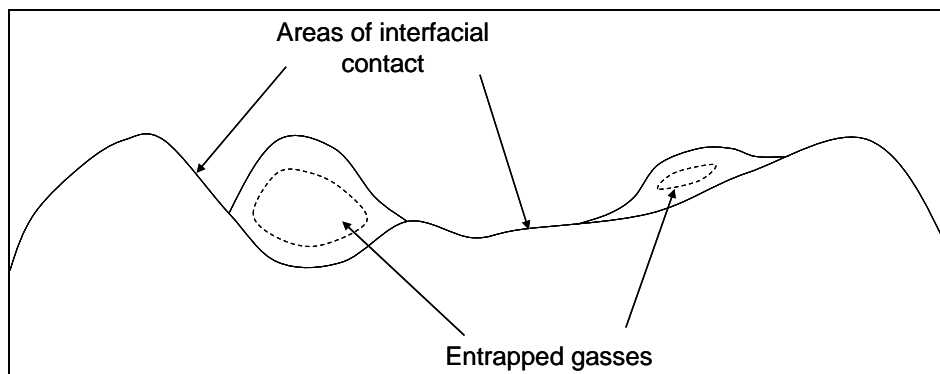


Figure 2-7. Schematic picture of a polymer-polymer interface.

Even then, if gases such as air or moisture are trapped in the interface, actual molecular contact between polymer chains of each surface will be prevented until these surface impurities diffuse into the bulk of the material. Incomplete molecular contact limits van der Waal's bonding (from an adsorption theory point of view) and interfacial diffusion (from the diffusion theory point of view) of polymer molecules. In order for the contact area to increase, the material must undergo viscous flow and displace pockets of entrapped gases.

Early studies were done in the sixties of last century by Korenyevskaya and coworkers²⁶: they studied the growth of the contact area with time to elucidate the importance of each stage of the formation of the adhesive joint, using an optical device of their own construction. They found that the joint strength increases with the completeness of the contact as a function of time and contact pressure. Further investigations done by Vouytskii and Lavrent'yev²⁷ lead to a contact formation model. Lavrent'yev assumed that the contact formation probability, W_c , is a function of time:

$$\begin{aligned} dW_c &= \text{const}(1 - W_c)dt \\ 0 &\leq W_c \leq 1 \end{aligned} \quad (2 - 37)$$

If the fractional contact area j is proportional to W_c , then:

$$dj = \alpha j_\infty (1 - j / j_\infty) dt \quad (2 - 38)$$

where j_∞ is the free surface and α is a constant. The solution of equation (2 - 38) for $j = j_\infty$ for $t = \infty$ and $j = j_0$ for $t = 0$ gives:

$$j = j_\infty [1 - \exp(-\alpha t)] + j_0 \exp(-\alpha t) \quad (2 - 39)$$

The authors assumed, that the contact formation process is governed only by the creep properties of a polymer. A first approximation of the deformation process in the contact zone can be based on the elementary Kelvin-Voigt element²⁸ (see Figure 2-8), for which the following retardation equation applies:

$$J(t) = J_i (1 - e^{-t/q_k}) \quad (2 - 40)$$

where $J = \frac{e}{\sigma}$ is compliance, e = deformation, σ = stress. Differentiating and rearranging this equation results in:

$$de = \frac{e_\infty}{q_k} \left(1 - \frac{e}{e_\infty}\right) dt \quad (2 - 41)$$

where q_k is the relaxation time of the Kelvin-Voigt element. If $\varepsilon/\varepsilon_\infty = \varphi/\varphi_\infty$, equations (2 - 38) and (2 - 41) are equivalent, and $\alpha = 1/q_k$. The dependence of $e(t)$ on

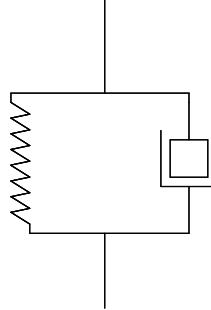


Figure 2-8. The Kelvin – Voigt model, spring combined with a dashpot in parallel alignment.

viscosity h and applied pressure P was described by Rebincev²⁹. The coefficient q_k behaves as:

$$q_k = he / P \quad (2 - 42)$$

Equation (2 - 41) then becomes:

$$hede = (e_\infty - e)Pdt \quad (2 - 43)$$

From the law of elastic deformation, the solution of the equation (2 - 43) is:

$$e_\infty \ln\left(\frac{e_\infty - e}{e_\infty}\right) + e = -\frac{Pt}{h} \quad (2 - 44)$$

With assumption $\varepsilon/\varepsilon_\infty = \varphi/\varphi_\infty$, equation (2 - 44) gives the apparent contact time dependence of the contact surface:

$$\ln(1 - j) + j = -pt/h \quad (2 - 45)$$

This equation was found to properly approximate the autohesion curves of different polymers^{23,30}.

It is important to note, that although the experiments of Voyutskii et al. have shown that the contact area formation is not instantaneous, the interface strength developed further even after full contact was achieved. Thus viscoelastic flow is a controlling factor only during the early stages of contact.

Hamed raised the following argumentation¹: when two surfaces are brought in contact, the interface forms in a progressive manner. Thus after certain time t ,

there will be different portions that achieved interfacial contact at times between 0 and t . As a result, interdiffusion also progressed to varying extents in these regions. The overall bond strength is then the sum of strengths derived from various microscopic interactions. Two borderline cases then can exist:

- 1) The rate of contact formation: R_{ct} is much larger than the rate of interdiffusion: R_i . The whole process is then interdiffusion controlled, and contact formation will finish before any substantial interdiffusion has occurred.
- 2) $R_{ct} \ll R_i$. The bond formation is contact-controlled, with interdiffusion completed quickly after the contact is achieved.

Skewis³¹ calculated the R_i of typical industrial elastomers by their diffusion coefficients. He calculated that after one second of contact an elastomer chain interdiffuses around 45Å: enough for substantial interpenetration. Thus, for common industrial elastomers with molecular weight around 200 000 to 300 000 the bond formation is contact limited.

A strong argument for the contact-controlled bond formation is also the fact, that diffusion should in fact be independent of pressure. Hamed³² in his study concluded, that in the case of NR and SBR tack was sensitive to the compression load applied, what also points to the contact-controlled mechanism.

Anand et al.^{33,34,35} also suggested that the increase in adhesive joint strength is due to an increasing degree of interfacial contact. The increase of adhesion strength Anand attributed to the formation of secondary, van der Waals forces across the interface. He calculated on the basis of Lennard-Jones potential³⁶ intermolecular forces for polystyrene and their contributions to the adhesive joint strength. However, when the quality of the joint was considered, especially with regard to the deformability under the forces causing stress cracking, it was clear that the connection through secondary forces only, does not give an adequate explanation³⁷ for the phenomena observed.

A model for random rough surfaces has been proposed by Greenwood and Williamson³⁸. They represented the surface as a series of asperities and craters of constant radius of curvature, R , but with a distribution of heights relative to a mean plane and a density of asperities per unit surface area: Σ . When a flat plane is brought into contact with such a surface, there will be contact with any asperity whose height z is greater than the separation distance d . The probability of contact is given by:

$$prob(z > d) = \int_d^{\infty} j(z) dz \quad (2 - 46)$$

and the total number of such contacts is:

$$n_c = N \int_d^{\infty} j(z) dz \quad (2 - 47)$$

where N is the number of asperities. The total area of contact can be calculated:

$$A_{tot} = NR \int_d^{\infty} j(z)(z-d) dz \quad (2-48)$$

and the total load:

$$P_{tot} = NER^{1/2} \int_d^{\infty} j(z)(z-d)^{3/2} dz \quad (2-49)$$

For high pressures the distribution of heights can be obtained by using an exponential distribution, given by:

$$j(z) \approx \frac{1}{s} e^{-z/s} \quad (2-50)$$

where s is the standard deviation of height distribution. With this distribution the total contact area and the total load are given by the following relationships:

$$A_{tot} = nsR \quad (2-51)$$

$$P_{tot} = nEs^{3/2} R^{1/2} \quad (2-52)$$

From these two expressions the relationship between load and area can easily be obtained:

$$A_{tot} \approx P_{tot} \left(\frac{R}{s} \right)^{1/2} \frac{1}{E} \quad (2-53)$$

where E is again the Young's modulus of the material. An important result is, that A is inversely proportional to the elastic modulus and proportional to the applied load pressure.

This result can be used to develop a molecular interpretation of tack³⁹. The simplest case is that of a monodisperse polymer above its glass transition temperature. Entanglements impose topological constraints on the motion of chains and control the relaxation process. There are two characteristic timescales that define three different regimes¹⁹. The entanglement time, τ_e , is defined as:

$$t_e \approx \frac{m_0 N_E^2 b^2}{kT} \quad (2-54)$$

where N_e is the number of monomers between entanglements, μ_0 is the monomer friction coefficient, and b is the monomer length, k is Boltzmann's constant and T absolute temperature.

The disentanglement time, τ_d , scales as:

$$t_d \approx t_e \left(\frac{Z}{N_e} \right)^3 \quad (2 - 55)$$

where Z is the polymerization index. For short timescales, $t_c < t_e$, relaxation occurs on short distances due to Rouse-like motions. As a result the modulus decreases according to a simple power relationship:

$$E(t_c) \approx E_N^{(0)} \left(\frac{t_e}{t_c} \right)^{1/2} \quad (2 - 56)$$

where $E_N^{(0)}$ is the plateau modulus on the E vs. $\log t$ curve in a relaxation experiment, see Figure 2-9.

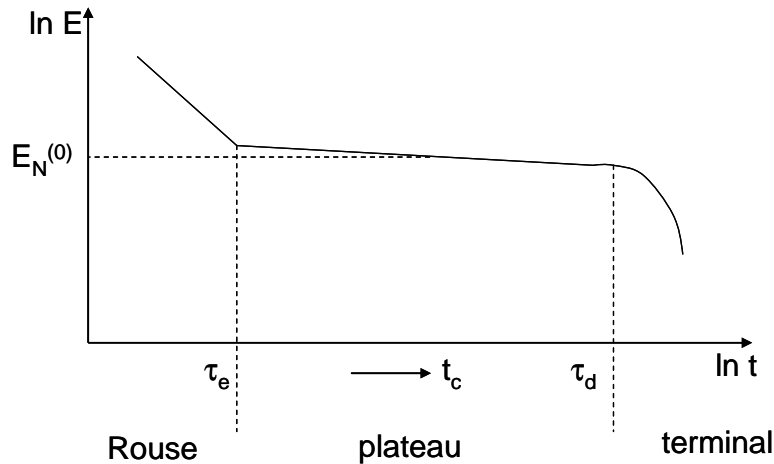


Figure 2-9. Schematic depiction of Young's modulus of a high MW polymer in a relaxation experiment.

For intermediate contact times, $t_e < t_c < t_d$, the modulus practically does not change. For relaxation, disentanglement of chains and times longer than t_d are required, thus only at contact times longer than t_d an adhesive joint deforms via viscous flow. In the context of a tack experiment: if the relevant transition is the one from the Rouse domain to the plateau region and is controlled by t_e , combining equations (2 - 53) and (2 - 56) at times shorter than t_e the area of contact scales with contact time: $A_{tot} \approx t^{1/2}$.

This description has some implications. First, the contact time at which the tack levels off should be strongly dependent on temperature, as it scales with the monomer friction coefficient. On the other hand, this time should be independent of the molecular weight of the chains, as long as the latter is larger than the critical value needed for entanglements. Another implication is, that the transition between good and bad tack is controlled by the disentanglement time: if $t_c > t_d$, viscous flow takes place and tack is good. At shorter times there is not enough viscous flow to create a good contact. If this is true, then the critical contact time for good tack should show strong molecular weight dependence.

2.4.2 THE HERTZ AND JKR CONTACT THEORIES

This field of contact mechanics, concerned with deformations of solid materials that are placed in contact with one another, has a long history, dating back to the work of Hertz⁴⁰ in 1882. He used optical microscopy to measure the size of the contact zone, as shown on Figure 2-8:

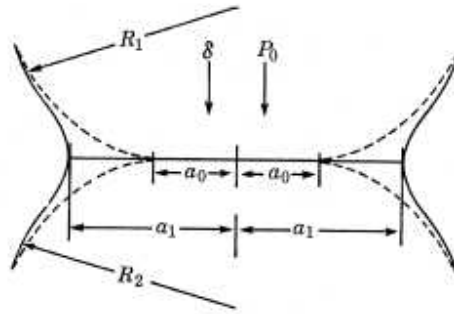


Figure 2-10. The contact between two elastic spheres.

The radius (a_0) of contact zone is given by:

$$a_0^3 = \frac{3}{4} p (k_1 + k_2) \frac{R_{s1} R_{s2}}{R_{s1} + R_{s2}} P \quad (2 - 57)$$

where P is again applied pressure, k_1 and k_2 are the elastic constants of the material of each sphere:

$$k_1 = \frac{1 - n_{p1}^2}{pE_1} \quad \text{and} \quad k_2 = \frac{1 - n_{p2}^2}{pE_2}$$

where n_p is the Poisson ratio and E is the Young's modulus of each material, R_{s1} and R_{s2} are the radii of the two spheres, respectively.

Johnson, Kendall and Roberts⁴¹ extended the Hertz theory. They noted that at low loads, the contact areas between these bodies were larger than those

predicted by Hertz, and tended towards a constant finite value as the load was reduced to zero. At high loads the results closely fitted the Hertz theory. These observations suggest that attractive surface forces are operating between the solids. Although they are of little significance at high loads, they become increasingly important as the load is reduced to zero. The Hertz equation modified to take into account the surface energy effect reads:

$$a^3 = \frac{R_c}{K} \left(P + 3WpR_c + \sqrt{[6WpR_c P + (3WpR_c)^2]} \right) \quad (2 - 58)$$

where $R_c = \frac{R_{s1}R_{s2}}{(R_{s1} + R_{s2})}$, $K = \frac{4}{3}p(k_1 + k_2)$, and W is the work of adhesion of both surfaces. The relationship between the pull-off force P_p and the work of adhesion for elastic bodies held together by interfacial surface forces is given by:

$$P_p = -\frac{3}{2}pR_cW \quad (2 - 59)$$

Derjaguin, Muller and Toporov presented a different approach, based on thermodynamics. In the DMT model⁴² the attractive forces act in the region outside the contact zone, which is still Hertzian. Due to the complexity of the analysis Derjaguin et al. limited the study to the contact of an elastic sphere with a flat surface, with the condition $E_{sphere}/E_{surface} \ll 1$ ⁴³. Moreover, E_{sphere} should not be too small, or the intramolecular interactions would deform the contact area. The relationship between pull-off force and contact area is given as:

$$P_p = \frac{Ka^3}{R_c} - 2pR_cW \quad (2 - 60)$$

The aforementioned theories look contradictory on first sight, and initially were considered competing each other. The controversy was resolved by Tabor⁴⁴ who proved that they apply to different limits of contact situations. Tabor introduced a dimensionless parameter, which can be interpreted as a ratio of elastic deformation to the range of action of surface forces, as defined by:

$$m_T = \frac{32}{2p} \left(\frac{RW^2}{2z_0^3 K^2} \right) \quad (2 - 61)$$

where z_0 is the smallest distance in which two crystalline bodies can be brought (depending on source: 3-4 Å⁴⁵) and K_{DMT} is the so-called combined elastic modulus:

$$\frac{1}{K_{DMT}} = \frac{3}{4} \left(\frac{1-n_1^2}{E_1} + \frac{1-n_2^2}{E_2} \right) \quad (2 - 62)$$

The DMT and JKR theories apply to the opposite extremes of the range of μ . The DMT theory is applicable for small diameter spheres, high Young's modulus and low surface energy, where $\mu < 1$. For highly adhesive systems, where $\mu > 1$, the JKR theory is most appropriate.

The JKR theory is a very broad subject, for a more in-depth overview the interested reader is referred to other texts^{41,46}.

2.5 CONCLUDING REMARKS

As was shown in the previous paragraphs, the phenomenon of elastomer-elastomer adhesion can be described in various ways. Different theories and models can be used to fit experimental data concurrently, but they disagree when it comes to molecular-level descriptions. Table 2-1 summarizes the different approaches and shows in a compact form the tack dependencies on contact time and pressure, as derived from the various theories and models:

Table 2-1: Summary of tack dependencies

	Tack time dependence	Energy time dependence	Tack pressure dependence
Reptation theory	$t^{1/4}$	$t^{1/2}$	P^0
Vouytskii's model	t	-	P
Greenwood-Williamson model	$t^{1/2}$	-	P

The JKR and adsorption theory are essentially different from the ones mentioned above. While Wool's and Greenwood's models deal with macroscale contacts, where the viscoelastic contributions from the sample bulk are important, the JKR and adsorption theory describe the adhesion phenomenon on a microscale. Especially the JKR model, while still dealing with elastic solids, focuses on forces acting on a surface and minimizes the rheological phenomena. These theories do not predict the time dependence, but rather the relationship between the contact load, pressure and contact area. The measuring techniques based on the JKR theory are most suitable to characterize the surface forces of solid materials, while in the case of macroscale contacts the main challenge is to decouple the thermodynamic work of adhesion from the viscoelastic effects. More on this subject can be found in Chapter 4 of this thesis.

¹ Hamed G.R., *Rubber Chem. and Technol.*, **54**, 576, 1981.

² Kammer H.W., *Acta Polym.*, **34**, 112, 1983.

- ³ Mittal K.L., *Polym. Eng. Sci.*, 17, 467, 1977.
- ⁴ Fowkes F.M., *Treatise on Adhesion and Adhesives*, R.L. Patrick (Ed.), Marcel Dekker: New York, 1967.
- ⁵ Young T., *Trans. R. Soc. London*, 95, 65, 1805.
- ⁶ Dupré A., *Theorie Mechanique de la Chaleur*, Gauthier – Villars, Paris, 1869.
- ⁷ Adamson A.W., *Physical Chemistry of Surfaces*, 5th ed. Wiley Intersciences (Ed.), New York, 1990.
- ⁸ Fowkes F.M., *Ind. Eng. Chem.*, 55, 40, 1964.
- ⁹ Owens D.K., Wendt R.C., *J. Appl. Polym. Sci.*, 13, 1741, 1969.
- ¹⁰ Good R.J., *J. Adh. Sci. Technol.* 6, 12, 1992.
- ¹¹ van Oss C.J., Chaudhury M.K., *Fundamentals of Adhesion*, L.H. Lee (Ed.), Plenum Press: New York, 1991.
- ¹² Wu S., *J. Adh.*, 5, 39, 1973.
- ¹³ Gent A.N., Hamed G.R., *Elastomer Technology – Special Topics*, ACS Rubber Division, Akron Ohio, 2003.
- ¹⁴ Voyutskii S.S., *Autohesion and Adhesion of High Polymers*, John Wiley & Sons (Ed.), New York, 1963.
- ¹⁵ Rouse P.E., *J. Chem. Phys.*, 21, 1272, 1953.
- ¹⁶ Zimm B.H., *J. Chem. Phys.*, 24, 269, 1956.
- ¹⁷ de Gennes P.G., *J. Chem. Phys.*, 55, 572, 1971.
- ¹⁸ de Gennes P.G., *C. R. Acad. Sc (Paris)* B291, 219 1980
- ¹⁹ Doi M., Edwards S.F., *The Theory of Polymer Dynamics*, Oxford: Clarendon Press, Oxford, 1988.
- ²⁰ Wool R.P., O'Connor K.M., *J. Appl. Polym. Sci.*, 52, 10, 1981.
- ²¹ Wool R.P. *Fundamentals of Adhesion*, L.H. Lee (Ed.), Plenum Press: New York, 1991.
- ²² Wool R.P., *Rubber Chem. and Technol.*, 57, 307, 1984.
- ²³ Mikos A.G., Peppas N.A., *Polymer*, 30, 84, 1989.
- ²⁴ Prager S., Tirrell M., *J. Chem. Phys.*, 75, 5194, 1981.
- ²⁵ Prager S., Tirrell M., *J. Chem. Phys.*, 78, 7015, 1983.
- ²⁶ Korenyevskaya N.S., Vouytskii S.S., *Polym. Sci. USSR*, 8, 1372, 1966.
- ²⁷ Plisko L.F., Lavrent'yev V.V., Vouytskii S.S., *Polym. Sci. USSR*, 14, 2501, 1972.
- ²⁸ Ferry J.D., *Viscoelastic Properties of Polymers*, 3rd edition, John Wiley & Sons (Ed.), New York, 1980.
- ²⁹ Rebincev P.A., S.S., *Polym. Sci. USSR*, 86, 239, 1951.
- ³⁰ Stacer R.G., Schreuder-Stacer H.L., *Int. J. Fracture* 39, 201, 1989.
- ³¹ Skewis J.D., *Rubber Chem. and Technol.*, 39, 217, 1966.
- ³² Hamed G.R., *Rubber Chem. and Technol.*, 54, 403, 1981.
- ³³ Anand J.N., Karam H.J., *J. Adh.*, 1, 16, 1969.
- ³⁴ Anand J.N., Balwinski R.Z., *J. Adh.*, 1, 24, 1969.
- ³⁵ Anand J.N., *J. Adh.*, 1, 31, 1969.
- ³⁶ Lennard-Jones J.E., *Proc. Phys. Soc.*, 43, 461, 1931.
- ³⁷ Bonten C., Schmachtenberg E., *Polym. Eng. Sci.*, 41, 475, 2001.
- ³⁸ Greenwood J.A., Williamson J.B.P., *Proc. R. Soc. Lond.*, A, A295, 300, 1966.
- ³⁹ Creton C., Leibler L., *J. Polym. Sci., Part B: Polym. Phys.*, 34, 545, 1996.
- ⁴⁰ Hertz H., Reine J., *Angew. Math.*, 92, 156, 1882.
- ⁴¹ Johnson K. L., Kendall K., Roberts A. D., *Proc. R. Soc. Lond. A.*, 324, 301, 1971.

-
- ⁴² Derjaguin B. V., Muller V. M., Toporov Y., *J. Coll. Int. Sci.*, 53, 314, 1975.
- ⁴³ Muller V.M., Yushchenko V.S., Derjaguin B.V., *J. Coll. Int. Sci.*, 77, 91, 1980.
- ⁴⁴ Tabor D., *J. Coll. Int. Sci.*, 58, 1, 1976.
- ⁴⁵ Rabinovich Y. I., Adler J. J., Ata A., Singh R. K., Moudgil B. M., *J. Coll. Int. Sci.*, 232, 17, 2000.
- ⁴⁶ Maugis D., Barquins M., *J. Phys. D: Appl. Phys.*, 11, 1989, 1978.

Chapter 3

Silicone Elastomers: Properties and Characterization

*“To know that we know what we know, and to know that we do not know what we do not know,
that is true knowledge.”*

Copernicus

In this chapter the silicone elastomers will be described, starting from the methods of synthesis from metallic silica. Then the methods of crosslinking are described with the emphasis on the hydrosilylation reaction as a method used further in the thesis for the preparation of samples. Next paragraphs describe NMR and IR characterization methods in relation to the crosslinking reaction, and finally some surface properties of silicone elastomers are mentioned. The experimental section describes the quantitative NMR measurements used for the vinyl group content determination.

3.1 INTRODUCTION

The term “silicones” is used to describe a whole family of organo-silicon compounds, based on a backbone molecular chain containing alternative silicon and oxygen atoms. Depending on the types of organic groups, silicone polymers exhibit a wide range of properties. Special attention will be paid to poly(dimethyl)siloxane (PDMS) rubbers, especially the ones containing vinyl-terminated polymer chains.

3.2 SILICONE CHEMISTRY

The unique chemistry of the silicone polymers is a result of their silicon-oxygen backbone. The primary difference between silicone and organic polymers is shown in Figure 3-1.

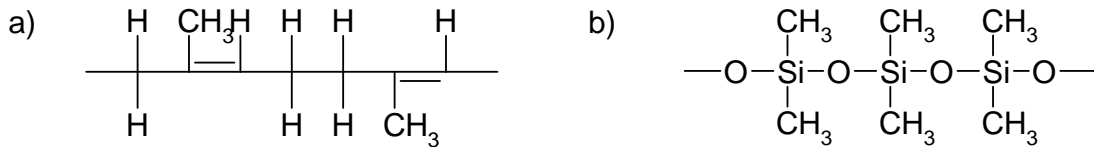


Figure 3-1. Organic polymer a) and silicone polymer b).

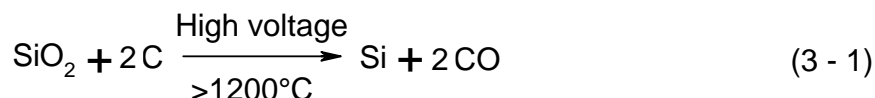
The silicone polymer molecules can be easily customized by the chemists to optimize their performance and adjust attributes needed for certain applications¹. Some examples of the organic side groups are shown on Figure 3-2:

Class	Silicone Type	Chemical structure
MQ	Dimethyl	$* \left[\begin{array}{c} \text{CH}_3 \\ \\ \text{---Si---O---} \\ \\ \text{CH}_3 \end{array} \right]_n *$
PMQ	Methyl phenyl	$* \left[\begin{array}{c} \text{CH}_3 \\ \\ \text{---Si---O---} \\ \\ \text{CH}_3 \end{array} \right]_n \left[\begin{array}{c} \text{C}_6\text{H}_5 \\ \\ \text{---Si---O---} \\ \\ \text{C}_6\text{H}_5 \end{array} \right]_m *$
		$* \left[\begin{array}{c} \text{C}_6\text{H}_5 \\ \\ \text{---Si---O---} \\ \\ \text{CH}_3 \end{array} \right]_n *$
VMQ	Methyl vinyl	$* \left[\begin{array}{c} \text{CH}_3 \\ \\ \text{---Si---O---} \\ \\ \text{CH}_3 \end{array} \right]_n \left[\begin{array}{c} \text{HC}=\text{CH}_2 \\ \\ \text{---Si---O---} \\ \\ \text{CH}_3 \end{array} \right]_m *$
FVMQ	Fluorosilicone	$* \left[\begin{array}{c} \text{CH}_3 \\ \\ \text{---Si---O---} \\ \\ \text{CH}_3 \end{array} \right]_n \left[\begin{array}{c} \text{HC}=\text{CH}_2 \\ \\ \text{---Si---O---} \\ \\ \text{CH}_2\text{CH}_2\text{CF}_3 \end{array} \right]_m *$

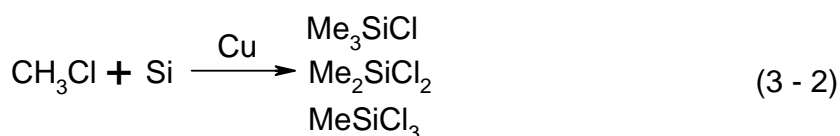
Figure 3-2. Examples of silicone polymer side groups.

3.2.1 SYNTHESIS

The silicone industry started in the late 1930's, after Rochow discovered the direct process for the production of chlorosilanes from elemental silicon and methyl chloride^{2,3}. The first step in production of a silicone polymer requires the reduction of silica to metallic silicon via the carbo-electro reduction process⁴:



The silicon is then converted to methylchlorosilanes by the before mentioned direct process reaction, a so-called MCS reaction, in a presence of copper as a catalyst.



The product mixture from a typical MCS reaction is subjected to several distillation steps, where the monomers are separated from the reaction residue; the residue usually contains siloxanes and disilanes. The dimethyldichlorosilanes are reacted with water to form silicone hydrolyzate, which rapidly condenses to form cyclic siloxanes and low molecular weight linear siloxanes. The latter are reacted with base to product cyclic siloxanes, especially dimethyl tetramer, so-called D₄, which is the primary input for the dimethyl silicone polymer. The further ring opening polymerization of D₄ is conducted with a strong base, resulting in linear polymers, of which the molecular weight is controlled by the addition of monofunctional silanes acting as chain stoppers. The process is schematically shown in Figure 3-3.

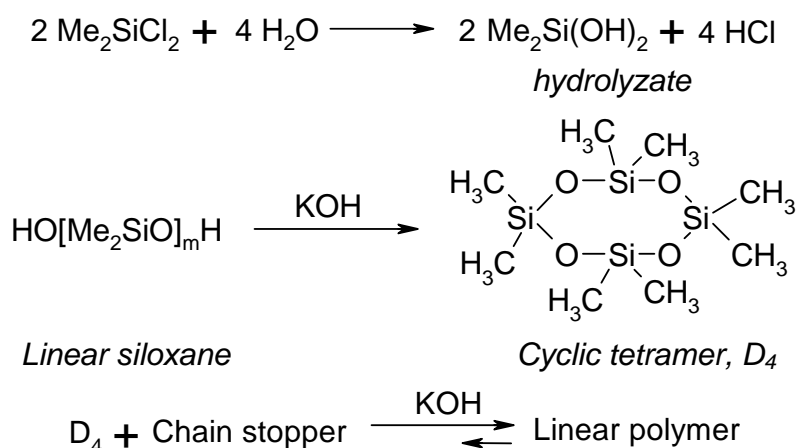


Figure 3-3. Synthesis of a siloxane polymer.

There is an alternative process consisting of the direct condensation of the hydrolyzate, using an acid catalyst to obtain linear polymers. This process is applicable rather for low molecular mass oils, since it results in higher levels of branching.

3.2.2 CROSSLINKING OF SILICONES

3.2.2.1 PEROXIDE CURE

The traditional curing systems for silicone rubbers are organic peroxides. When heated, peroxides generate free radicals that react with the pendant organic groups on the silicone polymer^{1,5,6,7}. This results in crosslink formation between the polymer chains. The presence of vinyl groups in the chain speeds up the reaction greatly, also improving the crosslink density. The peroxide cure reaction is schematically shown in Figure 3-4.

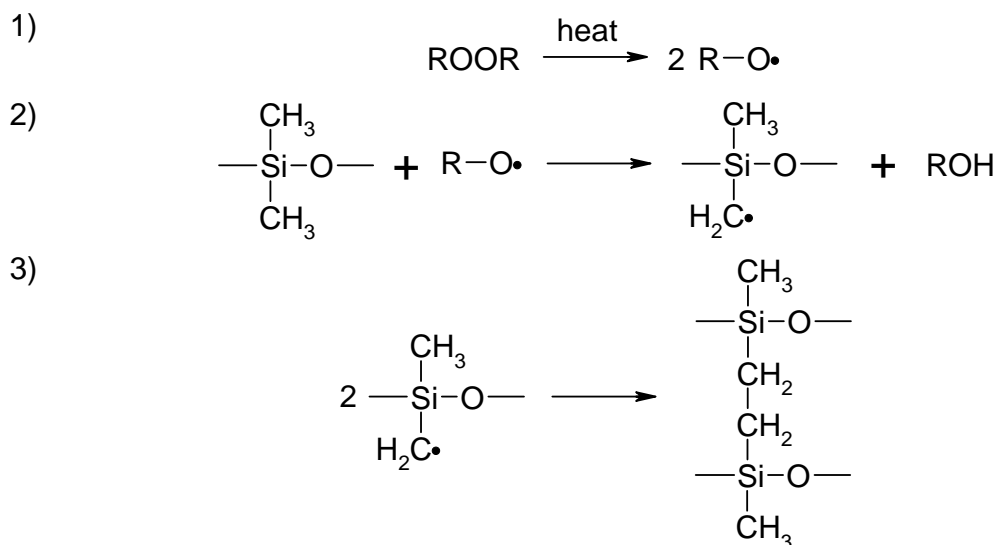


Figure 3-4. Peroxide vulcanization of silicone rubber.

The peroxide systems are commonly used. However, elastomers cured in such a way may release peroxide decomposition byproducts, such as cumyl alcohol or acetophenone, depending on a type of peroxide used⁷.

3.2.2.2 ADDITION CURE BASED ON A HYDROSILYLATION REACTION

An alternative method of curing silicone rubbers utilize the addition of a silane group to an unsaturated -C=C- bond, usually vinyl or allyl groups. It can be initiated in several ways, metal catalysis being the most common. The catalysts can be metal salts, supported metals or transition metal complexes⁸. A wide variety of catalysts has been investigated, but the most common ones in synthesis and industrial processes are platinum complexes⁹. Speier's catalyst, the hexachloroplatinic acid, is widely used in the commercial hydrosilylation of

unsaturated substrates^{10,11}. Other platinum compounds also exhibit high activity, especially in curing siloxanes containing vinyl groups, such as cis-dichlorobis(triphenylphosphine) platinum (II), $\text{PtCl}_2(\text{PPh}_3)_2$; di- μ -chloro-dichlorobis(ethylene) diplatinum (II), $\text{PtCl}_2(\text{C}_2\text{H}_4)_2$ or tetrakis (triphenoxyphosphine) platinum (IV), $[(\text{PhO}_3)\text{P}]_4\text{Pt}$ [11]. However, the Karstedt's catalyst¹², a 2% platinum divinyltetramethyl-disiloxane complex in xylene, is the preferred hydrosilylation catalyst^{13,14}. Its chemical structure is shown in Figure 3-5.

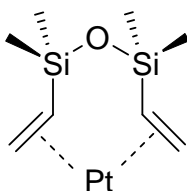


Figure 3-5. Karstedt's catalyst.

During the addition cure the hydride adds to a vinyl unsaturation, as illustrated in Figure 3-6, resulting in a uniformly crosslinked rubber.

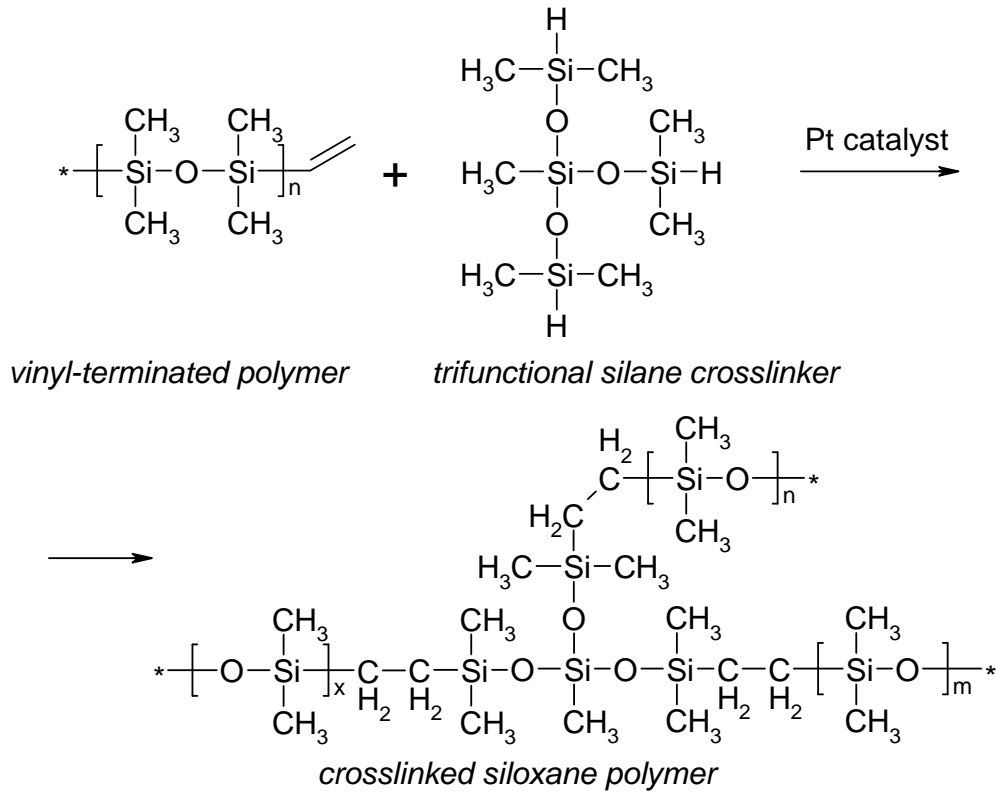


Figure 3-6. The hydrosilylation crosslinking reaction.

The addition occurs mainly on the terminal carbon. The following mechanism has been proposed¹⁵.

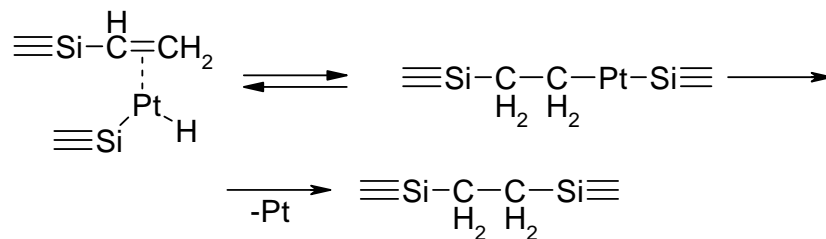
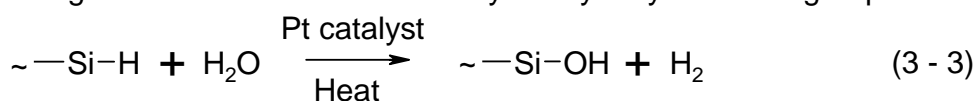


Figure 3-6. The simplified hydrosilylation reaction mechanism. Triple bonds represent the remaining valences of the silicon atom. Other Pt-ligands and Si substituents are omitted for simplicity of the picture.

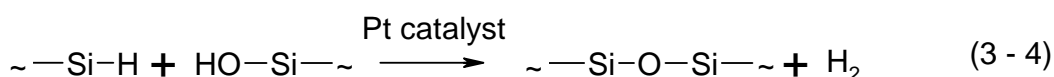
The reaction begins with an oxidative addition of the silicone to the platinum, then hydrogen transfer to the double bond and then reductive elimination of the platinum. Since the reaction proceeds actively at room temperature, inhibitors play a crucial role in assuring adequate mixing and cure rate control. Lots of different chemical compounds can act as inhibitors, including peroxides, copper salts, crown ethers, unsaturated organic compounds, amines or organophosphorous species. Unfortunately, the hydrosilylation reaction is very

sensitive to contamination. Chemical compounds capable of forming strong complexes with platinum can inadvertently poison the catalyst. Amines and thiols as electron-donating substances are the most detrimental. Despite this drawback, the hydrosilylation reaction is widely used in preparation of siloxane networks, due to its high selectivity, which tolerates many functional groups, including esters, ketones, amides, ethers, nitriles, etc.¹⁶ The absence of reaction by-products, the homogenous degree of crosslinking in thick sections of rubber goods and excellent reversion resistance, are additional benefits of using addition cure systems.

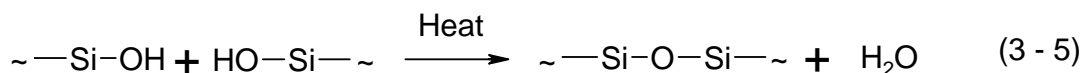
Secondary reactions during the hydrosilylation process may occur^{17,18} and are especially favored with an excess of crosslinker and during the so-called postcure stage. The reactions involve catalyzed hydrolysis of SiH groups:



Crosslinking also occurs during this stage, when the newly created SiOH groups catalytically react with the remaining SiH groups:



Another possible reaction for postcuring is the condensation of two SiOH groups created in reaction (3 - 3):



Reactions (3 - 3) and (3 - 4) are slower than the primary crosslinking reaction. The condensation reaction (3 - 5) is even slower than the reactions involving -SiH groups. The abovementioned processes are called postcure reactions, because they occur only when the system is allowed or forced to proceed towards complete conversion¹⁸.

3.3 CHARACTERIZATION OF SILICONE POLYMERS AND VULCANIZATES

3.3.1 INFRARED SPECTROSCOPY

Infrared spectroscopy is one of the oldest techniques for the molecular characterization of materials. It dates back to the work of Coblenz^{19,20} who worked on instrument design, development of the experimental technique and the determination of absorption and reflection spectra of a large number of compounds. In the field of structural analysis and identification of polymers, infrared spectroscopy has established a strong position. Much work has been

done in the field of IR spectroscopy of rubbers^{21,22}, including the silicone rubber materials as well. The spectral patterns of the groups attached to the siloxane chain are highly specific and identification can readily be made using the infrared spectroscopy.

The IR spectrum of vinyl-terminated PDMS polymer (pure polymer film) is shown in Figure 3-7a. Some characteristic peak assignments are as follows^{23,24}:

Adsorption band [cm^{-1}]	Chemical group
2800-3000	C-H (CH_3)
1596	Si-C=C
1373	CH_2
1264	Si- CH_3
1019	Si-O
880	-CH=CH ₂
800	Si-C

The extent of the hydrosilylation reaction can very conveniently be determined using the infrared spectroscopy^{18,25,26}. The Si-H bond gives a very characteristic absorption peak around 2160 cm^{-1} , as shown in Figure 3-7b. This band is intense and falls in the region where hardly any other chemical group gives a signal.

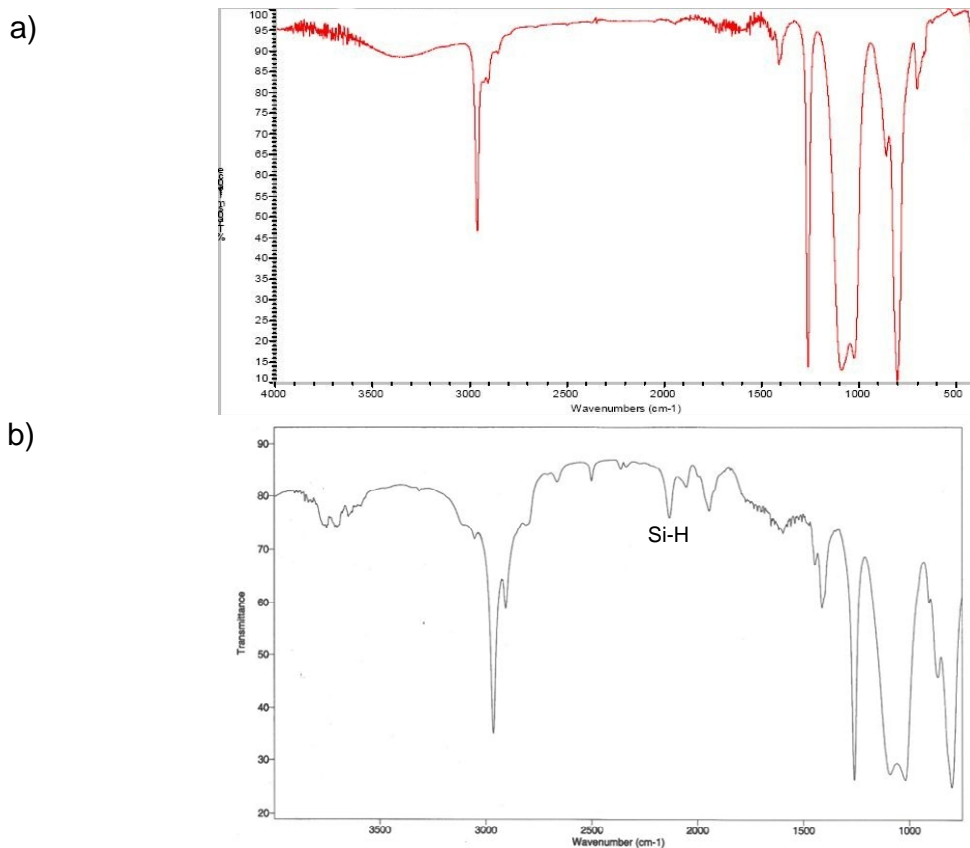


Figure 3-7: IR spectra of a) pure vinyl-terminated PDMS²⁷; b) hydrosilylation reaction mixture. The Si-H peak is marked.

Analysis of changes in the Si-H stretching adsorption band as a function of time, gives the possibility of studying the reaction kinetics as well²⁸. An example of how the concentration of silicone hydride in a crosslinker changes, like shown in Figure 3-6, with time is shown in Figure 3-8. The intensity of the band decreases with time and extent of the curing reaction. The hydrosilylation is known for the absence of significant side-reactions, so the changes can be taken to be the result of reaction between the hydrosilane and the vinyl groups²⁹. According to the sources, the hydrosilylation reaction appears to obey first order kinetics^{25,26}.

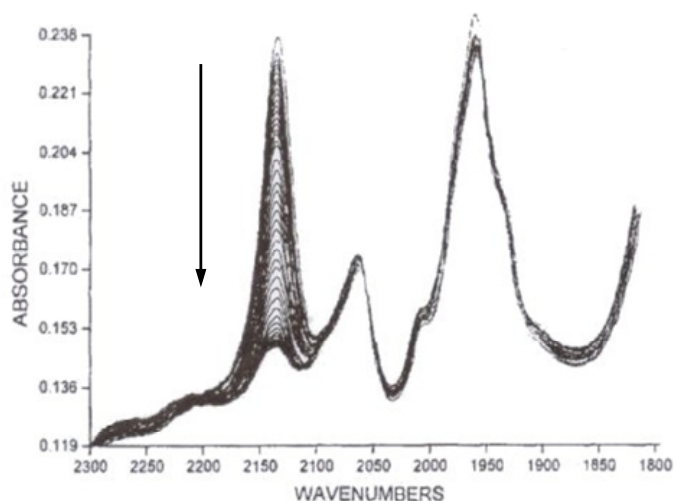


Figure 3-8: Decrease of the silyl adsorption band²⁸. The arrow represents increasing reaction time.

Though infrared spectroscopy can be used for end group analysis, it is limited mostly to siloxanes capped with Si-H or Si-Me₃. The first group takes advantage of the strong signal in the unpopulated region, while the other one uses a Fourier deconvolution to separate di- and trimethyl absorbances in the Si-C stretching band³⁰.

3.3.2 NMR

Many groups attached to the siloxane chain have distinctive proton resonances, and ¹H NMR is a useful technique for both qualitative and quantitative analysis. For identifying molecular structures it is widely used in conjunction with other NMR techniques, such as ²⁹Si or ¹³C NMR.

Quantitative spectra are useful for analyzing mixtures. The use of the hydrosilylation reaction for crosslinking requires knowledge of the Si-H/Si-vinyl ratio in the reaction mixture, to achieve the best or required quality of product. ¹H Nuclear Magnetic Resonance spectroscopy provides a very suitable tool for that purpose, since the vinyl groups can easily be detected with NMR. A sample spectrum of vinyl-terminated PDMS is shown in Figure 3-9.

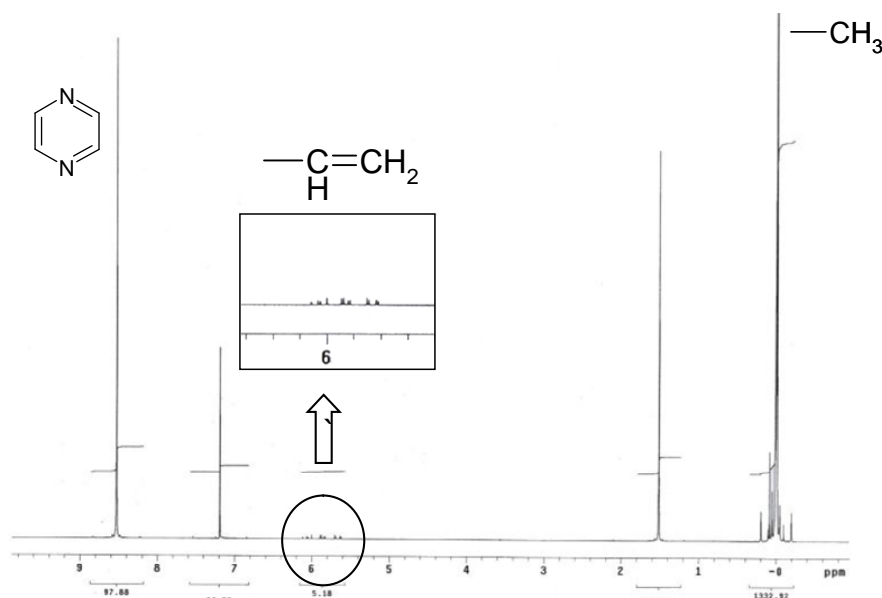


Figure 3-9: ¹H NMR spectrum of vinyl-terminated PDMS. The signals from vinyl groups are enlarged. Pyrazine is used as an internal standard for quantitative measurements.

Terminal vinyl groups in siloxane polymers are reported to give the signals at around 6 ppm^{31,32}. The intensity of the signal depends on the concentration of vinyl-groups in the polymer. For polymers with high molecular weight, sometimes special techniques have to be used to enhance the signal-to-noise ratio³², since the relative error of integration is proportional to the ratio. Thus the accuracy of the integration and further calculations can be improved.

3.4 SURFACE PROPERTIES OF PDMS.

The surface properties of silicones can best be described by taking the pendant groups as the primarily surface active entities. The polymer backbone then controls the way in which they appear on the surface³³. This is a useful simplification in explaining the unique surface properties of siloxanes in general, and PDMS in particular.

PDMS exhibits a uniquely low liquid surface tension ranging from 16 to 21 mN/m at room temperature³⁴; only fluorinated species have even lower surface tensions. Such low surface tension gives PDMS the tendency to accumulate at the surfaces in systems like polymer blends or block copolymers. This property is a reflection of the molecular structure. The rotation around the Si-O bond is virtually free, compared with an energy barrier of 14 kJ/mol for carbon-carbon bond rotation in polyethylene, and more than 20 kJ/mol for poly(tetrafluoroethylene)³⁵. This free rotation is reflected in a very low glass transition temperature of poly(dimethylsiloxane), of below -100 °C. Another structural feature worth noting is the wide variability of the Si-O bond due to its partially ionic nature, which also can contribute to the overall chain flexibility. This

gives siloxanes an extended and flexible chain system in which steric hindrances are little likely to impede the creation of a methyl-group rich, low surface energy configuration, as shown in Figure 3-10. In combination with the methyl pendant groups, which according to Owens and Wendt³⁶ exhibit one of the lowest intermolecular interactions, this explains the low surface tension properties of PDMS.

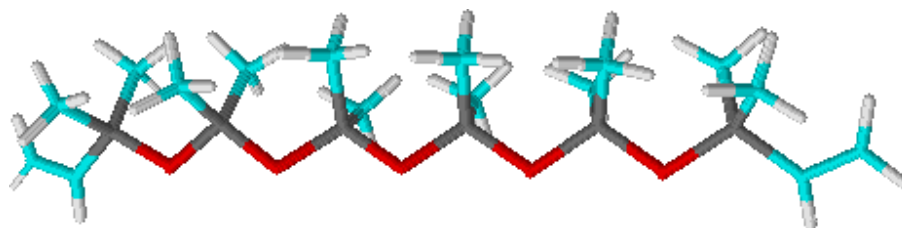


Figure 3-10: The methyl “comb”, the way methyl groups in PDMS are organized on the polymer surface.

The main consequence of the low surface energy of PDMS is, that this liquid polymer will spread over any high-energy substrate. PDMS will also spread over many low-surface energy materials, excluding various fluorocarbon polymers. The high chain flexibility allows “rebuilding” of a surface, like regaining hydrophobicity after exposition to corona or plasma discharges. Untreated polymer chains migrate to the surface or hydrophilic groups turn away from the surface³⁷. As a low surface energy component, PDMS tends to migrate and accumulate on the surfaces of polymer blends³⁸, its surface concentration can even reach 95% at very small bulk concentrations. Therefore, the surface properties of polymer blends can be altered by addition of poly(dimethylsiloxane).

3.5 QUANTITATIVE NMR MEASUREMENTS FOR VINYL-GROUP CONTENT DETERMINATION

As was mentioned above, the knowledge of the average vinyl-group content in a batch of siloxane polymer is of crucial importance for setting the stoichiometry of the hydrosilylation reaction, and thus controlling the degree of crosslinking of the resulting silicone rubber. ¹H NMR measurements have been done for every new batch of the siloxane polymer, before it was used to prepare silicone rubber.

3.5.1 SAMPLE PREPARATIONS

Materials. The PDMS polymers of various molecular weights were supplied by ABCR. Pyrazine (>99%) and CDCl₃ were obtained from Aldrich.

NMR sample preparation. Weighed amounts of PDMS oil and pyrazine were dissolved in CDCl₃ in a glass flask. The solution was then transferred to the NMR tube, the tube was further filled up with the solvent to the volume needed for best spectrum resolution, and the whole mixture was stirred again to ensure proper mixing.

3.5.2 ¹H NMR MEASUREMENT

Machine settings. The measurement was performed using a Varian Unity 300 MHz apparatus. The ¹H NMR spectra were recorded using the following machine settings:

Variable symbol	Explanation	Value
NS	Number of scans	16
DS	Number of dummy scans	0
O1p	Center of spectrum	5.333 ppm
TD	Datapoints time domain	32 K
SI	Datapoints spectrum domain	32 K
P0	Pulse	90°
D-1	Delay after pulse. Very important, because of the long T ¹ value of pyrazine protons in combination with the 90° pulse	30 sec
DE	-	5.50 μsec
SWH	Sweep width	6024.1 Hz
LB	Line broadening	1.0 Hz

A sample spectrum was already shown in Figure 3-9. The signals from vinyl-groups appear in the 6 ppm region. The peaks of pyrazine protons show clearly between 8 and 9 ppm, which range in the case of PDMS is always empty, thus nothing can interfere with the measurement. After baseline correction the spectra were integrated by hand. All the integrations included also the C¹³ “satellites” signals.

Calculations of the hydrogen-to-vinyl ratio. The amount of the vinyl functional groups was calculated according to the following formula:

$$\text{group count [mmol/kg]} = \frac{m_{\text{pyr}} \cdot 10^6 \cdot 4 \cdot I_{\text{vinyl}}}{80 \cdot 3 \cdot m_{\text{PDMS}} \cdot I_{\text{pyr}}}$$

The symbols are as follows:

m_{pyr} – mass of pyrazine in a sample (in grams)

10^6 – factor for calculations to mmol/kg

4 – the amount of protons in pyrazine

I_{vinyl} – the integration of vinyl signals

80 – the molar mass of pyrazine

3 – the amount of protons in a vinyl group

m_{PDMS} – the mass of PDMS in a sample (in grams)

I_{pyr} – the integration of pyrazine signal

The results from the measurements were compared with measurements made within Océ Technologies³⁹. They agreed within the measurement error of the method.

3.6 CONCLUDING REMARKS

Due to their unique molecular structure, silicone elastomers exhibit a wide range of properties. The way of synthesis allows for the preparation of polymers with different sidegroups, which in turn contribute to the overall flexibility of the polymer. Silicone polymers can be crosslinked in many different ways, depending on the type of sidegroups. One of the best methods to use, with almost no by-products and side reactions, is the hydrosilylation reaction. Still it depends heavily on the stoichiometry, thus requiring the knowledge of the amount of reactive groups in the polymer. This drawback can easily be overcome by using the ¹H NMR to determine the reactive group content. The measurement is accurate and easy to perform, but may require some additional tuning to enhance the signal-to-noise ratio, though.

Not only NMR, but infrared spectroscopy can also be used for the characterization of silicone polymers. It is especially well suited for detecting the types of sidegroups and changes in their concentration. The spectral techniques are a powerful tool in the field of silicone elastomers.

¹ Toub M., Finney D.L., *Basic Elastomer Technology*, ACS Rubber Division, the University of Akron (Ed.), Akron, Ohio, USA, 2001.

² Lewis L.N., *Chemistry of Organosilicon Compounds, Part 3*, John Wiley (Ed), Sussex, England, 1998.

³ Eugene Rochov, *Preparation of Organosilicon Halides*, U.S. patent 2,380,995, 1945.

⁴ Lewis L.N., *From Sand to Silicones. An Overview of the Chemistry of Silicones*, GE Research and Development Center, 1998.

⁵ Bueche A.M., *J. Polym. Sci.*, **15**, 105, 1954.

⁶ Ogunniyi S.D., *Prog. Rubb. Plast. Technol.*, **15**, 95, 1999.

⁷ Heiner J., Stenberg B., Persson M., *Polym. Test.*, **22**, 253, 2003.

⁸ Grate J.W., Kaganove S.N., *Polym. News*, **24**, 149, 1999.

⁹ Roth L.E., Vallés E.M., Villar M.A., *J. Polym. Sci.*, **41**, 1099, 2003.

¹⁰ Kishi K., Ishimaru T., Ozono M., Tomita I., Endo T., *Int. J. Adhes. Adhes.*, **20**, 253, 2000.

¹¹ *Comprehensive Handbook on Hydrosilylation*, Marciniak B. (Ed), Pergamon, Oxford, 1992.

¹² Karstedt B.D., *Platinum Complexes of Unsaturated Siloxanes and Platinum Containing organopolysiloxanes*, US Patent 3,814,730, 1974.

¹³ Dvornik P.R., Gerov V.V., *Macromolecules*, **27**, 1068, 1994.

¹⁴ Maric M., Ashurov N., Macosco C.W., *Polym. Eng. Sci.*, **41**, 631, 2001.

¹⁵ Colas A., Curtis J., *Biomaterials Science 2nd Edition*, Elsevier Academic Press (Ed.), 2004.

¹⁶ Grate J.W., Kaganove S.N., Nelson D.A., *Chem. Innovation*, **29**, 2000.

¹⁷ Thomas D.R., *Siloxane Polymers*, Prentice Hall: Englewood Cliffs, NJ (Ed.), 1993.

- ¹⁸ Simpson T.R.E., Tabatabaian Z., Jeynes C., Parbhoo B., Keddie J.L., *J. Polym. Sci., Part A: Polym. Chem.*, **42**, 1421, 2004.
- ¹⁹ Coblenz W.W., *Investigation of Infrared Spectra*, Paper No. 35, Carnegie Institution of Washington, 1906.
- ²⁰ Coblenz W.W., *Appl. Spectrosc.*, **7**, 109, 1953.
- ²¹ Hampton R.R., *Rubb. Chem. Technol.*, **45**, 546, 1972.
- ²² Prajna P. De, *Spectroscopy of Rubbers and Rubbery Materials*, 3rd chapter, Rapra Technology Limited (Ed.), Shawbury, UK, 2002.
- ²³ Roy S., De P.P., *Polym. Test.*, **11**, 3, 1992.
- ²⁴ Flipsen T.A.C., Derks R., van der Vegt H., Pennings A.J., Hadziioannou G., *J. Polym. Sci. Part A.*, **35**, 41, 1997.
- ²⁵ Simpson T.R.E., Parbhoo B., Keddie J.L., *Polymer*, **44**, 4829, 2003.
- ²⁶ Batch G.L., Macosko C.W., Kemp D.N., *Rubb. Chem. Technol.*, **64**, 218, 1991.
- ²⁷ Automotive Industry Standards, *Guidelines for Analysis of Automotive Rubbers by Fourier Transform Infrared Spectrometry (FTIR) and Thermogravimetry (TGA) Techniques.*, 2003.
- ²⁸ Oulad Hammouch S., Beinert G.J., Herz J.E., *Polymer*, **15**, 3353, 1996.
- ²⁹ Venkataraman S.K., Coyne L., Chambon F., Gottlieb M., Henning Winter H., *Polymer*, **30**, 2222, 1989.
- ³⁰ Lipp E.D., *Appl. Spectrosc.*, **40**, 1009, 1986.
- ³¹ Daum J., Erdodi G., Kennedy J.P., *J. Polym. Sci. Part A*, **44**, 4053, 2006.
- ³² Bontems S.L., Stein J., Zumburum M.A., *J. Polym. Sci. Part A*, **31**, 2697, 1993.
- ³³ Owen M.J., *Ind. Eng. Chem. Prod. Res. Dev.*, **19**, 97, 1980.
- ³⁴ Owen M.J., *Siloxane Surface Activity*, Silicone-Based Polymer Science: A Comprehensive Resource, American Chemical Society (Ed.), 1990.
- ³⁵ Tobolsky A.V., *Properties and Structure of Polymers*, Wiley & Sons (Ed.), New York, 1960.
- ³⁶ Owens D.K., Wendt R.C., *J. Appl. Polym. Sci.*, **13**, 1741, 1969.
- ³⁷ Hillborg H., Gedde U.W., *Polymer*, **10**, 1991, 1998.
- ³⁸ Chen X., Gardella J.A., *Macromolecules*, **27**, 3363, 1994.
- ³⁹ Océ AMmethode 1994-50.

Chapter 4

Development of the Tack Testing Device

"We are stuck with technology when what we really want is just stuff that works."
Douglas Adams

In this chapter the design of the tack testing device employed in this thesis is described. The main goal was to build an apparatus capable of measuring very low levels of tack on a macroscale. The chapter begins with an introduction into different adhesion testing methods, divided into destructive and non-destructive. Then a detailed description of the experimental setup and routine is given.

4.1 INTRODUCTION

To characterize the various properties of adhesives and adhesive joints, different methods of testing are needed. Because of the great variety and versatility of all sorts of adhesives, developing a universal testing method is not feasible. Till now, many different techniques were invented to deal with the characterization of surface phenomena. In general, these methods can be classified as destructive and non-destructive¹. The latter deal with the thermodynamic work of adhesion, while the former measure the practical side of adhesive joints.

4.1.1 NON-DESTRUCTIVE ADHESION MEASUREMENTS

These methods are mostly used to determine the thermodynamic work of adhesion. In this section some of the most characteristic techniques are briefly described.

4.1.1.1 CONTACT ANGLE MEASUREMENTS

One of the most common techniques to determine the surface energy of solids is the contact angle measurement. The method is depicted in Figure 4-1:

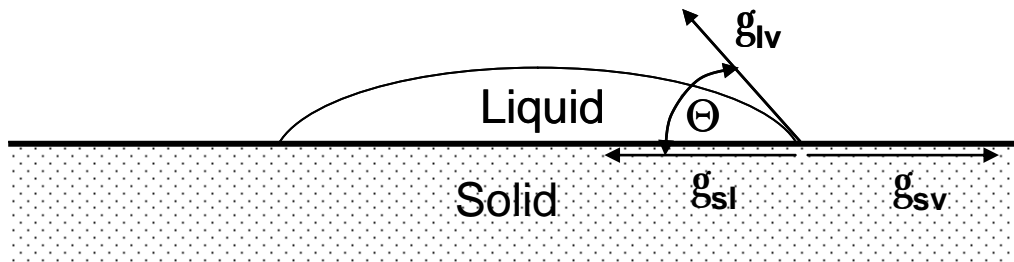


Figure 4-1. Schematic illustration of the contact angle of a liquid on solid. γ_{sl} , γ_{sv} and γ_{lv} are the solid-liquid, solid-vapor and liquid-vapor interface tensions, respectively.

For a drop of a liquid placed on a smooth, flat, rigid surface, the contact angle q is an indication of the wetting power of the liquid. If $q = 0$, the liquid wets the surface completely. This happens, when the attractive forces between the liquid molecules are smaller than the forces between the solid and liquid molecules. The attractive forces for the liquid are indicated by its surface tension. From the equilibrium of the components of surface tension and from the contact angle the following relationship can be used to estimate the surface tension of a solid:

$$g_{sv} = g_{sl} + g_{lv} \cos q \quad (4 - 1)$$

A widely used method for determining the value of surface energy of a solid is to measure the contact angle of a series of liquids of decreasing surface tension on the material of interest². The plot of $\cos q$ against g_{lv} is extrapolated to $\cos q = 1$ to find the surface tension of the solid. It should be noted, that the value generally depends on the choice of liquids.

4.1.1.2 ADHESION BETWEEN AN ELASTIC SPHERE AND A FLAT SURFACE

In 1971, Johnson, Kendall and Roberts published their theory on contact mechanics:³ paragraph 2.4.2 of this thesis. In their experimental set-up a probe of e.g. silicone rubber with a spherical shape was pressed against a flat surface of a second material: Figure 4-2.

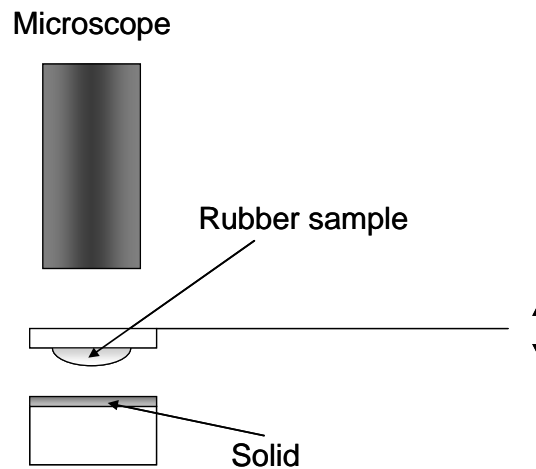


Figure 4-2. Schematic representation of a JKR experiment.

The JKR theory then predicts, that the contact area radius at equilibrium is a function of the adhesion energy G_a . When the applied load is reduced to zero, the radius r_0 of the residual contact provides a direct measure of G_a :

$$G_a = (1/6p)Kr_0^3 / R_c^2 \quad (4 - 2)$$

where K is the so-called combined elastic modulus and R_c is the radius of the sphere. The negative force P_p required to pull the probe away from the surface gives another measure of G_a :

$$G_a = (3p/2)P_p / R_c \quad (4 - 3)$$

4.1.1.3 AFM ADHESION MEASUREMENTS

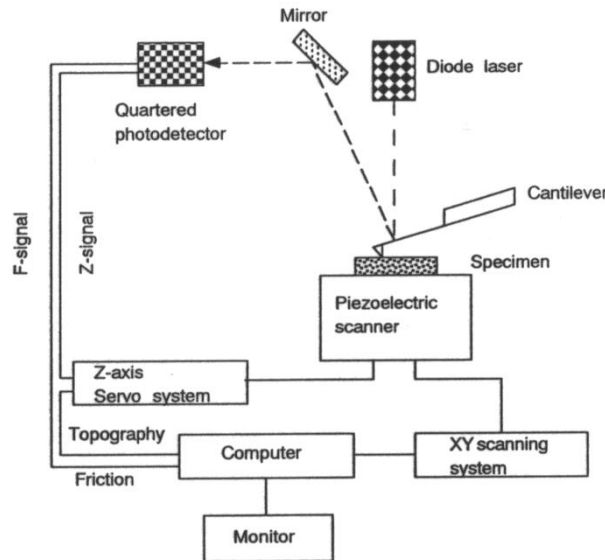


Figure 4-3. Schematic of an AFM apparatus.

Atomic Force Microscopy was primarily invented for surface imaging. A typical apparatus consists of a cantilever acting as a deflection sensor, a positioning mechanism and a cantilever-mounted tip, as depicted in Figure 4-3. AFM can operate in different modes, but for adhesion measurements the so-called force-distance curve recording is important⁴. The measured pull-off force can be related to the work of adhesion via the JKR theory, or the Derjaguin, Muller and Toporov (DMT) theory⁵. The DMT theory gives the following relationship between the pull-off force P_p and the work of adhesion W :

$$P_p = 2pRW \quad (4 - 4)$$

For proper calculations estimation of the tip radius is of crucial importance, as well as proper calibration of the signal. The latter requires knowledge of the spring constant of the cantilever. There are several methods, which provide an elegant way to measure or calculate the cantilever spring constant⁶.

4.1.2 DESTRUCTIVE ADHESION MEASUREMENTS

When these methods of adhesion testing are used, parts of a specimen undergo large deformations. Thus the values obtained are strongly affected by the viscoelastic properties of the tested materials.

4.1.2.1 WORK OF DETACHMENT

The work of detachment, W_d , is usually much larger than the thermodynamic work of adhesion W^a . Thus, detaching an adhering layer is an irreversible process and the measured values contain large contributions from dissipative processes in the bulk⁷. Andrews and Kinloch^{7,8} investigated adhesive joints of different geometry trying to evaluate the dissipation component. They assumed from the first law of thermodynamics, that the adhesive failure energy is the sum of two components: dissipative and adhesive:

$$W_d = W_{d0} + \gamma \quad (4 - 5)$$

where W_{d0} is the adhesive and γ dissipative component, respectively.

Another important aspect is the influence of the separation rate:

$$W_d = W_{d0} f(R_{sep}) \quad (4 - 6)$$

where $R_{sep} \cong \dot{c} a_T$ (\dot{c} is the crack propagation rate and a_T is a WLF shift factor). From this relationship authors tried to evaluate the dissipation factor. A similar approach was proposed by Gent and Schultz⁹. These considerations above are given to point out, that in order to understand the various destructive test methods one needs to know how the measured breaking stress depends on the test variables, as well as on the actual bond strength W_d .

4.1.2.2 PEEL TEST

The most common method of destructive testing of adhesive joints, a peel test, involves peeling away a thin elastic layer from a smooth, flat and rigid surface. The layout is illustrated in Figure 4-4.

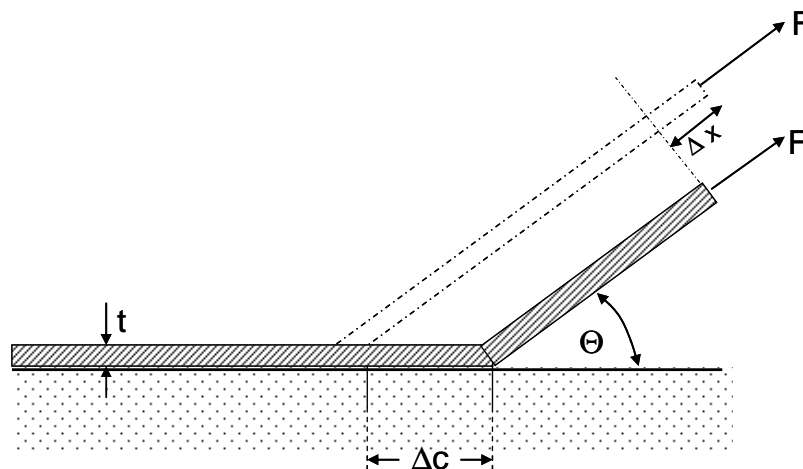


Figure 4-4. The principle of a peel test.

When the distance Dc is debonded, the point of application of the peel force F moves by distance Dx . From geometrical considerations:

$$\Delta x = (1 - \cos \Theta)\Delta c + e\Delta c \quad (4 - 7)$$

where e is the tensile strain of the sample after detachment. The work of peeling is expended, partially to cause detachment and partially to elongate the strip:

$$F\Delta x = [W_d w + U_v wh]\Delta c \quad (4 - 8)$$

where w is the width of the strip, h its thickness and U_v is the energy per unit volume spent to elongate the material after detachment. From combining (4 - 7) and (4 - 8), the work of detachment is given by the general relation:

$$W_d = (F/w)(1 + e - \cos \Theta) - U_v h \quad (4 - 9)$$

If the strip is linearly elastic:

$$e = F / whE \quad (4 - 10)$$

and

$$U_v h = (F/w)^2 / (2hE) \quad (4 - 11)$$

where E is the elasticity modulus. Equation (4 - 9) then takes form:

$$W_d = (F/w)(1 + e/2 - \cos \Theta) \quad (4 - 12)$$

When the strain is relatively small and the peel angle Q not close to zero, the following simple relation can then be obtained:

$$W_d \approx (F/w)(1 - \cos \Theta) \quad (4 - 13)$$

The special type of a peel test, where peeling is done at the angle of 0° is called a shear failure test. For linearly elastic layers, the work of detachment can be calculated from the following expression:

$$s_b^2 = 2EW_d / h \quad (4 - 14)$$

where h is the layer thickness and s_b is the tensile stress.

4.1.2.3 TEL-TAK DEVICE

The Tel-Tak device was introduced in 1969 by Beatty¹⁰. It belongs to the category of the tensile adhesion measurement devices, where thin layers of rubber are compressed between flat, rigid surfaces. The maximum tensile force required to break the bond is taken as a measurement of adhesion strength. The machine layout is shown in Figure 4-5. Beatty claimed the following criteria for the tack tester:

- simple and sturdy device;
- gives reproducible measurements;
- portable;
- able to give fast results;

The tested specimens are $\frac{1}{4}$ or $\frac{1}{2}$ inch by 2 inches strips of rubber placed in the machine at right angles to each other, and thus define the area of contact. The contact load can be varied. A timer is activated once the strips are pressed together, allowing the selection of variable contact times. A motor coupled with a gearbox provides a 2.4 mm (0.1 inch) per second separation speed. The maximum separation force is measured by the spring gauge, calibrated directly in psi (pounds per square inch). The device allows measuring rubber-rubber and rubber-steel tack.

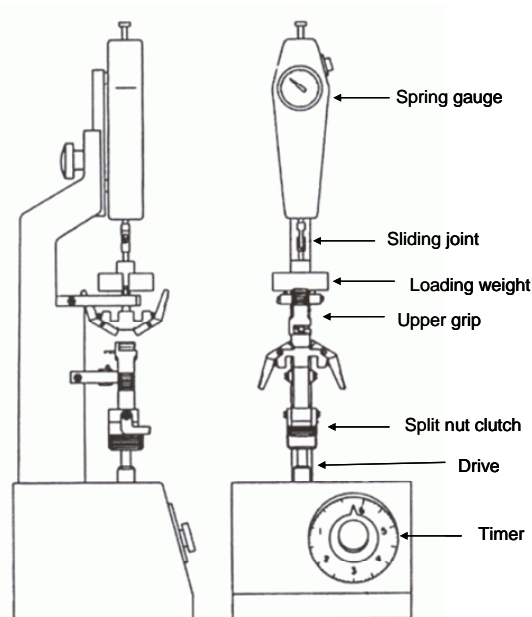


Figure 4-5. The layout of Tel-Tak device.

4.2 DESCRIPTION OF THE TACK TESTING DEVICE USED IN THE PRESENT RESEARCH

4.2.1 DESCRIPTION AND OVERVIEW

The Tel-Tak device was primarily designed to test rubber compounds for tire applications, mostly based on natural rubber, known for its tack behavior thanks to its ability to strain crystallize. Thus the usefulness of the Tel-Tak device for the

testing of the very low tack values of the non-crystallizing silicone rubbers was very limited. The spring gauge did not exhibit enough accuracy to properly register the pull-off adhesion force, and the clamping system designed for highly resilient natural rubber was unsuitable for holding samples of unfilled silicone rubber, which in general exhibits poor physical properties. Still, the general idea of an adhesion testing device developed for the purpose of this thesis, depends heavily on the Tel-Tak principle.

The scheme of the device is shown in Figure 4-6. The instrument is based on a tensile tester, Zwick Materials Testing Machine Z1.0/TH1S. The drive system of the machine allows precise control and settings of the clamps separation speed. The loadcell is capable of measuring small forces: in a range of milinewtons, which is important for experiments with silicone rubbers usually exhibiting a very low tack.

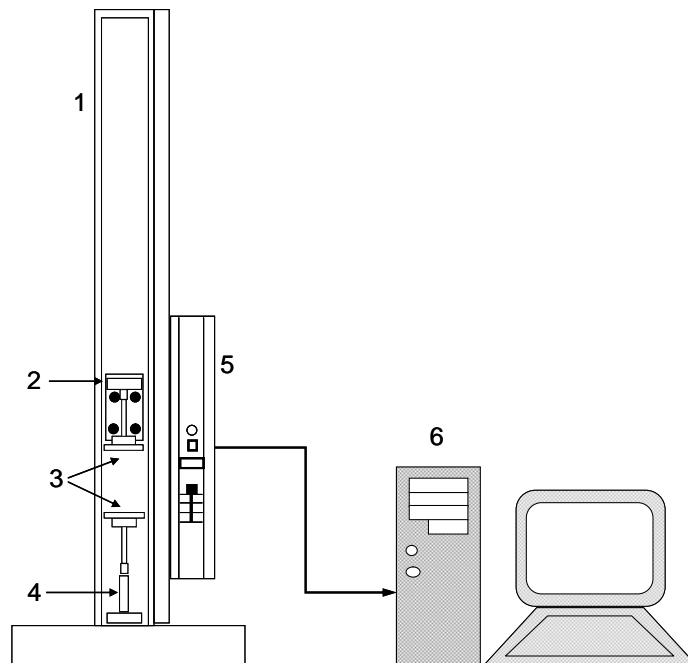


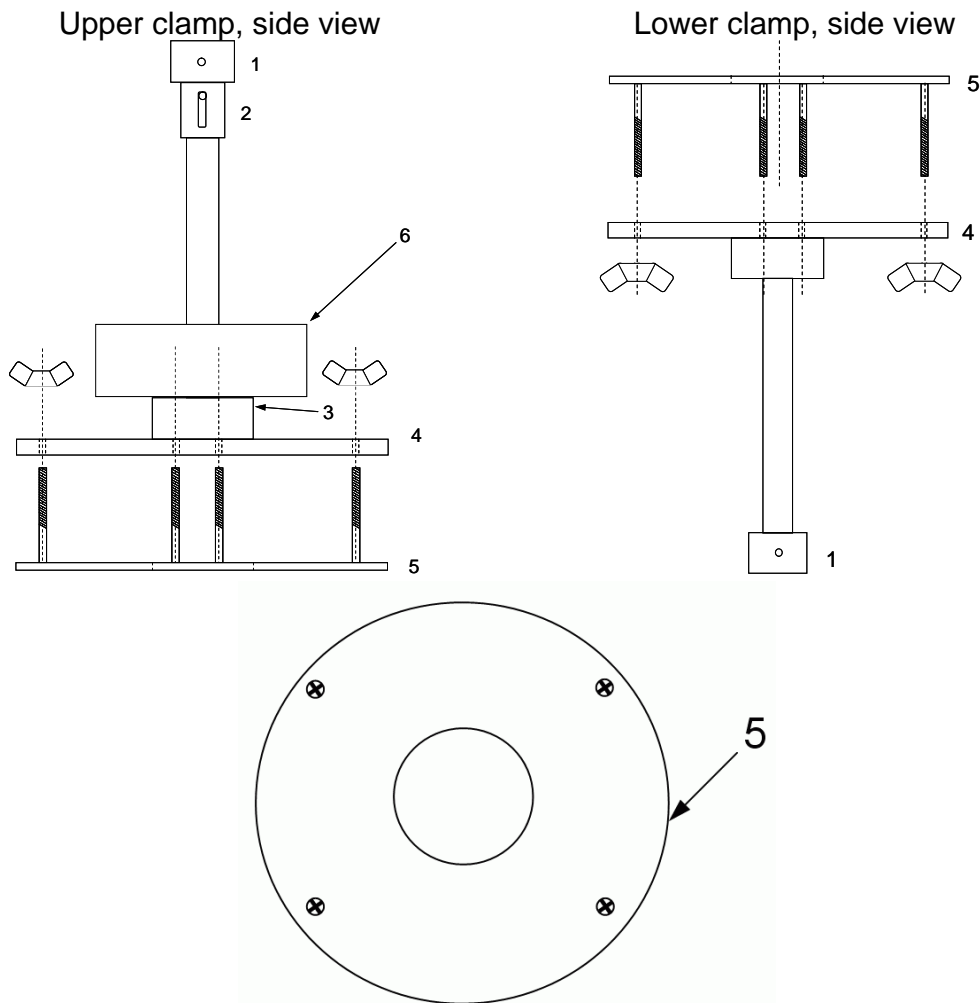
Figure 4-6. Layout of the rubber tack testing device. 1) Zwick tensile tester frame. 2) Moveable crosshead. 3) Clamps. 4) Loadcell. 5) Electronics console. 6) Computer.

In the original Tel-Tak experiment two flat samples are pressed together under a 90° angle. This allows for easy control of the contact area, but may create problems however with air entrapment during the compression stage. For this reason a completely different design of the clamps was chosen. The contact area was adjusted from flat rectangular to hemispherical, so that the contact between two hemispheres starts in the middle and proceeds towards the exterior. This minimizes the probability of air entrapment and allows for better control over the contact formation. During the separation stage of the tack experiment, this sort of experimental setup also avoids a suction effect, which can appear if the

contacting surfaces are flat. Thus the maximum separation force measured is a direct measure of rubber tack.

The scheme of the experimental setup is shown in Figure 4-7. To achieve the contact area curvature the rubber samples are pressed between steel plates (4) and an orifice disks (5), which are then firmly bolted together with butterfly screws. Part of the specimen is then forced through the opening in the orifice disk, forming the desired hemispherical shape – the portion of rubber protruding from the orifice represents the measurement area, as it is shown in Figure 4-8. To achieve a reproducible surface area, the Teflon-made separator is inserted between the two hemispheres, as seen in Figure 4-8. The separator has the same shape as the orifice disks. Thus during the compression stage, the surface area does not undergo any enlargement. This sort of setup has some limitations though: the rubber sample has to be soft or elastic enough to protrude through the opening.

Prior to the measurement the samples become under compression. The load placeholder allows placement of different weights, thus adjusting the compression force if necessary. This sort of setup also assures that the compression applied is always the same, providing better reproducibility of measurements.



Both clamps, bottom view of the orifice disk

Figure 4-7. The diagram of the tack testing device. 1) Clamp mount. 2) Freely moving joint. 3) Load placeholder. 4) Upper plate. 5) Orifice disk. 6) External changeable loading weights.

In order to ensure that during the compression no additional force is exerted on the samples, the upper clamp is equipped with a freely moving joint. During the contact formation it allows the machine crosshead to move freely to a position, where the upper clamp rests on the lower clamp and is compressed only by the weight of the applied load on the load placeholder.

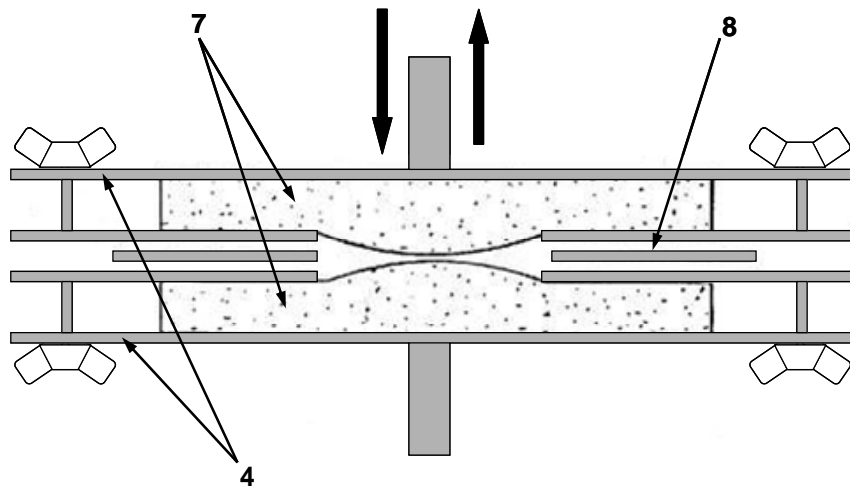


Figure 4-8. The specimens mount area. 7) Rubber sample. 8) Teflon separator. The downward arrow indicates the compression force, upward arrow indicates separation.

The signals from the force and displacement transducers: loadcell and the crosshead (see Figure 4-6), are coupled into a computer via a serial cable. For the data acquisition, treatment and machine operating, the computer uses the TestXpert 10.0 graphical user interface software supplied by Zwick GmbH. The program allows saving the whole test environment to disk, including any user comments during the testing procedure, as well as exporting the experimental results in text format, readable by all of the popular office suite programs.

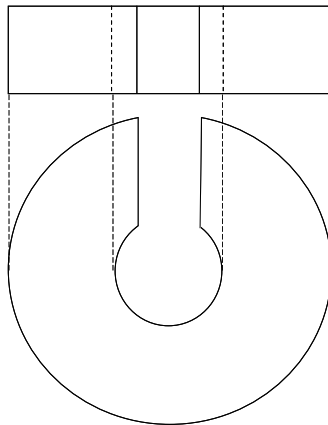


Figure 4-9. The external exchangeable load; side and top view.

4.2.2 COMPONENTS AND SPECIFICATIONS OF THE EXPERIMENTAL SETUP

In this section of the chapter the components of the tack testing device are described in technical details.

Upper clamp: The upper clamp basically consists of a 10 mm diameter steel rod with a mount (1) on one side to fix in the sample holder of a tensile tester, and a 6 mm thick plate on the other (4), with a diameter of 60 mm. The full length of the upper clamp is 92.5 mm, with 7.5 mm of extra extension available via the freely moving joint (2). The load placeholder (3), a steel ring with diameter 20 mm, allows the placement of external weights.

Lower clamp: The lower clamp has a similar construction to the upper one, with the exception that it does not have the freely moving joint and is mounted rigidly to the loadcell of the tensile tester; its length is 88.5 mm.

Orifice disk: The orifice disk (5) is a 1.5 mm thick, 60 mm diameter steel plate with a 17 mm diameter opening in the middle and four threaded bolts. The disks can be attached to the clamps using four M3 butterfly screws.

External loading weights: The weights (6) are brass cylinders with an opening allowing them to be placed on the loadholder, as shown in Figure 4-9. Two loads have been used: “Small” – 43 mm diameter, 10 mm height, 100 g weight; and “Large” – 60 mm diameter, 16 mm height and 325 g weight.

Separator: The separator (8) is a 1 mm thick 60 mm diameter Teflon[®] disk with 15 mm diameter opening in the middle, having 180 mm² net contact surface. It is used to keep the contact area from extending beyond the openings of the orifice disks. The use of Teflon[®] ensures the absence of measurable interactions between separator and sample.

Zwick tensile tester: The Zwick Z1.0/TH1S is a table-top materials testing machine with a maximum test load of 1.0 kN, equipped with 90 W DC drive system capable of achieving 0.1 – 1800 mm/min speeds. Speed control can be done with 1% accuracy. The drive system’s travel accuracy is 0.226 μm with crosshead positioning accuracy ± 20 μm.

Loadcell: The load cell converts the physical quantity force to a electrical, measurable signal. In the tensile tester the originally mounted model KAP-Z was used, with measurement range 1 – 500N (grade 1).

Computer: The computer was based on an ASUS P4 motherboard with the processor Intel Pentium™ PIV 2.4 GHz and 256 MB of RAM installed.

Software: The host computer utilizes the Microsoft Windows® 2000 Service Pack 4 operating system. The Zwick™ TestXpert 10.0 graphical user interface

was used for the acquisition and introductory processing of the experimental data. The user modified B069001.01 test method (ISO 37 standard tensile test for rubbers) was used for the experiments.

4.2.3 DATA ACQUISITION AND CALCULATION

The data acquisition was done in two stages: recording of the force-displacement curve and calculation of rubber tack. The first stage was done using the aforementioned TestXpert software with the B069001.01 test method loaded. A view of the program screen is shown in Figure 4-10.

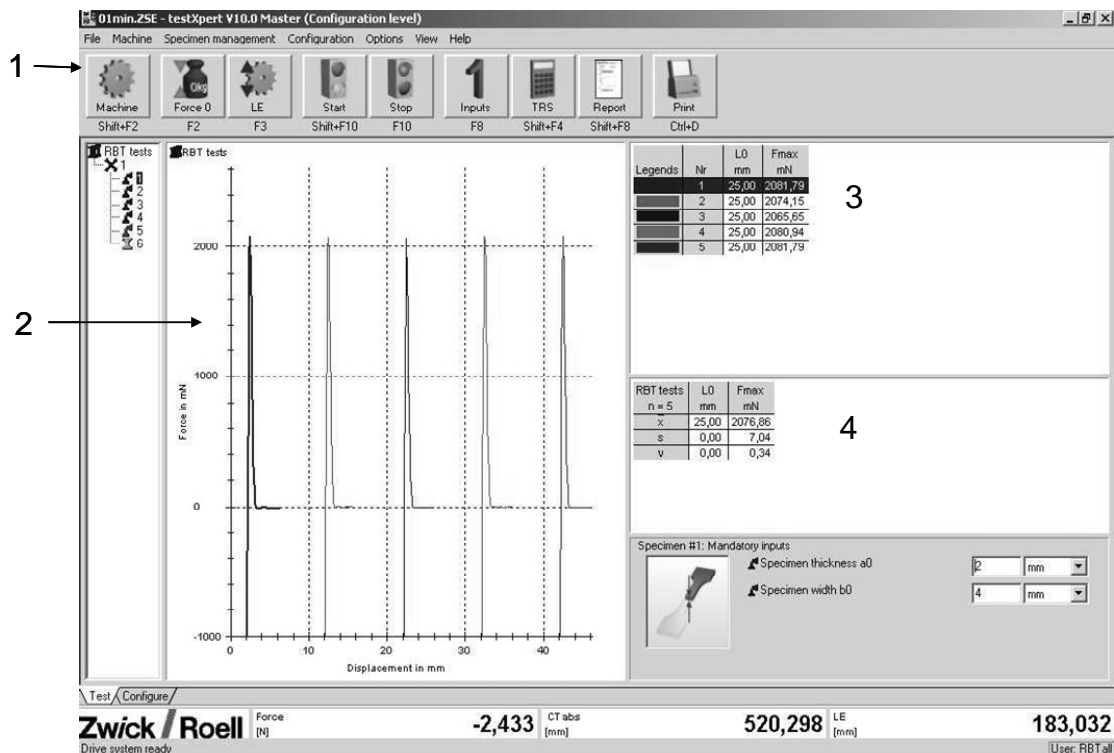


Figure 4-10. View of the TestXpert program screen. 1) Machine controls. 2) Graphical results. 3) Selected numerical results. 4) Statistics.

The most important parts are marked with the numbers 2 and 3. The graphical presentation screen (2) basically shows the recorded force-displacement curves of the tack experiment. A more detailed view of one of the curves is shown in Figure 4-11.

The sign of the loadcell signal depends on tensile vs. compression loading. On the graph the negative force means that the sample is under compression; a positive force indicates separation.

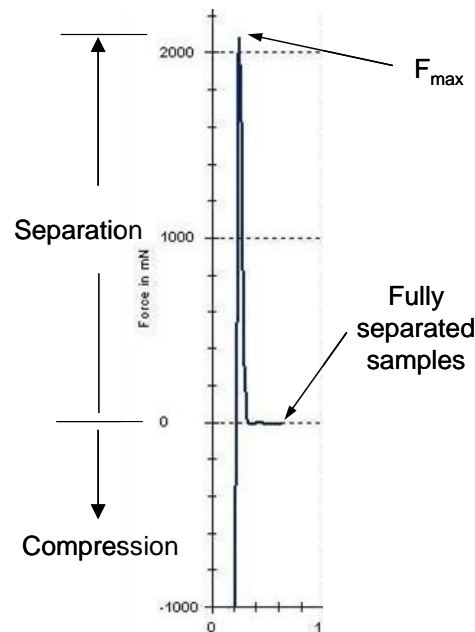


Figure 4-11. Force-displacement curve.

The force rises from negative to positive as the load on the sample is released, with beginning of separation at the value of $F = 0$. The ascending curve indicates that the two samples are still adhering to each other by the forces acting on the interface between the two rubber hemispheres. The maximum force signals the point where the two hemispheres are still in full contact. After that recorded force quickly drops to zero, when the two hemispheres progressively lose contact. The program records the maximum separation force for further calculations.

The measured values can be further interpreted in the terms of the fracture energy of tack. Gent and Hamed¹¹ propose the use of the fracture energy term, while Voyutskii¹², Wool¹³ and O'Connor¹⁴ show that the tack can be used as well. Since tack is defined as a unit of force per cross-sectional area, it simplifies the calculations. The cross-sectional area is constant during the experiment using the Teflon[®] separator, and this contact surface area of 180 mm^2 is taken for the calculations.

4.3 SAMPLE PREPARATION AND EXECUTION OF THE TACK MEASUREMENTS

The poly(dimethyl)siloxane rubber samples were prepared by mixing the vinyl-terminated poly(dimethyl)siloxane (PDMS) polymer with the silane crosslinker, a platinum cyclovinylmethylsiloxane complex: Karstedt-type catalyst, and 1-ethynylcyclohexanol used as reaction inhibitor. All of the above materials were obtained from ABCR, with the exception of the inhibitor, which was obtained from Aldrich. PDMS and crosslinker were mixed together at room temperature using a magnetic stirrer for 10 minutes, then $10 \mu\text{l}$ of inhibitor was added and subsequently $2 \mu\text{l}$ of the catalyst was added to the mixture. The hydrosilylation

reaction proceeds rapidly at room temperature, thus the order in which the components were added was important. The prepared reaction mixture was then stirred for five more minutes and subsequently degassed using an ultrasonic bath.

After mixing the degassed mixture was compression molded using a WLP 1600/5*4/3 Wickert laboratory press at 120 °C for 30 minutes. The sheet thickness was 2 mm. In order to avoid possible sample surface contamination, the cover plates of the mold were covered with thoroughly cleaned Teflon[®] foil. Molded samples were then postcured in an oven at 120 °C for 48 hours, still contained within the Teflon[®] foils.

Tack measurements: For the tack measurements square 30x30 mm strips were cut from the initial sheets. After removal of the Teflon foil measurements were performed in a manner described previously in this chapter. The load, compression time and separation speed varied according to the type of measurement. All experiments were performed under ambient conditions.

4.4 CONCLUDING REMARKS

A rubber tack testing device for low adhesion forces was constructed and successfully tested, after the principle of Tel-Tak. The setup allows accurate adhesion testing of soft rubbers and uncured rubber blends. The machine records the force-displacement curve, allowing for further data processing. The experimental setup was found to be capable of accurate measurements of tackiness of silicone rubbers, which are known to exhibit very low tack. The setup also allows a good control over a test contact area, which is a very important issue in tack testing.

¹ Packham D.E., *Handbook of Adhesion*, Longman Scientific & Technical (Ed.), Harlow, England, 1992.

² Zisman W.A., Fox H.W., *J. Colloid Sci.*, **5**, 514, 1950.

³ Johnson K. L., Kendall K., Roberts A. D., *Proc. R. Soc. Lond. A.*, 324, 301, 1971.

⁴ Carpick R.W., Salmeron M., *Chem. Rev.*, 97, 1163, 1997.

⁵ Derjaguin B.V., Muller V.M., Toporov Y.P., *J. Coll. Int. Sci.*, 53, 314, 1975.

⁶ Lévy R., Maaloum M., *Nanotechnology*, **13**, 33, 2002.

⁷ Andrews E.H., Kinloch A.J., *Proc. R. Soc. London Ser. A*, 332, 385, 1973.

⁸ Andrews E.H., Kinloch A.J., *Proc. R. Soc. London Ser. A*, **332**, 401, 1973.

⁹ Gent A.N., Schultz J., *J. Adhesion*, **3**, 281, 1972.

¹⁰ Beatty J.R., *Rubb. Chem. Technol.*, **42**, 1040, 1969.

¹¹ Gent A.N., Hamed G.R., *Elastomer Technology – Special Topics*, ACS Rubber Division, Akron Ohio, 2003.

¹² Voyutskii S.S., *Autohesion and Adhesion of High Polymers*, John Wiley & Sons (Ed.), New York, 1963.

¹³ Wool R.P. *Fundamentals of Adhesion*, L.H. Lee (Ed.), Plenum Press: New York, 1991.

¹⁴ Wool R.P., O'Connor K.M., *J. Appl. Polym. Sci.*, 52, 10, 1981.

Chapter 5

Silicone Rubber Tack in Relation to Network Structure^{*}

"The reward of a thing well done, is to have done it."
Ralph Waldo Emerson

In this chapter, the influence of telechelic silicone rubber network structure on static rubber-rubber tack is described. Telechelic polymers have crosslinking sites restricted to the ends of polymer chains only, giving well-defined networks. Rubber-rubber tack is related to the network structure, mostly to the amount of loose polymer chains not linked into the network, that can diffuse through the interface. By controlled variation of the degree of crosslinking of the telechelic silicone rubbers, various levels of tack are induced, which may be related to the network topology.

5.1 INTRODUCTION

In order to create a network, polymer molecules have to be tied together mostly by means of chemical reactions. This process, called vulcanization, differs depending on the rubber type. A three-dimensional network is created, with the junctions ordinarily formed by covalent bonds. However, in some instances physical combinations of chains in the form of crystals may serve the same purpose: conferring recoverability to the network¹.

Several theories were developed to predict the elastic or swelling properties of polymer networks. The network structure, however, is not easy to define. In the commonly used vulcanization processes primary chains are crosslinked randomly leading to the formation of network defects: pendent, "dangling" chains, loops, trapped entanglements, etc., which cannot be avoided during the reaction.

^{*} Part of the work described in this chapter has been presented at the International Rubber Conference in Lyon, July 2006, and this chapter has been submitted for publication to Journal of Adhesion.

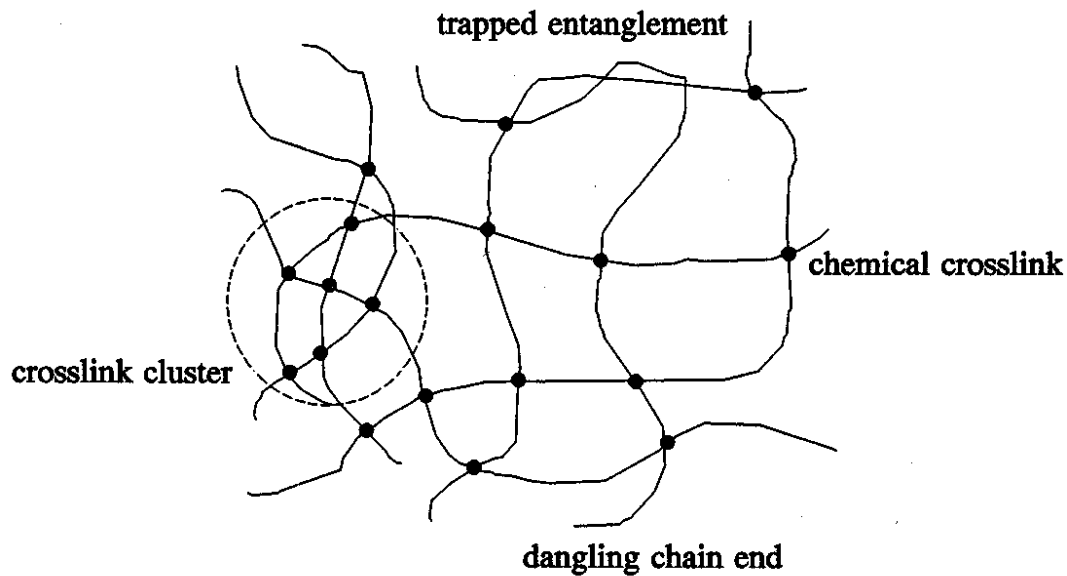


Figure 5-1. Network structure: crosslinks and network defects²

5.1.1 THE IDEAL NETWORK

For the definition of a network the concept of the ideal network of polymer chains was developed. The “ideal” network can be defined as a collection of Gaussian elastic chains connected with f -functional crosslinks³. The definition of the ideal network has some additional requirements as well:

- the chains between crosslinks must consist of statistical chain elements having the same length;
- the network should be Gaussian: every elastic chain between crosslinks has to contain enough statistical chain elements to obey Gaussian statistics;
- the network should be homogeneous, macroscopically as well as microscopically. The segment density and crosslink density should be equally distributed throughout the whole network;
- the functionality of the crosslinks should be known and constant throughout the entire network.

5.1.1.1 AFFINE NETWORK

The first theory of rubber elasticity was developed by Kuhn⁴. The structural assumption was made, that upon macroscopic deformation the dimensions of polymer chains change exactly proportional to the macroscopic deformation⁵. This assumption is called “the affine deformation”. In addition to that, Kuhn assumed that crosslinking immobilizes the junction points, which defines the macroscopic state of the network. The variation of the elastic free energy DA induced by the deformation I is expressed by the following relation:

$$\Delta A(I) = \frac{1}{2} k_B T n (I_x^2 + I_y^2 + I_z^2 - 3) \quad (5 - 1)$$

where k_B is Boltzmann's constant, v is crosslink density expressed as the number of elastically active chains per unit volume [cm^{-3}], I_x , I_y , and I_z are the deformations along the three Cartesian coordinates x , y , and z respectively, and T is the absolute temperature. The uniaxial stress, s the force per unit of undeformed cross-sectional area is given as:

$$s = k_B T n (I_x - I_x^{-2}) \quad (5 - 2)$$

With the Young's tensile E-modulus defined as:

$$E = \frac{S}{e} \quad (5 - 3)$$

with e being deformation equal to $I - 1$, and expanding the right hand term of equation (5 - 2) in series, it results in the following expression for the tensile modulus:

$$E = \frac{S}{e} = 3k_B n T \quad (5 - 4)$$

assuming a Poisson's constant of 1.5.

5.1.1.2 PHANTOM NETWORK

The phantom network model was developed by James and Guth⁶. In the phantom network polymer chains have no material properties: they may pass through each other freely and they are not subjects to the volume exclusion requirements. Under these circumstances, network junctions are free from constraints, thus they undergo displacements that are affected only by the connections to the network, not by their immediate surroundings⁷. The chains pass through each other like phantoms. The variation of an elastic free energy is expressed by the following relation:

$$\Delta A(I) = \frac{1}{2} k_B A T n (I_x^2 + I_y^2 + I_z^2 - 3) \quad (5 - 5)$$

where the front factor A is unspecified. This theory was then developed by Duiser and Staverman⁸, and further by Graessley⁹:

$$A = \frac{f - 2}{f} \quad (5 - 6)$$

where f is an average functionality of the crosslink junctions. Combination of equations (5 - 5) and (5 - 6) yields the following expression:

$$\Delta A(I) = \frac{f-2}{f} n k_B T \left(\frac{I_x^2 + I_y^2 + I_z^2 - 3}{2} \right) \quad (5-7)$$

For a trifunctional network $A = 1/3$ and for tetrafunctional $A = 1/2$. More generally, assuming no loop formation happens, the variation of elastic free energy for a macroscopic network exhibiting ν elastically effective chains and m_e elastically effective junctions is expressed as:

$$\Delta A(I) = (n - m_e) k_B T \left(\frac{I_x^2 + I_y^2 + I_z^2 - 3}{2} \right) \quad (5-8)$$

For a perfect f-functional network:

$$2n = f m_e \quad (5-9)$$

After taking into account the abovementioned contributions, Flory reconsidered his initial elasticity theory to be valid for networks of any functionality and irrespective of their structural defects. The elastic free energy variation is then most generally expressed as:

$$\Delta A(I) = x k_B T \left(\frac{I_x^2 + I_y^2 + I_z^2 - 3}{2} \right) \quad (5-10)$$

where x is the cycle rank of the network. For a perfect f-functional network with number m_e of elastically effective junctions:

$$x = (n - m_e) = n \left(1 - \frac{2}{f} \right) \quad (5-11)$$

Note that $\Delta A(I)$ of equation (5 - 10) for the phantom network for an average crosslink functionality $f=4$ is half of that of equation (5 - 1) for the affine network. Flory^{10,11} considered that a real network should be expected to exhibit a behavior intermediate between these two extreme cases, depending upon chemical composition, topological structure and structure of defects, like pendent chains.

5.1.2 MODEL NETWORKS – SYNTHESIS AND PROPERTIES

Crosslinks based on an end-linking process are very important for preparation of model networks, useful for testing the validity of different network theories. But, even if the reaction conditions are chosen very carefully, it cannot be assumed that the model networks are really fully developed. At least, they should satisfy the following requirements:

- the linear chains of a model network should have known length, and, if possible, a narrow molecular mass distribution;
- each elastic chain should be connected by its two ends to two different branching points;
- the model network should be homogeneous, the segment and crosslink density should be constant throughout the total volume;
- the functionality of branching points should be known and constant.

The preparation of a model network requires a polymer fitted at both chain ends with appropriate functional groups. Polyurethanes¹² and siloxane polymers are commonly used for this purpose, poly(dimethyl)siloxane (PDMS) being a good example. PDMS chains are chemically stable, with good resistance to chemical and thermal degradation. Due to its extremely low glass transition temperature ($T_g = -113^\circ\text{C}$) PDMS can be considered a low viscosity, highly mobile polymer at room temperature, which allows the study of its elastic behavior in absence of diluents³.

The synthesis of model PDMS networks has been the subject of many previous studies^{13,14}. In many cases, networks were prepared by crosslinking linear PDMS with γ radiation. Networks obtained in this way are statistical in nature and their structure is not well defined. Coupling end-linked chains, on the other hand, may lead to networks with well-defined topological structures. The reaction depends on the type of functional groups. For example, tetrafunctional model networks have been prepared using PDMS with -OH groups at the chain ends:

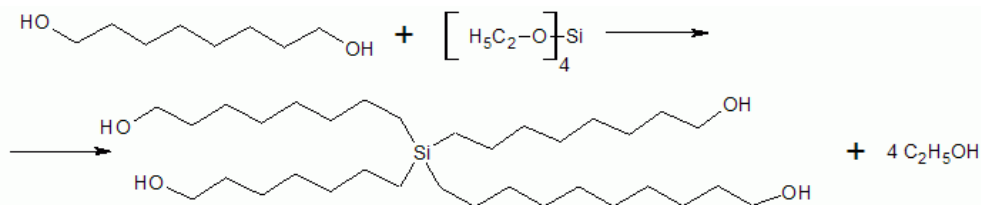


Figure 5-2. Tetrafunctional PDMS network preparation.

Networks with different functionalities can be prepared in a similar manner.

Hydrosilane functions, -SiH, are known to readily react with vinyl and allyl double bonds in the presence of catalysts such as Karstedt's catalyst: a 2% platinum divinyltetramethyl-disiloxane complex in xylene. The substrates can be PDMS fitted at the chain ends with vinyl groups, or with silane groups. The former requires the use of a multifunctional silane as crosslinker, while the latter requires compounds with multiple vinyl or allyl bonds, like tetraallyloxyethane, which is shown in Figure 5-3.

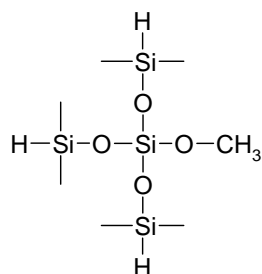
Table 5.1. Materials characterization: polymers.

Material	Viscosity [Pa·s]	M _w [g/mole]	Average vinyl group content [mmole/kg]	Supplier
MQ 6	100	6 000	~400 ^{*)}	ABCR
MQ 9	200	9 400	~230 ^{*)}	ABCR
MQ 17	500	17 000	166	ABCR
MQ 28	1000	28 000	98	ABCR
MQ 50	5000	50 000	64	ABCR

^{*)} the VGC varies depending on the batch of polymer used.

The structures of the tri, and tetrafunctional silanes used as crosslinkers are shown in Figure 5-4. A multifunctional silane was also employed, provided by a proprietary source, of which the structure was not disclosed. The platinum-cyclovinyldimethylsiloxane complex was used as cure reaction catalyst. All the above materials were obtained from ABCR, Germany, with the exception of the multifunctional silane. 1-ethynylcyclohexanol (99%) was used as a temporary reaction inhibitor, as obtained from Aldrich. The solvents used were all of pro analysi quality.

a)



b)

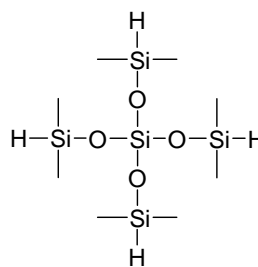


Figure 5-4. Chemical structures of a) tri and b) tetrafunctional silane crosslinkers.

Sample preparations: For every batch of polymer the exact amount of vinyl groups was determined using NMR measurements (Varian 300 MHz apparatus) with pyrazine as an internal standard, as described in Chapter 3 of this thesis. The results of these measurements are included in Table 5.1. From those results and the molecular structure of the crosslinker, the hydrogen-to-vinyl ratio (H/V) was calculated.

The samples were prepared using H/V ratios of 1.0, 1.2, 1.4 and 1.7, which means starting with the stoichiometric amount, up to 1.7 times excess of crosslinker. The curatives were mixed together with the polymer using a magnetic stirrer. During the preparation it was important, that the inhibitor was added to the reaction mixture before the catalyst. Without the presence of the

inhibitor, the cure reaction proceeds quickly even at room temperature. While the amount of crosslinker varied depending on the VGC of the polymer used, the amounts of catalyst and inhibitor were kept constant: 10 and 50 ppm respectively. The mixture was degassed and cured in a compression molding machine (WLP 1600/5x4/3 Wickert laboratory press) at 120°C for 30 min. Clean Teflon foil was placed between the cured mixture and the mold plates to avoid surface contamination and sticking of the material to the mold. The resulting 90x90x2 mm sheets were post-cured in an oven at 120°C for 48 hours.

Tack measurements: Samples were compressed under a load of 2.5 N for 10 minutes. For each sample, several tack measurements were done and the average was taken as the final result. The measurements were always performed at room temperature. The separation speed was constant at 4 mm/sec.

Crosslink density: Crosslink density measurements were made by swelling the rubber samples in toluene for 48 hours; calculations were performed using the well-known Flory-Rehner equation¹⁵:

$$n = \frac{cv_r^2 + \ln(1 - v_r) + v_r}{V_0(0.5v_r - v_r^{1/3})} \text{ [mol/cm}^3\text{]} \quad (5 - 12)$$

where v is the crosslink density, v_r is the equilibrium volume fraction of rubber in the swollen state and V_0 is the molar volume of the solvent. A polymer-solvent interaction parameter χ of 0.456³ was used for all calculations.

Sol-gel analysis: Sol-gel analysis was performed by extracting the samples in toluene for 2 weeks. The samples were then dried till no further mass loss was observed, and then the total weight loss was calculated.

5.3 RESULTS

5.3.1 TRIFUNCTIONAL CROSSLINKER

Figure 5-5 shows the rubber-rubber tack and crosslink density dependence on hydrogen-to-vinyl (H/V) ratio for PDMS with different molecular weights crosslinked with the trifunctional silane. Note the different scales used for the various PDMS in order to accentuate the large differences in measured tack and – to a lesser extent – in crosslink densities between the PDMS with varying molecular weights.

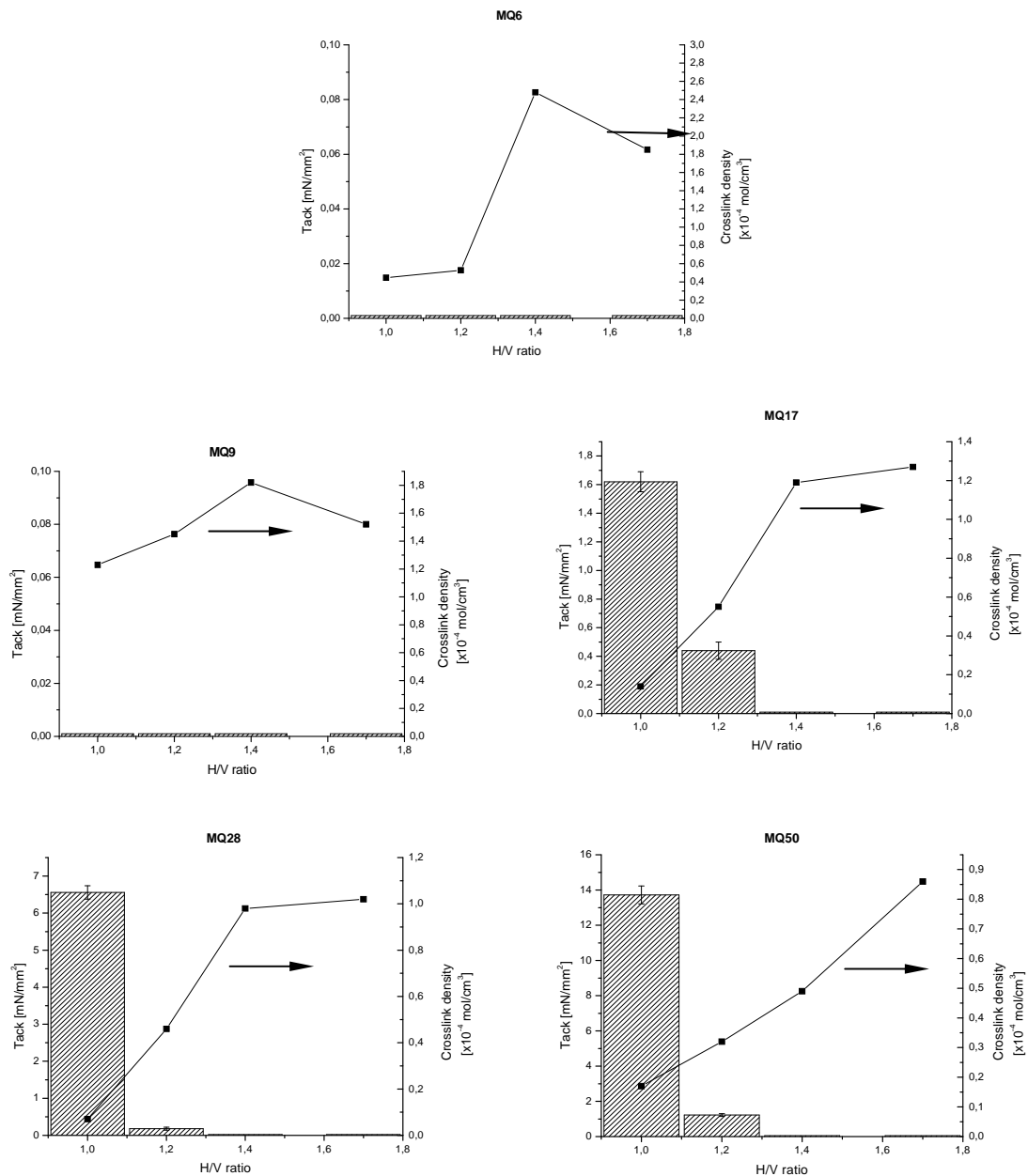


Figure 5-5. Tack and crosslink density of different molecular weight PDMS as a function of H/V ratio. Trifunctional crosslinker.

The trend observed in crosslink density is interesting. In all cases, the crosslink density increases at first with increasing amount of silane crosslinker. For the stoichiometric amounts of crosslinker: H/V = 1.0, the samples are still clearly undercrosslinked. The crosslink density of MQ 6 rises strongly with increasing H/V ratio between 1.2 and 1.4, reaching a maximum at H/V = 1.4. Then the crosslink density starts to decrease again. A similar trend is observed for MQ 9.

The maximum is positioned at the $H/V = 1.4$ as well, but the crosslink density increase at lower H/V ratios is much smaller: the starting crosslink density at $H/V = 1.0$ is already quite high, though the overall maximal crosslink density is lower than is the case for MQ 6.

For both lowest molecular weight PDMS, MQ 6 and MQ 9, no detectable tack can be measured, no matter the crosslink density obtained.

The samples of MQ 17 crosslinked with $H/V = 1.0$ and 1.2 exhibit detectable values of rubber-rubber tack. Tack decreases with increasing crosslink density, finally falling below the detection level of the apparatus at $H/V = 1.4$. The absolute tack values are quite low, in the range of 1.6 mN/mm^2 for the lowest crosslinked sample. A small increase in crosslink density already causes the tack to drop about four fold to 0.4 mN/mm^2 . The crosslink density trend is somewhat similar to the lowest molecular weight polymer, but the crosslink density increases more linearly with increasing silane excess. It can be seen, that at $H/V = 1.7$ the maximum in crosslink density has not been reached yet. The crosslink density is also much lower than that of MQ 9 and 6.

With molecular weight close to 30 000, MQ 28 starts to exhibit a substantial amount of tack at low crosslinking levels, much larger than the tack of MQ 17 at H/V ratio 1.0. The tackiness levels down much quicker though, with almost a tenfold decrease with change from $H/V = 1.0$ to 1.2 . At higher crosslink densities rubber-rubber tack again becomes undetectable. The crosslink density trend is very similar to MQ 17: a linear increase at the start followed by the beginning of a maximum. The crosslink maximum or "saturation" point obviously has not been reached in the investigated H/V range.

The highest molecular weight polymer tested, MQ 50 exhibits the highest tack, approximately twice as high as MQ 28. Just like in the case of MQ 28, the rubber-rubber tack levels down very fast with increase in crosslink density, becoming one order of magnitude lower at $H/V = 1.2$. Higher crosslinked MQ 50 samples do not exhibit any detectable tack again, similar to the other tested PDMS samples. The crosslink density trend of MQ 50 is strictly linear: crosslink density rises proportionally to the increase in silane excess. The plateau visible for lower molecular weight PDMS does not appear in the range tested.

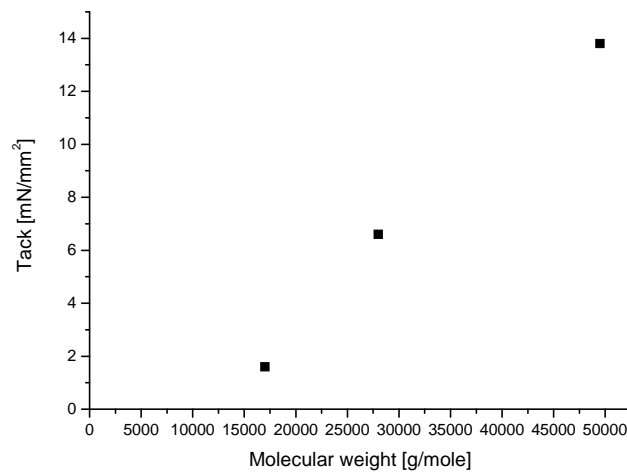


Figure 5-6. The tack – molecular weight relation for $H/V = 1.0$, trifunctional crosslinker.

Figure 5-6 shows the influence of the molecular weight of the prepolymer on rubber-rubber tack for samples crosslinked with the $H/V = 1.0$, with a trifunctional crosslinker. Tack rises substantially and more or less linearly with increase in molecular weight of the prepolymer.

5.3.2 TETRAFUNCTIONAL CROSSLINKER

Figure 5-7 shows the rubber-rubber tack and crosslink density dependence on hydrogen-to-vinyl (H/V) ratio for different molecular weight PDMS, crosslinked with the tetrafunctional silane. Note the same scale used for the tack values of the various PDMS, but different scales for the crosslink densities.

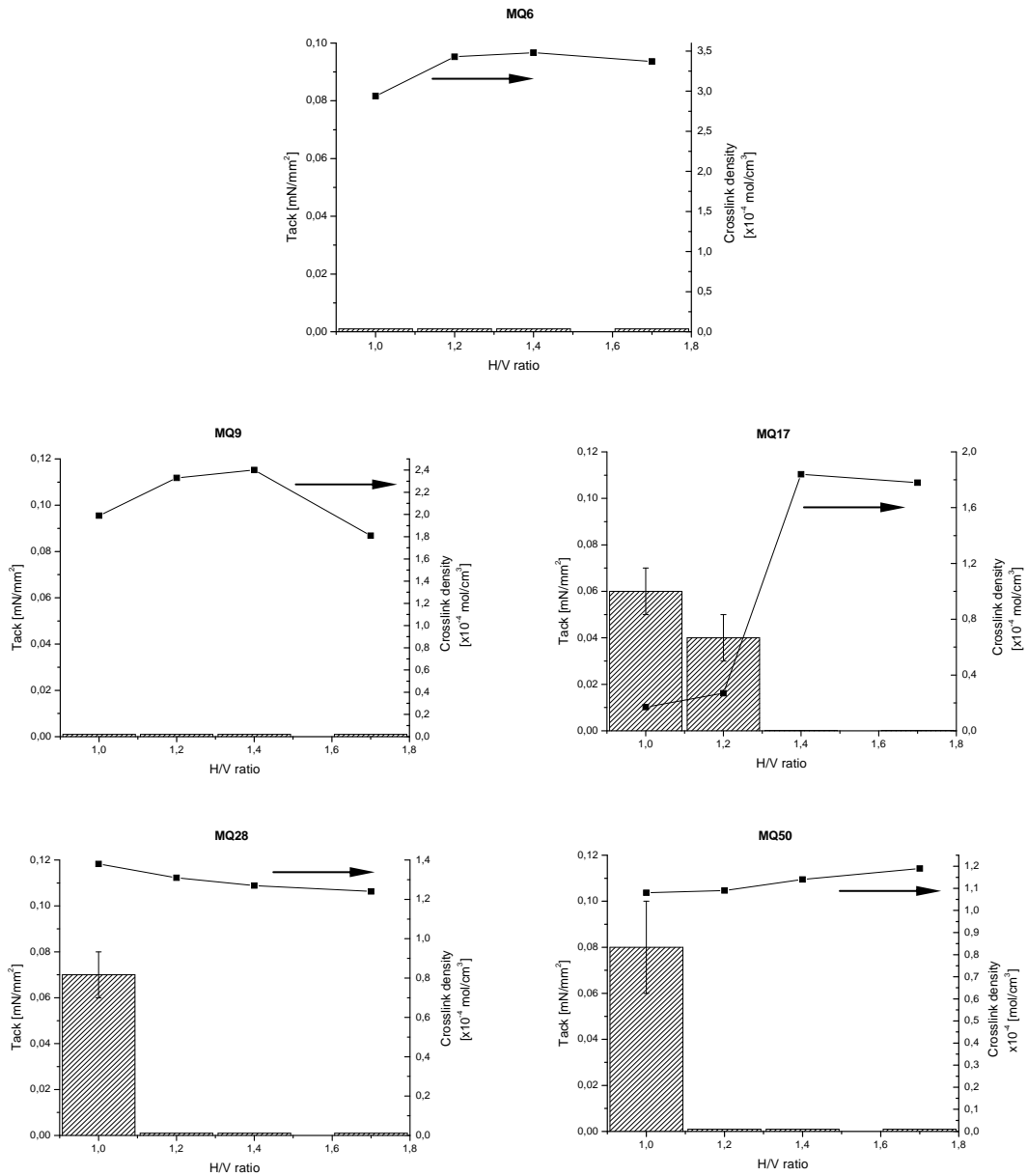


Figure 5-7. Tack and crosslink density of different molecular weight PDMS as a function of H/V ratio. Tetrafunctional crosslinker.

It can be seen, that for the tetrafunctional crosslinker the trend in tackiness change is similar to the trifunctional crosslinker. However, the overall values of recorded tack are significantly lower than those seen in Figure 5-5. MQ 6 and 9 lack any detectable rubber-rubber tack. Tetrafunctional-crosslinked MQ 17 shows very low tackiness, almost two orders of magnitude lower than MQ 17 crosslinked with the trifunctional silane. The difference is even more pronounced with increased molecular weight: almost three orders of magnitude lower in the case of MQ 50. In addition, MQ 28 and 50 do not exhibit any tack at H/V = 1.2 anymore.

The crosslink densities follow a slightly different trend as well; the absolute values are in general higher than those of the trifunctional-crosslinked samples at the same H/V ratios. MQ 6 exhibits only a slight increase between H/V ratios 1.0 and 1.2, and then at higher ratios the crosslink density stays more or less constant. MQ 9 shows a maximum at H/V = 1.4, while at H/V = 1.7 the crosslink density drops below the level of H/V = 1.0. The MQ 17 behavior differs from the lower molecular weight polymers: there is a large increase between H/V ratios 1.2 and 1.4, after which the crosslink density reaches a plateau. MQ 28 and 50 exhibit mutually similar behavior: the crosslink densities are almost constant, with a slight decreasing trend for MQ 28 and slight increase for MQ 50 with increasing H/V ratio. The values of crosslink density of MQ 28 are higher than the values for MQ 50.

5.3.3 MULTIFUNCTIONAL CROSSLINKER

Figure 5-8 shows the rubber-rubber tack and crosslink density dependence on H/V ratio for MQ 17 and 50, crosslinked with the multifunctional silane.

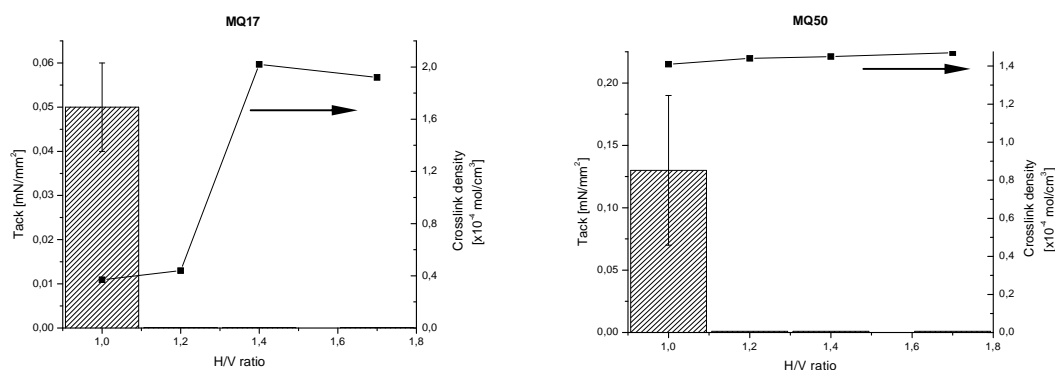


Figure 5-8. Tack and crosslink density of MQ 17 and 50 as a function of H/V ratio. Multifunctional crosslinker.

It can be seen, that the increase in crosslinker functionality above four does not cause significant changes anymore. MQ 17 and 50 show very similar behavior as

in the case of the tetrafunctional crosslinker, only MQ 17 loses tackiness quicker: there is no detectable tack left at $H/V = 1.2$.

The changes in rubber-rubber tack caused by the crosslinker functionality are further illustrated in Figure 5-9:

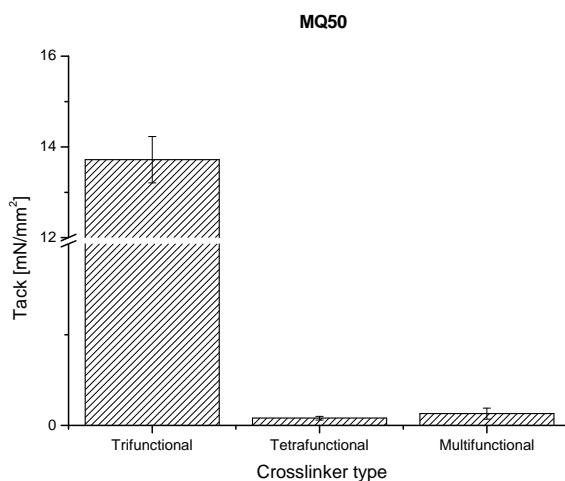


Figure 5-9. The effects of crosslinker functionality on rubber-rubber tack of MQ 50, H/V ratio 1.0.

The data have been taken for MQ 50 and $H/V = 1.0$. Using the trifunctional crosslinker gives samples high tackiness, which levels down drastically after increase of crosslinker functionality by one. Further increase in functionality does not cause significant changes anymore. The effect is basically the same for MQ 17 and 28, although the tack decrease is not as pronounced.

5.3.4 SOL-GEL ANALYSIS

Figure 5-10 shows the sol fractions of the crosslinked PDMS samples as a function of H/V ratio for both trifunctional and tetrafunctional crosslinker. In all cases the tetrafunctional crosslinker gives slightly, till significantly lower sol fractions than the trifunctional one, indicating the better crosslinking ability of the tetrafunctional crosslinker.

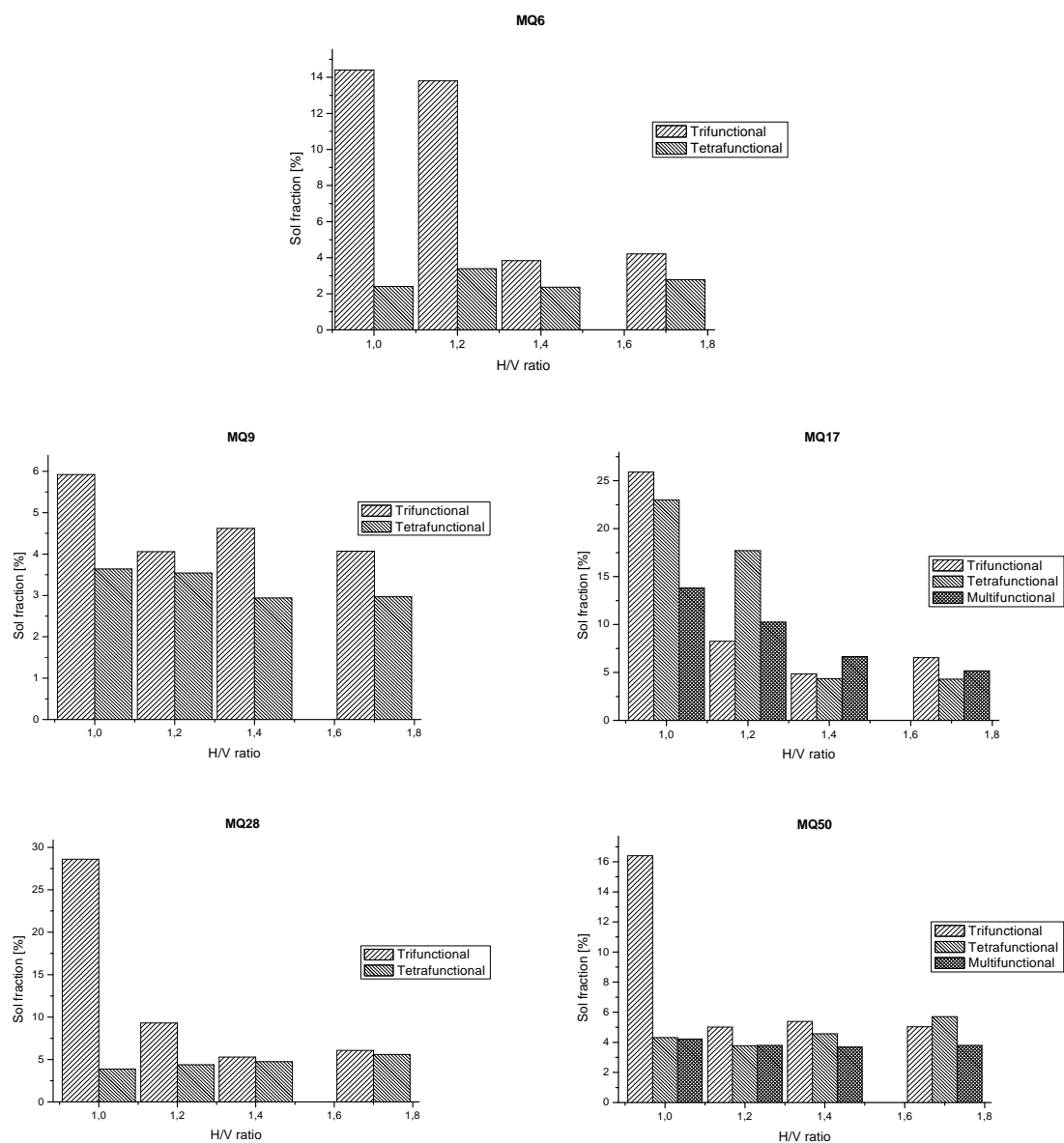


Figure 5-10. The sol fractions as a function of H/V ratio.

The amounts of sol fraction in crosslinked samples correspond well with the trends in crosslink density. MQ 6 samples crosslinked with the trifunctional crosslinker exhibit high amounts of extractable fractions for H/V = 1.0 and 1.2, whereas the amounts drop significantly with higher H/V ratios. For the tetrafunctional crosslinker, the sol fraction stays more or less the same for every MQ 6 sample. MQ 9 exhibits a different behavior. The amounts of sol fraction are smaller than in any other samples, and the sample with H/V = 1.4 and trifunctional crosslinker shows a little high extractable fraction. The tetrafunctionally crosslinked samples show a trend corresponding to that of

crosslink density. A similar situation can be seen in the case of MQ 17: the extractable fractions follow the crosslink density trend closely. The amounts of extractable fraction are in general higher than the amounts of low molecular weight polymers, especially for $H/V = 1.0$.

The high molecular weight PDMS, MQ 28 and 50, perform in a similar manner. Samples crosslinked with the trifunctional crosslinker and $H/V = 1.0$ have very high sol fraction, which levels down quickly with increase in crosslink density. Interestingly, the MQ 50 samples have a lower extractable fraction than the MQ 28 samples crosslinked at the same H/V ratio with trifunctional crosslinker. The changes disappear when crosslinker functionality is increased.

5.4 DISCUSSION

5.4.1 THE NETWORK STRUCTURE AND CROSSLINK DENSITY

The crosslink density – H/V ratio relationships show different trends, depending mostly on the molecular weight of the prepolymer and on the crosslinker type. First, with the densities of all PDMS samples being the same, the maximum attainable crosslink density for MQ 6 would have been eight times higher than for MQ 50, as determined by the ratio of their molecular weights. A correction needs to be made for the fact, that for MQ 6 eight times more crosslinker needs to be added relative to MQ 50 to correspond to the same H/V ratio. However, this correction does not account for the fact, that for MQ 6 in either case of the tri- and tetrafunctional crosslinker only approximately three times higher maximum crosslink density is found. It is an indication of problems involved in obtaining a perfect telechelic network, particularly with the lower molecular weight PDMS.

Trifunctional crosslinker added in stoichiometric amounts: $H/V = 1.0$, to the telechelic PDMS results in low levels of crosslinking. The amount of crosslinker molecules per unit volume is too low, for the polymer chain ends to find and attach themselves to the three-fold possible junctions, once the system solidifies. Increasing the crosslinker amount results in a higher probability of reaction happening, thus the increase in crosslink density. However this goes at the cost of crosslink junction functionality: from three to a lower value. Once the crosslinker excess reaches some threshold value, the crosslink density approaches a maximum, see Figure 5-5, and then starts to decrease again. There are most likely only two chain ends left to react with one silane crosslinker molecule in spite of its 3-functionality. But if only two chain ends of a prepolymer react with the crosslinker, then nothing else happens than a chain extension and no network formation. So somewhere along the H/V ratio range an optimum exists, where the best possible network is obtained. However, unfortunately, not a perfect telechelic network. The more so, the lower the molecular weight of the prepolymer, because there are more crosslink sites competing with each other for crosslinkable chain ends. Therefore the position of the maximum is dependent on the molecular weight of the prepolymer: where the maximum is reached at silane

excess 1.4 for MQ 6 and MQ 9, MQ 17 and MQ 28 approach their plateau at 1.7. For the high molecular weight MQ 50 the “oversaturation” level is not reached within the measured range. The mobility of the long prepolymer chains and the availability of crosslink sites are too low, that even 1.7 times excess of crosslinker still causes a further increase in crosslink density. Interestingly, MQ 50 shows a slightly higher crosslink density at $H/V = 1.0$ than MQ 17. This is most likely the influence of the measurement method used. During determination of crosslink density by equilibrium swelling also chain entanglements are taken into account. MQ 50 with its long chains forms a loosely crosslinked network with a small amount of chemical, but lots of physical crosslinks, like the entanglements.

Increase in crosslinker functionality from three to four does not create large behavioral changes in the case of the low molecular weight polymers, except that the crosslink density is in general higher as explained before. MQ 6 and MQ 9 show maxima in crosslink density vs. H/V ratio, but shifted to somewhat lower H/V ratio relative to the trifunctional crosslinker. Obviously, because of the increase in available crosslink sites per crosslinker molecule: the chance of simple chain extension by mere 2-fold attachment is much lower. The high molecular weight polymers, MQ 28 and MQ 50 behave in a most conspicuously different manner than when crosslinked with the trifunctional silane. Both of the polymers show a saturation effect, crosslink density is high and an increase in crosslinker excess causes only relatively small changes. This seems a little contradictory behavior, if we consider that the concentration of tetrafunctional silane molecules in the reaction mixture is actually smaller for the same H/V ratio, than for the trifunctional ones. However, it confirms, that the tetrafunctional crosslinker is much more effective compared to the trifunctional one by its reduced chance of chain extension. The actual maximum in crosslink density for MQ 28 and MQ 50 for the tetrafunctional crosslinker is therefore reached at H/V ratios close to 1.0. At higher H/V ratios a decrease of crosslink density should happen again (theoretically), however, the effect is so little that either a small increase or a small decrease may be found, depending on experimental fluctuations. Samples crosslinked with tetrafunctional silane have a much lower extractable fraction than samples crosslinked with the trifunctional one, which supports this conclusion.

MQ 17 behaves a little bit different, in particular in the case of the tetrafunctional crosslinker. We tend to relate this to either a somewhat less well defined molecular structure of the MQ 17 prepolymer (not extensively investigated) or experimental fluctuations in preparing the compounds for the curing process.

The little difference in behavior after further increase in functionality of the crosslinker to the polyfunctional one is now an obvious matter. There are problems with reacting all, or even most of the silane groups on the crosslinker, in addition to troubles with getting a relatively large number of polymer chain ends all into a small space next to the crosslinker molecule¹⁶. However, the large surplus of crosslinking sites on the crosslinker makes sure, that practically all

crosslinks have a functionality of at least three, and so contribute to network formation and not to chain extension.

5.4.2. TACK

There is a clear trend visible: the rubber-rubber tack decreases sharply with increase in crosslink density for most of the combinations investigated. This phenomenon has been observed for many types of polymers^{17,18}: although crosslinking of a polymer melt may initially increase tack, further increase in crosslink density causes the opposite effect. Lower crosslink density results in larger amounts of unattached chains, pendant network chains, as well as in a less constrained network. All these phenomena are known to promote tack by partial migration of polymer entities across the contact interface. Naturally, during the contact polymers may also exchange other interactions, like van der Waals forces or hydrogen bonding. However, it was already proven by others, that for PDMS-PDMS contact the forces are dispersive: van der Waals in nature, due to the presence of numerous methyl groups on the interface¹⁹. The contribution from these is negligible, thus the tack increase for low crosslink densities is mainly due to the presence of pendant chains and increased chain mobility. In the telechelic networks, crosslink sites are situated at the ends of the polymer chains, thus free chains and pendant (dangling) chains are the most common defects²⁰. Taking this into consideration, the mechanism of tack formation can be explained on basis of the de Gennes reptation model²¹. Crosslinking creates topological constraints – a crosslinked polymer network can be considered as fixed obstacles, limiting the movement of chains. Second, increasing the amount of crosslinker increases the probability, that the chain will get attached to more than one crosslinking site, thus being effectively trapped and unable to cross the interface. This explains the fast tack-decrease with increase in the H/V ratio, particularly for the tetrafunctional crosslinkers, where much lower chance of chain extension exists, which otherwise still would have allowed reptation and crossing the interface.

The samples of MQ 6 and 9 in Figure 5-5 and 5-7 exhibit no detectable tack at all. It could be expected, that very low molecular weight polymer would create many more pendant and unattached chains per unit of volume than higher molecular weight species. A different mechanism comes into play, though. In order to create a strong enough interface to result in measurable tack, polymer chains do not only have to cross the interface, but also entangle on the other side. Thus the molecular weight (and length) of the pendant and loose chain should be at least equal to the critical molecular weight needed to form entanglements. The borderline for PDMS seems to be a molecular weight of around sixteen thousands^{22,23}; MQ 6 and 9 are thus physically unable to form entanglements, which severely limits the possibility of creating interface strength. MQ 17 is just a borderline, which may explain its somewhat erratic behavior.

The increase in molecular weight of the polymer results in large increase in a tack values for the samples crosslinked with the trifunctional silane: Figure 5-5. Again, the balance between the decreasing amount of possible bonds and consequent pendant and loose chains, because of increase in molecular weight, and increased ability of the chains to penetrate the interface and entangle should be taken into account. Also, during separation the chains are extended before full release. The extensions and disentanglements cost more energy for the longer, higher molecular weight chains²⁴, also resulting in more energy dissipation.

5.5 CONCLUDING REMARKS

For telechelic PDMS the trends in crosslink density are strongly affected by the molecular weight of the prepolymer and by the crosslinker functionality. High molecular weight prepolymers react strongly on changes in crosslinker functionality, whereas low molecular weight species only increase the overall crosslink density. On the other hand, low molecular weight PDMS strongly react to crosslinker excess, showing saturation effects on the crosslink density.

The network structure of telechelic polymer has a very substantial influence on rubber-rubber tack. The pendent and left-over loose chains created during the crosslinking reaction must be able to reptate through the interface and entangle on the other side to contribute to the overall strength. For the very low molecular weight rubbers, MQ 6 and MQ 9, where no tack is detected due to their inability to entangle at the other side of the interface: their molecular weight is substantially lower than the critical molecular weight between entanglements. When the possibility of entanglement increases, rubber-rubber tack increases significantly. Using crosslinkers with higher functionality and hence better ability to bind polymer chains leads to a large decrease in tack, as visible especially for the high molecular weight silicone rubber, MQ 50.

¹ Mark H.F., Bikales N.M., Overberger C.G., Menges G., *Encyclopedia of Polymer Science and Engineering* John Wiley & Sons (Ed.), New York, 1987.

² van Bevervoorde E.E., *PhD Thesis*, University of Twente, 1998.

³ Hild G., *Prog Polym Sci.*, **23**, 1019, 1998.

⁴ Kuhn W., *Koll. Zeitschrift*, **76**, 258, 1936.

⁵ Kuhn W., *J. Polym.Sci.*, **1**, 380, 1949.

⁶ James H.M., Guth E., *J. Polym. Sci.*, **4**, 15, 1949.

⁷ Flory P.J., *Proc. R. Soc. London Ser. A.*, **351**, 351, 1976.

⁸ Duiser J.A., Staverman A.J., *Physics of Non Crystalline Solids*, J. A. Prins. North Holland Publishing Co. (Ed.), Amsterdam, 1965.

⁹ Graessley W.W., *Macromolecules*, **8**, 186, 1975.

¹⁰ Flory P.J., *J. Chem. Phys.*, **66**, 5720, 1977.

¹¹ Flory P.J., *Proc. R. Soc. London, Ser. A*, **351**, 1666, 1976.

¹² Dušek K., *Rubb, Chem Technol.*, **55**, 1, 1982.

¹³ Chen R.Y.S., Yu C.U., Mark J.E., *Macromolecules*, **6**, 746, 1974.

- ¹⁴ Johnson R.M., Mark J.E., *Macromolecules*, **5**, 41, 1972.
- ¹⁵ P.J. Flory, J. Rehner, *J. Chem. Phys.*, 521, **11**, 1943.
- ¹⁶ Sharaf M.A., Mark J.E., *J. Polym. Sci.*, **33**, 1151, 1995.
- ¹⁷ Gent A.M., Kim E.-G., Ye P., *J. Polym. Sci. B: Polym. Phys.*, **35**, 615, 1997.
- ¹⁸ Wootthikanokkhan J., Burford R.P., Chaplin R.P., *J. Appl. Polym. Sci.*, **67**, 1277, 1998.
- ¹⁹ Galliano A., Bistac S., Schultz J., *J. Coll. Interface Sci.*, **265**, 372, 2003.
- ²⁰ Roth L.E., Vega D.A., Vallés E.M., Villar M.A., *Polymer*, **45**, 5923, 2004.
- ²¹ de Gennes P.G., *J. Chem. Phys.*, **55**, 572, 1971.
- ²² Dollase T., Wilhelm M., Spiess H.W., Yagen Y., Yerushalmi-Rozen R., Gottlieb M., *Interface Sci.*, **11**, 199, 2003.
- ²³ Orrah D. J., Semlyen J. A., *Polymer*, **29**, 1452, 1988.
- ²⁴ Hillborg H., Gedde U. W., *Polymer*, **39**, 1991, 1998.

Chapter 6

The Time-dependent Autohesion for Symmetric Rubber-Rubber Contacts of Silicone Rubber*

“The order, the symmetry, the harmony enchant us...”
Gottfried Leibniz

In this chapter, the time-dependent autohesive behavior of crosslinked poly(dimethyl)siloxane is described. Loosely crosslinked, telechelic siloxane rubber networks give some interesting options to test the applicability of the Wool/DeGennes model for the crosslinked silicone elastomers. In this chapter the interface healing, as well as the separation rate behavior of symmetric rubber-rubber contacts will be shown.

6.1 INTRODUCTION

The problem of time dependence of polymer autohesion attracted lots of attention for many years. It addresses the strength of materials, which is connected to many practical engineering problems, such as polymer fusion and welding, rubber tack, etc. Research in this field brings fundamental insights into the physical processes of adhesive bond formation. Controversies, however, still exist when it comes to determining the controlling physical process. It is believed, that there are two basic mechanisms responsible for the time dependence of polymer autohesion^{1,2}: contact area formation through viscous flow; and the bond formation via chain penetration and entanglements across the interface.

As was mentioned in more detail in Chapter 2, Voyutskii appears to be the earliest person to work on this problem. He investigated the contact formation of the rubber-rubber interface and its influence on the joint strength³. With

* The work described in this chapter has been presented at the 1st International Conference on Self Healing Materials, April 2007, Noordwijk, the Netherlands and this chapter has been submitted for publication to Journal of Adhesion. Part of the work in this chapter has been presented at the Rapra Silicone Elastomers 2006 Conference, September 2006, Frankfurt, Germany.

Lavrent'yev he constructed a model for the contact area-time dependence, with the following time relationship as a result:

$$\ln(1 - j) + j = -Pt/h \quad (6 - 1)$$

where φ is the fractional contact area, related to the development of tack in time as: $\varphi \sim \text{tack}(t)/\text{tack}(\infty)$, P is the applied pressure and h is the viscosity of the polymer. The experiments of Voyutskii et al. showed that the contact area formation is not instantaneous; the interface strength developed further even after full contact was achieved. Thus viscoelastic flow is a controlling factor during the early stages of contact.

Wool⁴ used the reptation theory of deGennes⁵ to depict the process of a polymer-polymer interface crack healing. Incomplete molecular contact limits the interfacial diffusion of polymer molecules. Thus, for simplicity, Wool assumed instantaneous wetting of the interface. According to the theory of reptation, polymer chains are confined to a "tube" having a shape similar to the random coil conformation of the chain. Due to the Brownian motion the chain migrates from the tube, allowing it to cross the interface. The strength of the interface develops in time, and the rate of adhesion development is a function of contact time, temperature and molecular weight of the polymer. On the basis on the relations summarizing the description of a linear polymer chain movement in an entangled melt, Wool developed a molecular description of the interface as a function of time, molecular weight of the polymer, contact pressure and temperature. The topic is discussed in more details in Chapter 2 of this thesis, only the most important theoretical predictions are summarized in Table 6.1.

Table 6.1. Summary of scaling laws for Wool's theory of crack healing^{4,6}

Molecular aspect	Symbol*	Relation	Remarks
Number of chains	$n(t)$	$t^{1/4} M^{-5/4}$	$t \leq t_\infty$
Number of molecular bridges	$\rho(t)$	$t^{1/2} M^{-3/2}$	$t \leq t_\infty$
Average monomer penetration depth	$X(t)$	$t^{1/4} M^{-1/4}$	$t \leq t_\infty$
Average bridge length	$l_p(t)$	$t^{1/4} M^{-1/4}$	$t \leq t_\infty$
Tack	$\sigma(t)$	$\begin{cases} t^{1/4} M^{-3/4} \\ M^{1/2} \end{cases}$	$\begin{cases} t \leq t_\infty \\ t \geq t_\infty \end{cases}$
Strain energy at fracture	$U_c(t)$	$\begin{cases} t^{1/2} M^{-3/2} \\ M \end{cases}$	$\begin{cases} t \leq t_\infty \\ t \geq t_\infty \end{cases}$
Time to reach equilibrium	t_∞	M^3	-

^{*)} For the symbols, reference is made to Chapter 2.

where t_∞ is the time needed to reach equilibrium. Since $X(t) \sim t^{1/4} \sim \sigma$, this model regards the average monomer interpenetration depth as the controlling factor for σ , the macroscopic interfacial bonding strength. Still, it is important to note that not every chain crossing the interface will be able to support the bonding. Only those chains or chain segments are effective, which after crossing are able to hook into entanglements, at least one on each side. This may be considered a modification of Wool's model described before in the sense, that a minimum molecular weight of the reptating polymer is required to be able to span the distance across the interface and to reach two effective entanglements, one at each side. Below a certain minimum molecular weight the load bearing bonding strength will not develop. Wool's theoretical model was a depiction of an ideal case, where every chain is equally effective. A more general approach can be summarized in the following relation⁷:

$$\frac{\sigma(t_c)}{\sigma_\infty} = \frac{n(t, M_w, M_e)}{n(t_\infty, M_w, M_e)} \quad (6 - 2)$$

where $n(t_c, M_w, M_e)$ is the number of effective crossings per unit area as a function of contact time t , weight average molecular weight M_w , and molecular weight between entanglements M_e . The denominator is the number of effective crossings per unit area of the interface after equilibrium conditions have been reached. The total number of effective crossings is still predicted to scale with $t^{1/4}$ and is considered to be the mechanism behind the time dependence of autohesive bonding.

The proponents of the surface wetting mechanism point out, that the contact cannot develop instantaneously between two surfaces. On a microscale there will always be a rough topography, creating voids and disabling intimate molecular contact. Under pressure, material spreads with time, filling the voids via viscous flow. Increase in the apparent contact area e causes the overall bonding strength to rise. The bond strength develops in time with first-order kinetics of wetting.

Skewis⁸ calculated the rate of interpenetration of typical industrial elastomers from their diffusion coefficients, determined using radioactive-labeled polymers. He calculated that after one second of contact an elastomer chain interdiffuses around 45Å: enough for substantial interpenetration. On the other hand, tack development can take up to days to reach the equilibrium state. This would lead to the point, that for common industrial elastomers with molecular weights around 200 000 to 300 000, the adhesive bond formation is surface contact limited.

Another strong argument for the contact-controlled bond formation is the fact, that interpenetration should in fact be independent of contact pressure. Hamed⁹ in his study observed, that in the case of NR and SBR tack was sensitive to the compression load applied, what also points to a contact-controlled mechanism. However, the diffusion process is not strictly fully independent of pressure, because of an influence of free volume¹⁰, where the free volume depends on

pressure. This dependency, however, is several orders of magnitude lower than the effect of the small loading pressure used in the present tack experiments on viscous flow. This effect is thus negligible.

6.2 EXPERIMENTAL

Materials: Table 6.2 lists the vinyl-terminated polydimethylsiloxanes that were used for the study.

Table 6.2. Vinyl-terminated poly(dimethyl)siloxane polymers.

Material	Viscosity [Pa·s]	M _w [g/mole]	Vinyl group content [mmole/kg]	Supplier
MQ 17	500	17 000	166	ABCR
MQ 28	1000	28 000	98	ABCR
MQ 50	5000	50 000	64	ABCR

As crosslinker trifunctional tris(dimethylsiloxy)ethoxysilane was used. The platinum-cyclovinylmethylsiloxane complex was used as cure reaction catalyst. All the above materials were obtained from ABCR, Germany, with the exception of the multifunctional silane, which was provided by a proprietary source. 1-ethynylcyclohexanol (Aldrich, 99%) was used as a temporary reaction inhibitor. Pyrazine (Aldrich, 99%) was used as an internal NMR standard without further purification. The solvents used were all of pro analysi quality.

Sample preparations: For every batch of polymer the exact amount of vinyl groups was determined using NMR measurements (Varian 300 MHz apparatus) with pyrazine as an internal standard, as described in Chapter 3 of this thesis. The results of these measurements are included in Table 6.2. From those results and the molecular structure of the crosslinker, the hydrogen-to-vinyl ratio (H/V) was calculated.

The samples were then prepared using a H/V ratio of 1.0. The curatives were mixed together for 10 minutes with the polymer using a magnetic stirrer. During the preparation it was important, that the inhibitor was added to the reaction mixture before the catalyst. Without the presence of the inhibitor, the cure reaction proceeds quickly even at room temperature. While the amount of crosslinker had to be varied according to the vinyl group contents of the polymers used, the amounts of catalyst and inhibitor were kept constant: 10 and 50 ppm, respectively. The mixture was degassed and cured in a compression molding press (WLP 1600/5x4/3 Wickert laboratory press) at 120°C for 30 min. Clean Teflon foil was placed between the cured mixture and the mold plates to avoid surface contamination and sticking of the material to the mold. The 90x90x2 mm sheets were post-cured in an oven at 120°C for 48 hours.

Tack time-dependence measurements: The cured samples of MQ 17, 28 and 50 with hydrogen-to-vinyl ratio 1.0 were compressed under a load of 2.5 N in the

tack device described in Chapter 4. Times of compression were varied from 1 to 1000 minutes. For each compression time, several tack measurements were collected and the average was taken as the final result. After each series of measurements, samples were exchanged, to provide a fresh, uncontaminated surface. The measurements were always performed at room temperature. The separation speed after the compression was varied from 0.25 to 15 mm/s.

6.3 RESULTS

6.3.1 AUTOHESION BEHAVIOR

Figure 6-1 shows the beginning of PDMS autohesion development for short compression times.

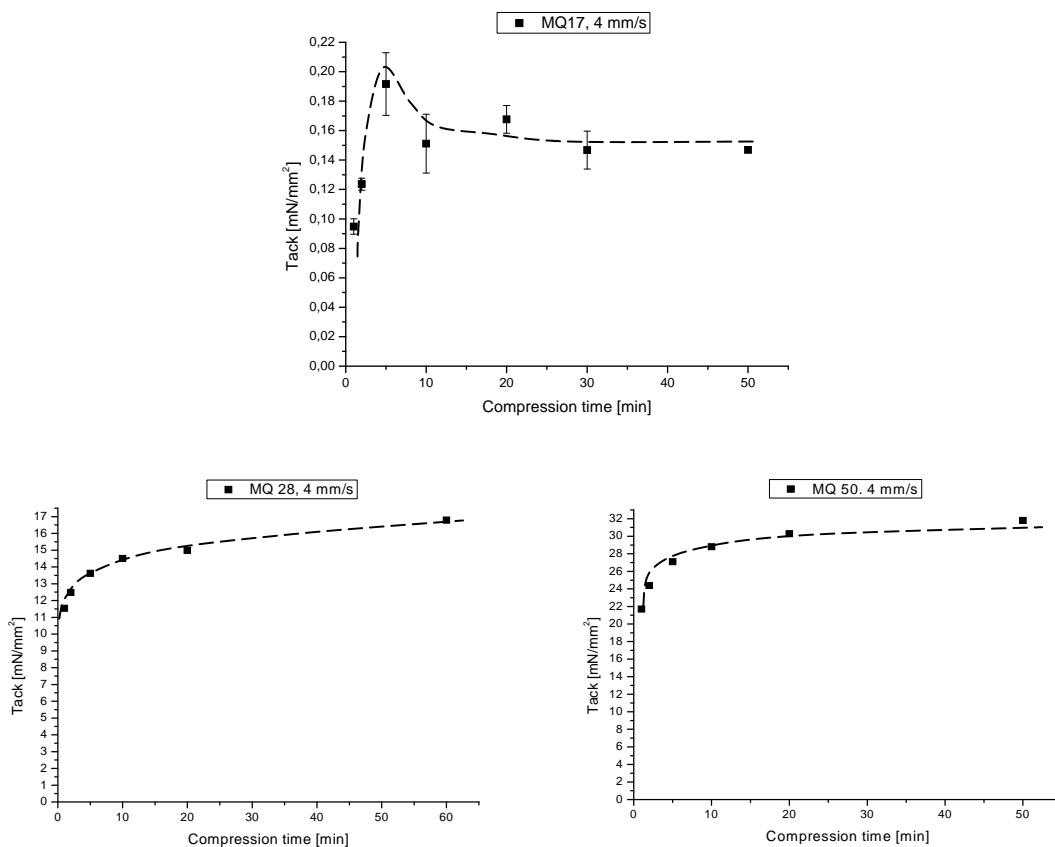


Figure 6-1. Tack as a function of compression time for MQ 17, MQ 28 and MQ 50, all cured with H/V = 1.0.

Notice the large difference in tack values between MQ 17 and the other two samples, MQ 28 and MQ 50. While the low molecular weight MQ 17 apparently shows a maximum in autohesion level for short contact time, the shape of the curve for the high molecular weight MQ 50 is more logarithmic of nature. The low

molecular weight PDMS quickly reaches a peak in tack, and after that point tack decreases again to a plateau. The situation is different in the case of the high molecular weight PDMS: the tack level rises slower but steadily; within the timescale of the measurement it cannot be determined if a saturation level is already reached. In fact, the tack still rises after very long compression times, ranging over 1000 minutes (not shown). That means that the ultimate interface strength has not already been reached after that period: a further increase in rubber autohesion was observed by Stacer et al. for times longer than 10 000 minutes, when finally the fracture stress achieved values independent of contact time¹.

6.3.2 THE COMPRESSION-TIME-DEPENDENT AUTOHESION OF INTERMEDIATE AND HIGH MOLECULAR WEIGHT PDMS MQ 28 AND MQ 50

In order to test, if silicone rubbers behave according to deGennes/Wool's theory, another variable was introduced: testing speed. The theory predicts that the slopes of the tack-time curves should change with separation speed from $t^{1/4}$ to $t^{1/2}$, indicating the change in the chain unraveling mechanism. The pull-out mechanism is favored at low separation speeds, low molecular weights and high testing temperatures. The chain fracture mechanism would be favored at high separation speeds and high molecular weight of tested polymers. Where the testing temperature remained constant, polymer molecular weight and separation speed could be varied.

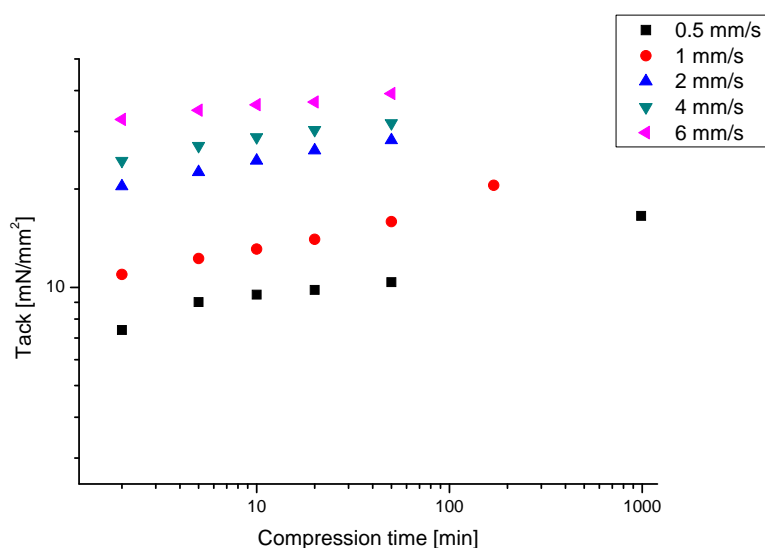


Figure 6-2. Autohesion curves for MQ 50 at different separation speeds.

Figure 6-2 shows an example, how the autohesion of the PDMS – PDMS interface of MQ 50 proceeds with compression time and increasing separation

speed. With the increase in separation speed, the maximum forces of autohesion increase as well.

This behavior is better illustrated in Figure 6-3, which shows how the slopes of the log tack vs. log time curves change with increase in separation speed. The slopes exhibit a local minimum at the speed of 4 mm/s, after which the exponent values rise monotonically with increase in separation speed. When the separation speed is decreased below 4 mm/sec, the exponent values also increase very fast.

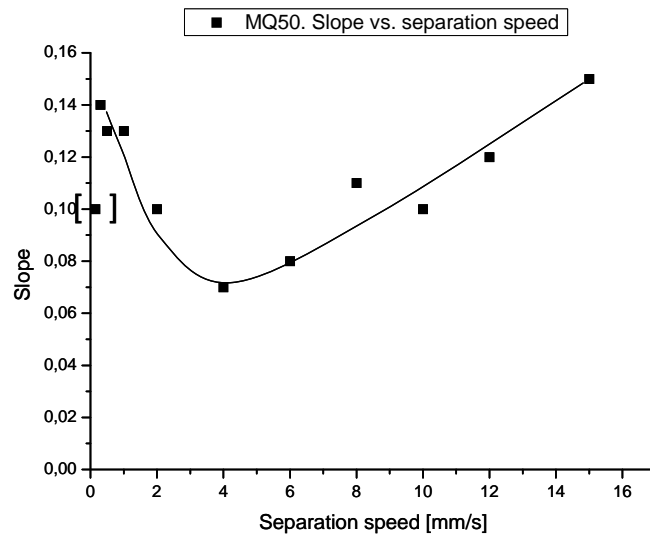


Figure 6-3. Slopes of the double logarithmic autohesion vs. compression time curves of MQ 50 in relation to separation speed. The line is intended to guide the eye.

The situation is similar for the intermediate molecular weight PDMS: MQ 28.

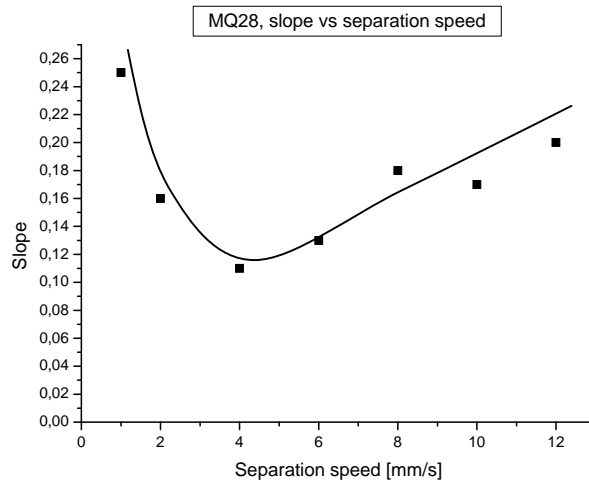


Figure 6-4. Slopes of the double logarithmic autohesion vs. compression time curves of MQ 28 in relation to separation speed. The line is intended to guide the eye.

The tack-time relationship for MQ 50 was measured over a somewhat broader range of separation speeds. Still, the behavior of both types of PDMS is similar: the minimum is located at the 4 mm/s speed and the exponent values rise later practically linearly with separation speed. When the speed is decreased below 4 mm/s the exponents rise very quickly. The slope values observed for MQ 28 are generally higher and closer to 0.25, as predicted by Wool, than for MQ 50.

The application of Vouytskii's equation for the autohesion data of MQ 28 and MQ 50 is shown in Figure 6-5. With j of equation (6 - 1) defined as $tack(t)/tack(\infty)$, plotting the $\ln(1-j)+j$ versus compression time should yield a straight line, if the contact formation obeys the first order kinetics of wetting. A limitation of the approach is, that $tack(\infty)$ was never actually reached. The tack after the longest compression time employed was taken for the equilibrium value.

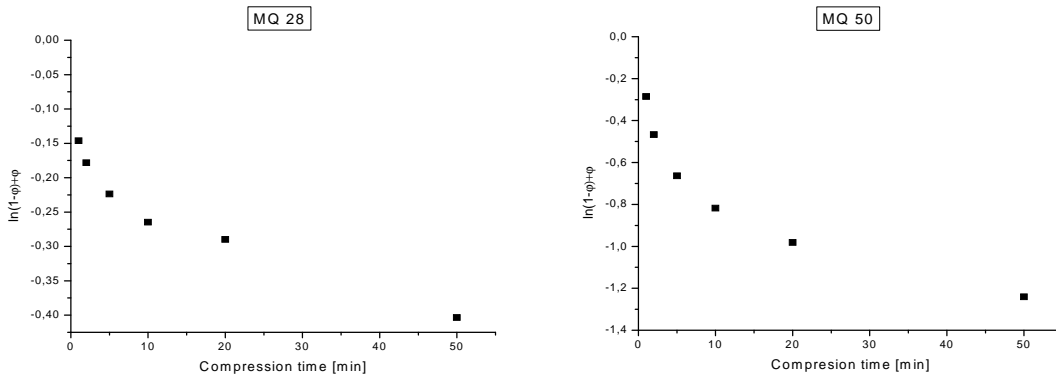


Figure 6-5. The application of the first order kinetics of wetting for autohesion data description for 4 mm/s separation speed.

For both MQ 28 and MQ 50, the plots do not give a straight line. It demonstrates that wetting is not the predominant process.

A closer look at the influence of separation speed on tack, after constant compression time, is given in Figure 6-6 for MQ 50 and MQ 28. For simplicity of the picture, only the values of tack after 10 minutes of compression were taken for comparison. MQ 50 clearly exhibits a maximum in tack, which levels down with the increase in separation speed. The tack values for MQ 28 are unfortunately much more scattered.

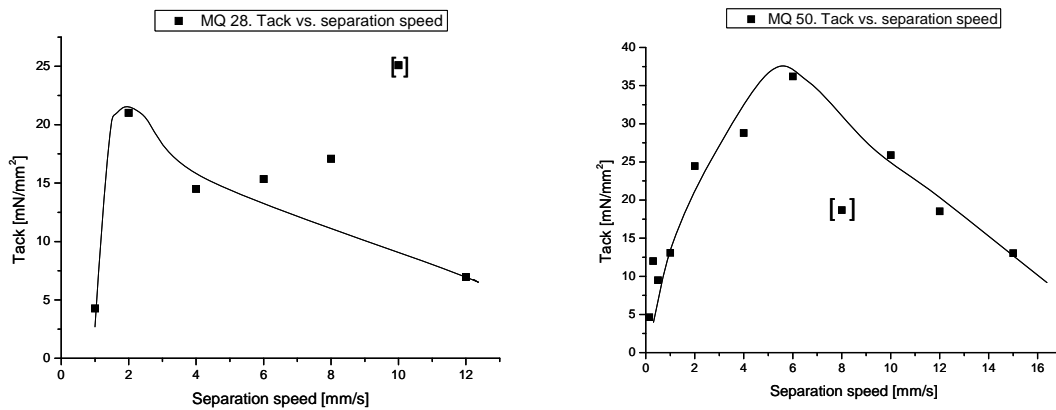


Figure 6-6. The tack as a function of separation speed for MQ 28 and MQ 50. The values after 10 minutes of compression were taken. The line is intended to guide the eye.

6.3.3 THE COMPRESSION-TIME-DEPENDENT AUTOHESIVE BEHAVIOR OF LOW MOLECULAR WEIGHT PDMS MQ 17

The behavior of the low molecular weight PDMS is very different. First of all, the tack curves clearly show the presence of a maximum at short contact times: the tack rises quickly to its maximum value and then lowers down to a plateau. This sort of behavior is completely absent for the higher molecular weight polymers. The presence of this maximum makes it very difficult to fit a curve – fitting results are obtained with a very large error. The maximum is present on each tack curve for separation speeds ranging from 4 to 10 mm/s. Moreover, it shifts with increasing separation speed to shorter contact times, vanishing completely at 12 mm/s. The absolute values of tack increase with increasing separation speed, but the increase stops at 8 mm/s.

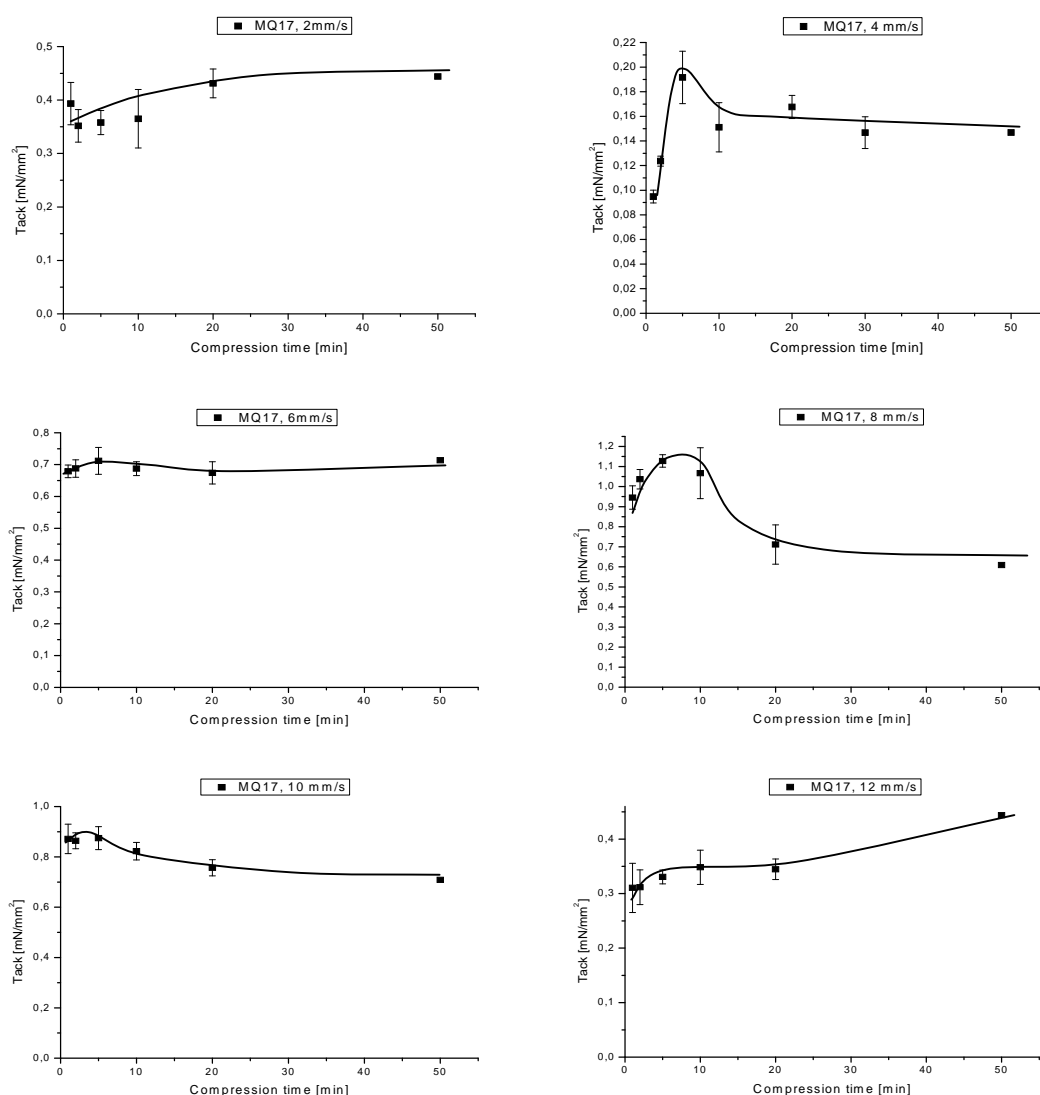


Figure 6-7. The beginning parts of the tack vs. compression time curves for MQ 17 at different separation speeds.

It is important, however, to look at the tack curve for MQ17 at extended compression times. Even after the tack seems to have decreased to the plateau values after several minutes, after a long compression time, at 1000 minutes and more, a substantial increase in rubber-rubber tack can still be seen. Figure 6-8 shows two autohesion curves of MQ 17, for 4 and 10 mm/s separation speeds. The increase in the tack is very substantial for the low separation speed, and decreases when the separation speed increases.

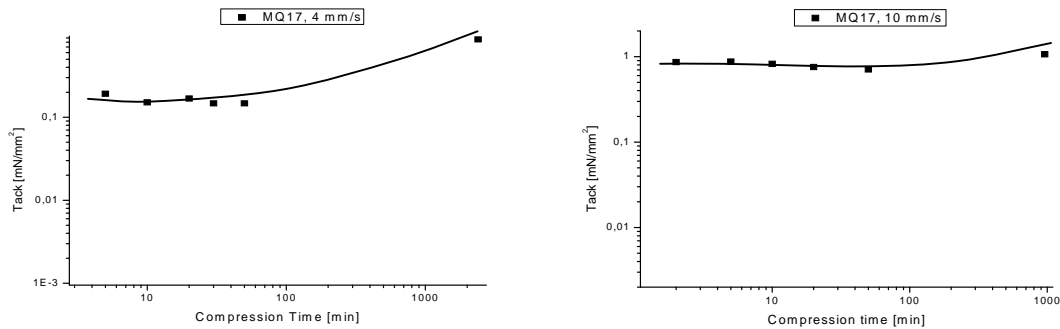


Figure 6-8. Tack curves for MQ 17, at 4 and 10 mm/s separation speed.

This trend is better visualized in Figure 6-9, where the difference in tack values between the plateau, measured at 50 minutes of compression and at 1000 minutes compression time are printed as a function of separation speed.

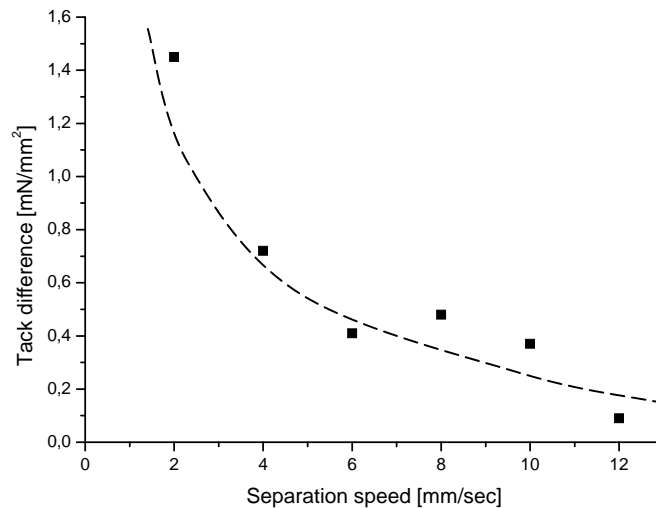


Figure 6-9. The difference between the 50 min and 1000 min compression time tack as a function of separation speed for MQ 17.

The difference in tack between 50 and 1000 minutes compression time decreases very quickly with increase in separation speed, being close to zero at the 12 mm/s.

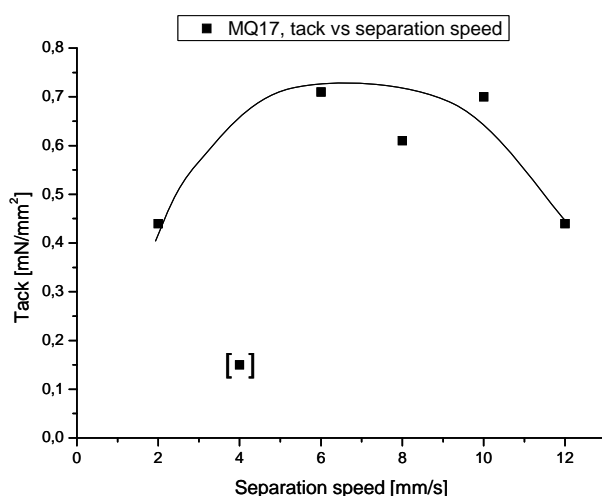


Figure 6-10. The tack as a function of separation speed for MQ 17. Tack at plateau (50 minutes of compression) was taken.

If the tack is plotted as a function of a separation speed, see Figure 6-10, it can be seen that there is roughly one broad maximum, spreading over the range of separation speeds. An exception is the 4 mm/s tack, which is anomalously low compared to the other results.

As it was done for MQ 28 and MQ 50, the applicability of Voyutskii's model was tested. The results are plotted in Figure 6-11:

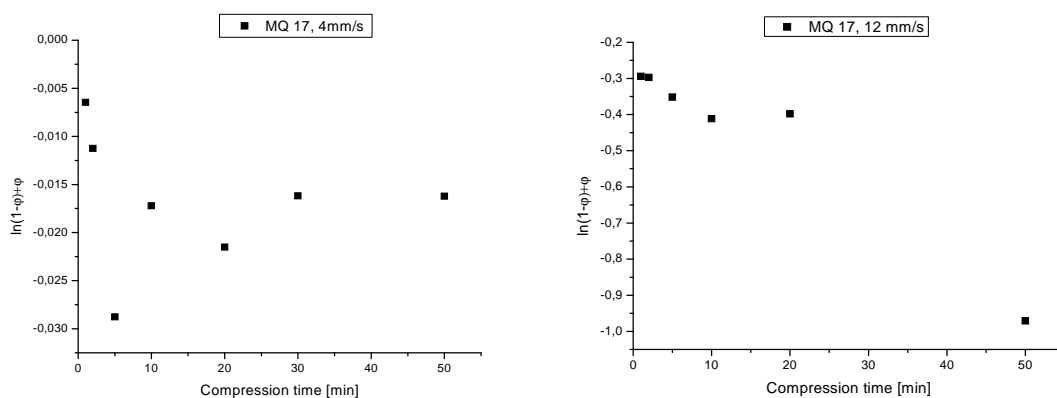


Figure 6-11. The application of the first order kinetics of wetting for autohesion data description of MQ 17 for 4 and 12 mm/s separation speed.

If an overshoot maximum is present in the autohesion data in Figure 6-7, the Voyutskii's model does not seem to be applicable: the points are scattered. But when the overshoot maximum has disappeared with increase in separation

speed, the plot gives a linear relationship, as opposed to the fitting results for MQ 28 and 50.

6.4 DISCUSSION

The presented results demonstrate, just like others have seen with different systems¹¹, how difficult it is to accurately and reproducibly measure tack, respectively to analyze the data on basis of the few models available. The main reason is, that the tack measurement encompasses two opposing, non-equilibrium effects:

- the development of tack or autohesion during compression time, with extra variables: compression load, temperature and a major effect of molecular weight;
- cutting short the development of tack with time at the moment where separation is imposed, is where the separation speed comes in as an extra parameter.

As to the first effect, Wool's model assumes that the separation resistance of the interface is dominated by molecules which diffuse through the interface. Basically, it is the strength required to pull the molecules from the "tube" created by the surrounding polymers and back from the interface. The longer the molecules are, the deeper the interpenetration may be, and the stronger the separation resistance. From this model there is a relationship predicted for the time needed for achieving equilibrium t_e . This time scales with the third power of the molecular mass of the polymer, see Table 6.1.

With the molecular weights of the two extremes MQ 17 and MQ 50 differing by a factor of 2.9, the time span required for MQ 50 to reach a similar state of equilibrium compared to MQ 17 is already 25 times larger! In other words, if we assume that equilibrium has been reached in the experiments with MQ 17 after compression time of approximately 50 minutes (see Figure 6-6), then for MQ 50 a time span of 20 hours or more would have been required, which is a little impractical experimental condition within the scope of this research. Therefore, it is reasonable to assume, that the tack-values measured for MQ 17 more closely resemble an equilibrium situation, while those for MQ 28 and far more for MQ 50 are tack values when equilibrium molecular interpenetration has not been reached yet.

6.4.1 HIGH MOLECULAR WEIGHT PDMS: MQ 28 AND MQ 50.

The tack stress should obey a time dependence t^x with $0.25 < x < 0.5$, depending on whether a pull-out or a chain fracture mechanism prevails: Table 6.1. How well this describes the autohesion data, can be seen from Figures 6-2 and 6-4. Although the time dependence of autohesion manifests itself in forms of double

logarithmic-type curves, the exponent values are lower than the theory predicts. It is important to note, however, that the exponents were predicted for monodisperse polymers. The data for polydisperse elastomers obtained by other researchers show a slower increase of the stress with contact time^{1,12}. Values of x lower than 0.25 can be explained by the polydispersity of the initially used polymer, which in the present case is around $\frac{\overline{M}_w}{\overline{M}_n} = 2$. This polydispersity is

related only to the material before crosslinking; after the crosslinking $\frac{\overline{M}_w}{\overline{M}_n} = \infty$, because of the infinite molecular mass of the crosslinked polymer matrix related to the uncrosslinked polymer and left over pendant chains that cross the interface. Wool's model was developed primarily for uncrosslinked polymers. A very important question to ask is how far it still applies for the partially crosslinked species.

The other model, known to describe the tack time development, was based on a first order kinetics of wetting. If the contact formation is flow-controlled, the plots in Figure 6-5 should have yielded a straight line. This is not the case, which strongly suggests, that the viscous flow is not the controlling process even during the early stages of contact. These results, however, should be taken with caution: in order to properly calculate the fractional fracture stress the value of tack at equilibrium ($j(\infty)$) was required. It was already mentioned, that during the timescale of the experiment equilibrium was not reached yet.

The interesting behavior observed during the separation speed experiments (Figures 6-6 and 6-10) is, that a maximum in tack is observed over the range of separation speeds. These results are similar to those obtained by Gent and Petrich¹³. They measured the force-separation rate dependence for butadiene-styrene random copolymer and found a very similar pattern, as shown in Figure 6-12:

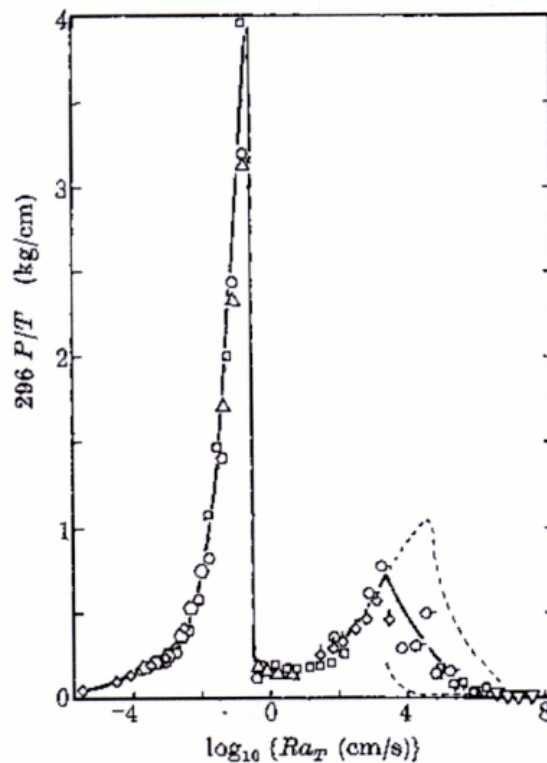


Figure 6-12. Master relation for peel force against rate of peeling for butadiene-styrene random copolymer, reduced to 23°C¹³.

There are two transitions visible, one at low and one at high peeling rate. The maximum of the transition observed for MQ50 and perhaps for MQ 28 falls in the area of 0.1 cm/s separation speed (Figure 6-6); or -1 on the scale seen in Figure 6-12. The authors attributed the sudden change in strength at low separation rates to an alteration of the sample bulk viscoelastic behavior during pulling. At a certain speed the rate of deformation is so high, that the material is not capable of liquid-like flow anymore and starts to exhibit rubber-like behavior. It should be noted again, that the experiments of Gent et al. were performed on uncrosslinked polymer. The crosslinked rubber is very unlikely to exhibit a liquid-like behavior. However, silicon elastomers are known for their extraordinary chain mobility, due to the very low glass transition temperature of below -100 °C compared to other rubbery polymers. The results of separation rate experiments for PDMS suggest, that there may be a second transition region at higher separation speeds than have been measured.

The scattering of the MQ 28 data in Figure 6-6 is a result of an artifact from the sample preparation stage. The liquid, uncrosslinked PDMS prepolymer always contains some amount of an uncrosslinkable fraction: silicon oil. This is the remains of the polymerization process, where the amount of oil varies from batch to batch. Samples of MQ 50 were all prepared from a single, large batch of material, while the samples of MQ 28 were prepared from different batches.

During the testing stage, the oil can diffuse towards the interface, forming a thin liquid layer interrupting the interface formation process. As a result, the absolute tack values for MQ 28 differ, while for MQ 50 they form a consistent picture – this is a problem often encountered in elastomer technology. Note, that the interface strengthening process is not affected by this phenomenon, the slopes of tack-time dependence curves are unchanged.

DeGennes extended the presence of maximum from the uncrosslinked to the loosely crosslinked systems with large amounts of entangled free chains and dangling ends¹⁴. In this view, the increase in force indicates a transition from *soft rubber*, with the network dominated by few crosslinks, to *hard rubber*, with network dominated by “frozen” entanglements. Figure 6-13 shows a schematic visualization of the fracture profile:

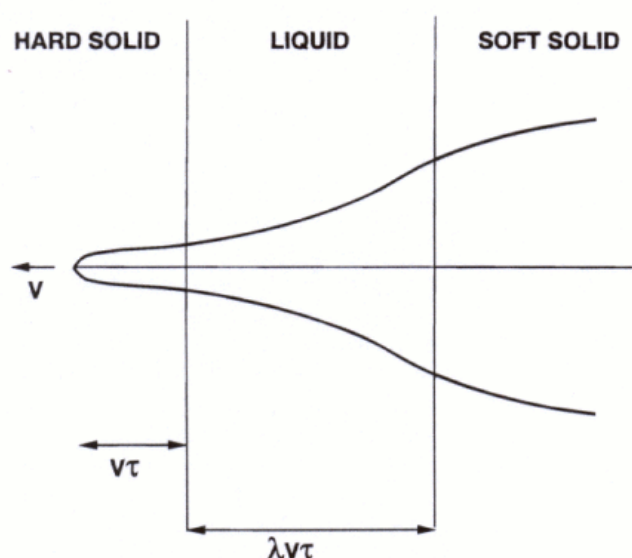


Figure 6-13. The crack tip profile¹⁴. V is the separation speed, t relaxation time and I is the low to high frequency modulus ratio.

If the crack propagation velocity is high enough, the entanglements do not have time to relax and retract. The relaxation time of the polymer chains therefore plays a crucial role here.

6.4.2 LOW MOLECULAR WEIGHT PDMS: MQ17

The tack behavior of the low molecular weight PDMS is more complicated. The tack curves show well-pronounced maxima for short compression times, after which the tackiness levels down to a plateau. However, after very long compression times, there is still an increase in tack level, showing that interpenetration and chain entanglements at least partially take place at the interface on the long term. Because of that sort of behavior, the fitting of the curves of log tack vs. log time to obtain the exponent value is virtually impossible:

it yields a large error. The maxima visible in Figure 6-7 shift to shorter contact times with increasing pulling speed. This behavior is very similar to the viscoelastic phenomenon known as stress overshoot¹⁵, where the shear stress vs. time passes through a maximum for large shear rates. Actually it is quite logical, if the timescale of the experiment is taken into account: where the surface chain interpenetration needs many hours to achieve an equilibrium value, pulling takes place in a time of seconds, thus the chains do not have time to orderly disentangle themselves¹⁶. It is interesting, that this sort of phenomenon did not appear during testing of the high molecular weight polymers, where one could expect it to be even more pronounced if the effect was based purely on viscoelastic dissipation. It should be noted however, that for the high molecular weight polymer the saturation level may or will not have been reached at all for interpenetrating chains in the range of contact times applied.

MQ 17 still shows a tack increase after very long compression times. Surprisingly, the relative increase depends heavily on separation speed: Figure 6-9. The explanation of this phenomenon may be related to the minimum molecular weight between the entanglements. Depending on the specific author, M_e of PDMS can be as low as 8100 g/mol, based on retardation spectrum measurements¹⁰, but the most often used value is 12300 g/mol¹⁷. The molecular weights of MQ 50 and MQ 28 are high enough to form entanglements, contributing to the strength of the interface. MQ 17 is a borderline case. According to some sources, PDMS with a molecular mass around 16000 can be regarded as practically non-entangled^{18,19}. Even if the molecular mass of MQ 17 may be high enough for the chains to still entangle, they cannot bear the stress well enough. If the interface is separated quickly, the polymer chains unravel very easily, hence their contribution to the joint strength diminishes. This can be the explanation for the different tack-separation speed behavior for MQ 17 (Figure 6-10), where instead of the abrupt transition like in a case of high molecular weight PDMS (Figure 6-6), one broad maximum over a whole range of separation speeds can be observed. The very low tack values for the 4 mm/s separation speed are again the result of the sample preparation process, mentioned before.

Fitting the first order kinetics to the autohesion data of MQ 17 encounters the same problem as fitting the power curve. Where the maximum is present, fitting yields a large scatter. It is striking, however, that when the maximum is gone, the graph takes the form of a straight line. This would suggest that the interface forming process for low molecular weight rubber MQ 17 is mostly wetting controlled. This correlates well with the critical entanglement molecular weight hypothesis.

6.4 CONCLUDING REMARKS

Wool's theoretical model for the diffusion-driven interface formation seems to have somewhat limited application for the PDMS telechelic network. The

autohesion curves of high molecular weight PDMS show a double logarithmic tack-time-dependence, but the generally accepted $t^{1/4}$ power law does not apply. Possibly due to the high polydispersity of the polymers used, but more probably because the theory was developed for uncrosslinked polymer melts.

The autohesion curves of the low molecular weight PDMS exhibit an anomalous behavior, most probably due to the polymer chains being at the edge of minimum molecular weight needed for entanglements. The tack-time development quickly reaches equilibrium, but the molecular weight is too low to follow Wool's model. Fitting another model, i.e. Voyutskii's, shows that the interface forming can be described in this way, when the maximum is not present, at least for the lowest molecular weight PDMS.

For MQ 28 and MQ 50 the interpenetration process is not quite in equilibrium yet, in spite of the fact that the molecular weight is high enough for the Wool's model to apply.

The tack – separation speed relationships exhibit sharp transitions for high molecular weight PDMS MQ 50 and broad for the low molecular weight. These are the signs of a viscoelastic response of the material, where the separation speed exceeds the retardation abilities of polymer chains. The intermediate molecular weight PDMS exhibits different behavior, due to the way samples have been prepared.

The question whether the contact development for a silicone rubber-rubber interface is diffusion, or viscous flow controlled, cannot be unequivocally determined from the experiments shown in this chapter.

¹ Stacer R.G., Schreuder-Stacer H.L., *Int. J. Fracture*, **39**, 201, 1989.

² Hamed G.R., *Rubb. Chem. Technol.*, **54**, 576, 1981.

³ Voyutskii S.S., *Autohesion and Adhesion of High Polymers*, John Wiley & Sons (Ed.), New York, 1963.

⁴ Wool R.P., *Rubber Chem. and Technol.*, **57**, 307, 1984.

⁵ de Gennes P.G., *J. Chem. Phys.*, **55**, 572, 1971.

⁶ Wool R.P., O'Connor K.M., *J. Appl. Phys.*, **52**, 5953, 1981.

⁷ Prager S., Tirrell M., *J. Chem. Phys.*, **75**, 5194, 1981.

⁸ Skewis J.D., *Rubber Chem. and Technol.*, **39**, 217, 1966.

⁹ Hamed G.R., *Rubber Chem. and Technol.*, **54**, 403, 1981.

¹⁰ Ferry J.D., *Viscoelastic Properties of Polymers*, 3rd edition, John Wiley & Sons (Ed.), New York, 1980.

¹¹ Galliano A., Bistac S., Schultz J., *J. of Coll. And Interface Sci.*, **265**, 372, 2003.

¹² D. Adolf, M. Tirrell, S. Prager, *J. Polym. Sci., Polym. Phys. Ed.*, **23**, 413, 1985.

¹³ Gent A.N., Petrich R.P., *Proc. R. Soc. London, Ser. A*, **310**, 433, 1969.

¹⁴ DeGennes P.G., *Langmuir*, **12**, 4497, 1996.

¹⁵ Bird R. B., *Dynamics of Polymer Liquids. Volume 1: Fluid Mechanics*, Wiley & Sons (Ed.), New York, 1977.

¹⁶ Bistac S., *J. Coll. Interf. Sci.*, 1999, 219, 210.

¹⁷ Aharoni S., *Macromolecules*, 19, 426, 1986.

¹⁸ Dollase T., Wilhelm M., Spiess H.W., Yagen Y., Yerushalmi-Rozen R., Gottlieb M., *Interface Sci.*, 11, 199, 2003.

¹⁹ Orrah D. J., Semlyen J. A., *Polymer*, 29, 1452, 1988.

Chapter 7

Adhesion of Dissimilar Rubber-Rubber and Rubber-Steel Contacts of Silicone Rubber

*“The universe is asymmetric and I am persuaded that life, as it is known to us, is a direct result of the asymmetry of the universe or of its indirect consequences. **The universe is asymmetric.**”*

Louis Pasteur, *Works* Vol. 1 (1 June 1874)

In this chapter, the influence of different various contact substrates on the adhesion to PDMS rubber is described: steel and PDMS with varying molecular weight and crosslink density. The tack phenomenon heavily depends on the type of combination used; thus by changing the contacting substrates, their molecular weight, respectively type and degree of crosslinking, different behavior is observed. One of the most commonly used combinations, especially in industry, is the rubber-steel combination. Due to the lack of possibilities for interpenetration of chains into the steel substrate, the mechanism behind the rubber-steel tack is mainly surface wetting and physical or chemical bond formation. Dissimilar rubber-rubber tack strongly depends on the various crosslinking levels of the interface forming samples, as well as on the differences in molecular weight of the polymers used, due to changes in concentration of obstacles obstructing chain interpenetration.

7.1 INTRODUCTION

The adhesion of elastomers is an important problem from the technological point of view. In the field of elastomer-elastomer adhesion most of the studies in literature considered similar, like-to-like autohesive joints, where chemical composition, degree of crosslinking and physical properties were the same. Much more work was devoted to adhesion of elastomers to rigid surfaces, like steel, glass or plastic. The main difficulty in such studies arises from the amounts of parameters that influence the dissimilar joint adhesion and have to be taken into account.

7.1.1 RUBBER - RUBBER DISSIMILAR JOINTS

Restricting the consideration to compatible polymers of the same chemical nature, three main mechanisms are responsible for creating interfacial strength¹: polymer chains interdiffusion through the interface (the compatibility of the contacting polymers is an important issue here), adsorption and co-crosslinking of polymer chains through the interface.

Very much work on covalent bonding at the interface was done by Gent et al. Gent and Chang checked the influence of the interfacial degree of chemical interlinking on the adhesion strength of rubbers joints². The strength of adhesion was directly proportional to the degree of crosslinking at the interface, with the limit being the tear strength of the material. If interlinking took place at contact of dissimilar rubbers, with previously fully cured sheets of rubber, the measured strength of adhesion was noticeably lower³. Vallat et al.¹ have studied the curative migration on the contacts of dissimilar IR rubbers, crosslinked to different degrees. They attributed a noticeable migration of curatives through the interface as one of the reason for high interfacial strength.

The chain interdiffusion in dissimilar polymer contacts is more complicated than for symmetric systems, since it involves the compatibility of the contacting polymers. Voyutskii et al. studied the diffusion on interfaces of different crosslinked polymer systems as a function of contact time⁴ using electron microscopy. For contacts of compatible polymers, noticeable chain interdiffusion occurred after around 30 minutes compression times. The rate of interdiffusion was higher for low molecular weight polymers. In incompatible polymer contacts chain interdiffusion occurred to some extent as well, however the times needed to achieve noticeable change on the interface were in the range of hours.

The problem of compatibility of polymer interfaces was investigated by Wool as well⁵. The equilibrium structure of the interface is determined by the balance of two forces. A favorable decrease in free energy due to entropic relaxation of the surface chains is counterbalanced by the unfavorable enthalpy of mixing. The postulated interface strength development with time should still proceed as:

$$\frac{G_f(t)}{G_{f,\infty}} \sim \left(\frac{t}{t_r} \right)^{1/2} \quad (7 - 1)$$

where G_f is the fracture energy in time t or at equilibrium (∞), and t_r is a reptation time for the polymer chains. For tack it means, that the interface strength should develop with time as $t^{1/4}$; see Chapter 2, equation (2–34) and following text.

7.1.2 RUBBER-HARD SURFACE CONTACT

The general difference between rubber-rubber and rubber-hard surface contacts is the absence of interdiffusion of polymer chains. Thus the possible adhesion influencing mechanisms mostly involve all kinds of viscous flow and chemical

interactions between the two surfaces. Tack will increase with growing completeness of contact.

Surface roughness turns out to be an important factor. Materials capable of flow may fill asperities, increasing the actual contact area. If the surface is porous, during contact formation rubber can penetrate into the pores; threads formed in this way must either be pulled out or broken in order to detach the two adhesive sides. Studies have shown that the strength of adhesion can largely be improved in this way⁶. Surface roughness affects crosslinked elastomers as well, as they are less capable to flow. The studies of Gent have shown, that adhesion of crosslinked elastomers to a rough steel surface resulted in a 100% interface strength increase compared to adhesion to a smooth steel surface⁷.

The adhesion development is not only influenced by surface wetting, additional physical and chemical bonds may develop during contact time. A good example is sulfur-cured natural rubber adhesion to brass-plated steel. Sulfur and by-products of the cure reaction migrate to the metal surface and form a copper sulfide film⁸. Vondraček and Gent performed some studies on adhesion of lightly peroxide crosslinked silicone rubber to glass and quartz substrate⁹. They found, that the adhesion to glass rises linearly with time of contact, the strength of the joint increased strongly with increased compression temperature. A similar trend was found during silicone rubber - steel contact. Authors attributed this to hydrolytic processes within the silicone rubber, followed by creation of reactive groups capable of reacting with surface groups on the steel. The formation of surface covalent bonds can be augmented by addition of special chemical compounds, called adhesion promoters¹⁰.

It is well known, that silicone rubber chains are capable of reorganizing due to the outstanding flexibility of the polymer backbone, so that either the polar backbone or apolar methyl side groups can present themselves on the surface. PDMS is well-known for recovering its hydrophobic surface properties, even after it was destroyed by plasma treatment¹¹. Similar behavior is then expected during contact with different, polar or non-polar surfaces. The polymer chains will rearrange to form as many bonds as possible.

7.2 EXPERIMENTAL

Materials: For the experiments MQ 17 and MQ 50 silicone rubbers were used, with specifications described in Table 6.1, Chapter 6.

Sample preparations: The samples were prepared in the way as described in Chapters 5 and 6 of this thesis.

Rubber-rubber tack measurements: Samples were compressed under a load of 2.5 N for 10 minutes. For each sample, several tack measurements were done

and the average was taken as the final result. The measurements were always performed at room temperature. The separation speed was constant at 4 mm/sec.

Rubber-steel tack measurements: Rubber sample was compressed against a polished chrome steel plate (see number 4 Figure 4-7, Chapter 4) under a load of 2.5 N for 10 minutes. For each sample, several tack measurements were done and the average was taken as the final result. The measurements were always performed at room temperature. The separation speed was constant at 4 mm/sec. The plate was carefully cleaned with acetone and dried before every measurement.

Tack-time-dependence measurements: The cured samples of MQ 17 and 50 with hydrogen-to-vinyl ratio 1.0 were compressed under a load of 2.5 N in the tack device, as described in Chapter 4. Times of compression were varied from 1 to 50 minutes. For each compression time, several tack measurements were collected and the average was taken as the final result. After each series of measurements, samples were exchanged, to provide a fresh, uncontaminated surface. All measurements were performed at room temperature.

7.3 RESULTS

7.3.1 RUBBER-STEEL TACK

Figure 7-1 shows the rubber-steel tack dependence on hydrogen-to-vinyl (H/V) ratio for PDMS with different molecular weights, crosslinked with the trifunctional silane. Note the different scales used for the various PDMS in order to accentuate the large differences in measured tack between the PDMS with varying molecular weights. The rubber-rubber tack values are the ones presented in Chapter 5 and have been included for comparison purposes.

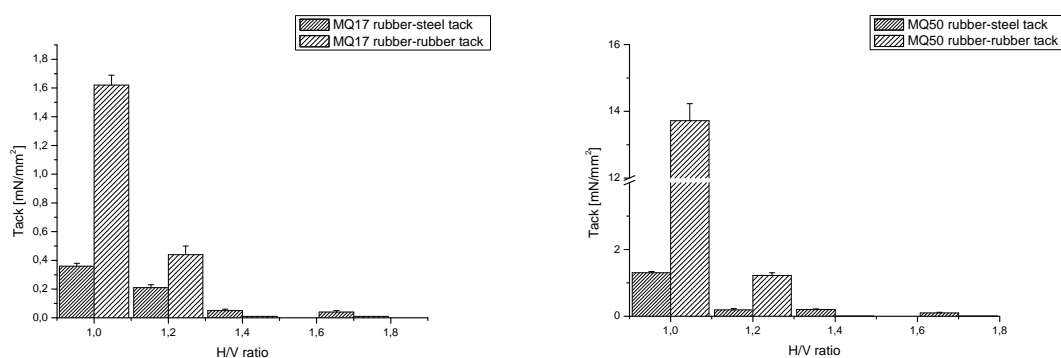


Figure 7-1. Rubber-steel tack for different molecular weight PDMS as a function of H/V ratio in comparison with the rubber-rubber tack. Trifunctional crosslinker.

The PDMS rubber-steel tack is in general much lower than the rubber-rubber tack. The difference is visible for both MQ17 and MQ50, however it is much more pronounced for MQ50, where tack differs by a factor of ten. Still, for both tested rubbers, for H/V ratios where rubber-rubber tack vanishes completely, there is still some detectable rubber-steel tack present. Besides that, the trends in rubber-steel tack are similar to the rubber-rubber ones. The H/V ratio = 1.0, and thus the lowest crosslink density, gives the highest tack, which then levels down with increasing H/V, but never completely disappears. The decrease with H/V ratio is much less pronounced for MQ17: it is more like a linear decrease; whereas for MQ50 the decrease is fast and resembles the decline of the rubber-rubber tack.

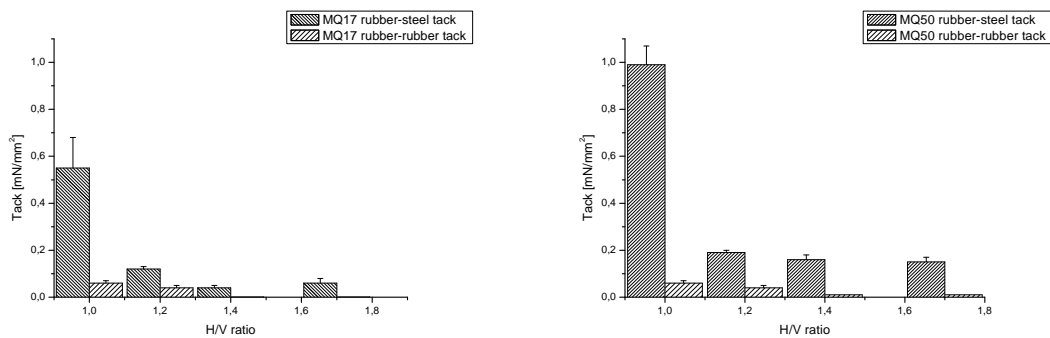


Figure 7-2. Rubber-steel tack for different molecular weight PDMS as a function of H/V ratio in comparison with the rubber-rubber tack. Tetrafunctional crosslinker.

Figure 7-2 shows the rubber-steel tack dependence on hydrogen-to-vinyl (H/V) ratio for PDMS with different molecular weights crosslinked with the tetrafunctional silane. The results are quite different, when the crosslinker functionality changes from three to four. PDMS crosslinked with the tetrafunctional crosslinker actually exhibits a higher rubber-steel tack than the corresponding rubber-rubber tack, although at a level generally in the same range as for the trifunctional crosslinker. The difference is again more pronounced in the case of MQ50 – a factor of ten – but still the levels of tack are overall very low and do not exceed 1 mN/mm². Just like in the case of the trifunctional crosslinker the rubber-steel tack does not disappear after reaching a H/V ratio of 1.2, it just seems to reach a constant level. The rubber-steel tack of MQ17 again shows a less pronounced tack decrease with increasing H/V ratio, although slightly sharper than when crosslinked with the trifunctional crosslinker. The tack decrease of MQ50 is more conspicuous, it reaches the constant tack level already at H/V ratio of 1.2.

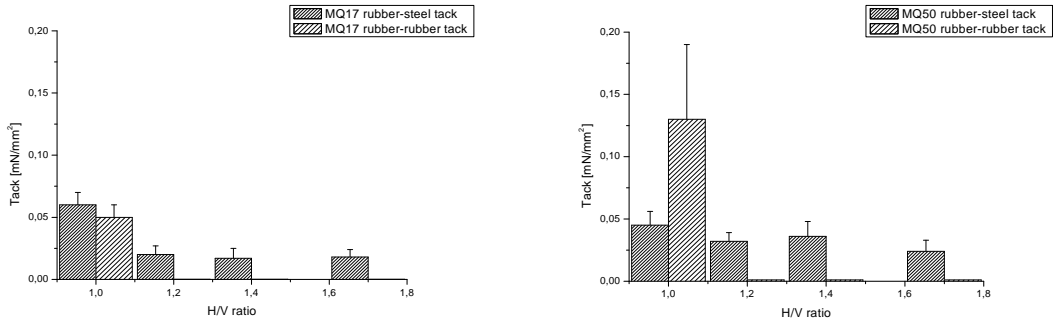


Figure 7-3. Rubber-steel tack for different molecular weight PDMS as a function of H/V ratio in comparison with the rubber-rubber tack. Multifunctional crosslinker.

Figure 7-3 shows the rubber-steel tack dependence on H/V ratio for MQ 17 and 50, crosslinked with the multifunctional silane. After crosslinking PDMS with the multifunctional crosslinker, the rubber-rubber and rubber-steel tack for H/V ratio of 1.0 becomes more or less equal for MQ17; the rubber-rubber tack is slightly higher for MQ50. Besides that, the picture remains very similar, after increasing the H/V ratio to 1.2 rubber-steel tack lowers down to a constant level. It is interesting to note, that the constant level of rubber-steel tack goes down with the increase in crosslinker functionality, to reach generally very low values for the multifunctional crosslinker.

7.3.2 TACK AND TACK TIME-DEPENDENCE FOR DISSIMILAR RUBBER-RUBBER CONTACTS

Figure 7-4 shows the tack values at 10 minutes of compression time for different dissimilar rubber-rubber contacts.

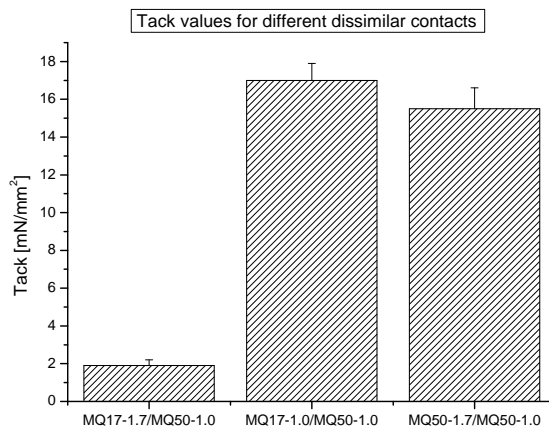


Figure 7-4. The tack values for dissimilar MQ17 and MQ50 contact.

The tack values for MQ17-1.0/MQ50-1.0 and MQ50-1.7/MQ50-1.0 (where 1.0 refers to H/V ratios) contacts are comparable in the range of measurement error. They are also approximately on the level of the MQ50 H/V = 1.0 tack, which was shown in Chapter 5 of this thesis to be in the range of 14 mN/mm². Using the fully crosslinked (H/V = 1.7) MQ17 as one side of the interface results in a large tack decrease, to the level of 2 mN/mm². Still, the tack of MQ17-1.7/MQ50-1.0 contact is significantly larger even than the MQ17=1.0 contact, not to mention the MQ17=1.7 contact which does not exhibit any detectable tack at all, as it was shown in Figure 5-5, Chapter 5.

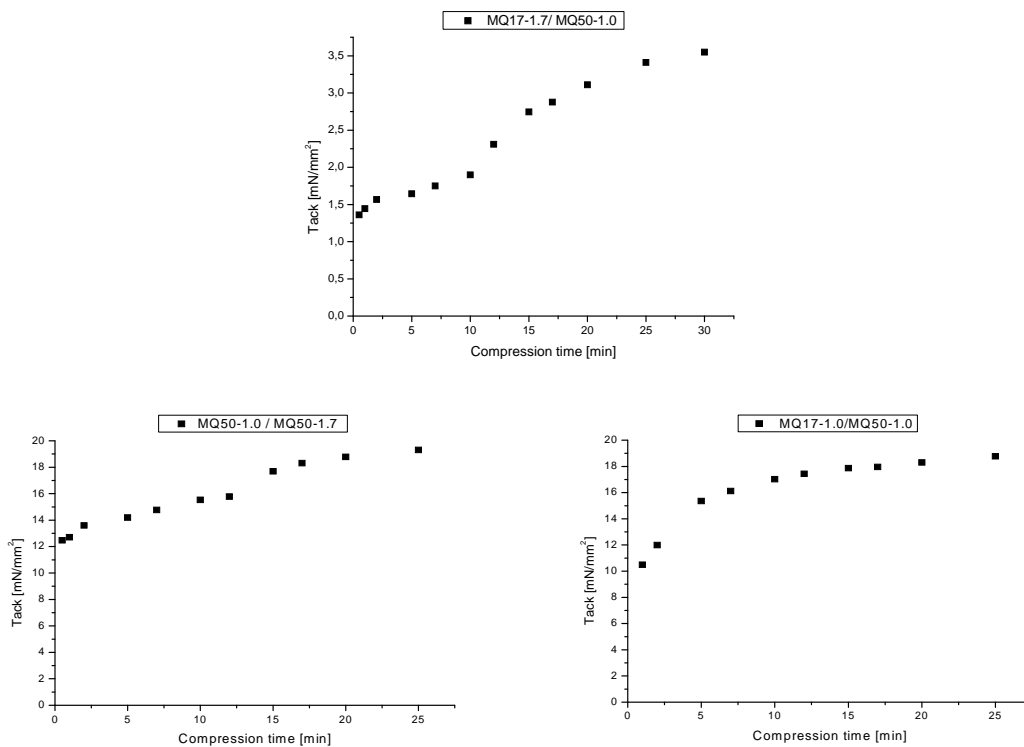


Figure 7-5. Tack as a function of compression time for MQ17 and MQ50 dissimilar contacts.

Figure 7-5 shows the tack-time dependence curves for the different dissimilar rubber-rubber contacts for short contact times till max. 25 minutes. Notice the large difference in tack values between the MQ17-1.7/MQ50-1.0 interface and the other two samples. The most striking feature in this tack-time development curve is the clearly visible induction period at short compression times, when tack rises much slowly compared to the other curves. This effect is most pronounced for the MQ17-1.7/MQ50-1.0 interface tack-time development curve. The tack rises very slowly till 10 minutes of compression, and then it rises much quicker forming the logarithmic-type curve, similar to the tack-time development curves as shown in Chapter 6 of this thesis. If fully cured MQ50 is used, instead of MQ17, the situation is similar. The tack values are much larger, but an induction

period of similar length is still visible followed by further increase in tack, although not as pronounced as in the previous case. Replacing fully crosslinked MQ50 with loosely crosslinked MQ17 results in a well-known logarithmic type tack development, without any induction period.

Fitting the power curve to the MQ17-1.0/MQ50-1.0 data yields the exponent of $t^{0.18}$. The other systems are more difficult to deal with. The results of plotting the tack data of MQ17-1.7/MQ50-1.0 and MQ50-1.7/MQ50-1.0 on a double logarithmic scale as a function of compression time are shown in Figure 7-6.

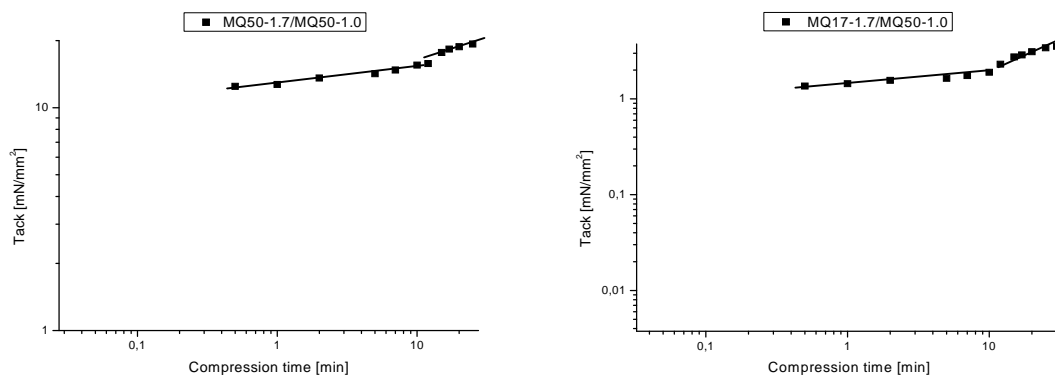


Figure 7-6. Tack of dissimilar rubber-rubber contacts vs. compression time on a double-logarithmic scale.

There are two tack developments present, that differ a lot in speed. The results of curve fitting are shown in Table 7.1:

Table 7.1. The exponents of dissimilar contacts.

Contact	Induction period exponent	Tack development exponent
MQ17-1.0/MQ50-1.0	-	0.18
MQ50-1.7/MQ50-1.0	0.07	0.17
MQ17-1.7/MQ50-1.0	0.09	0.55

Both observed induction periods are characterized by a very similar low exponent, the tack development with time is almost the same. The situation is different in the case of further tack development. The MQ17-1.0/MQ50-1.0 contact lacks the induction period; tack develops with an exponent of 0.18. MQ50-1.7/MQ50-1.0 contact tack after the induction period develops with a very similar speed. MQ17-1.7/MQ50-1.0 contact tack development is characterized by an anomalously high time exponent 0.55, which is much higher than could be expected.

First order kinetics of wetting¹² was applied for both induction and further tack development periods for the dissimilar rubber-rubber interfaces. The calculations

were done in the same way as described in Chapter 6 according to the equation (6 – 1). The results are shown in Figure 7-7.

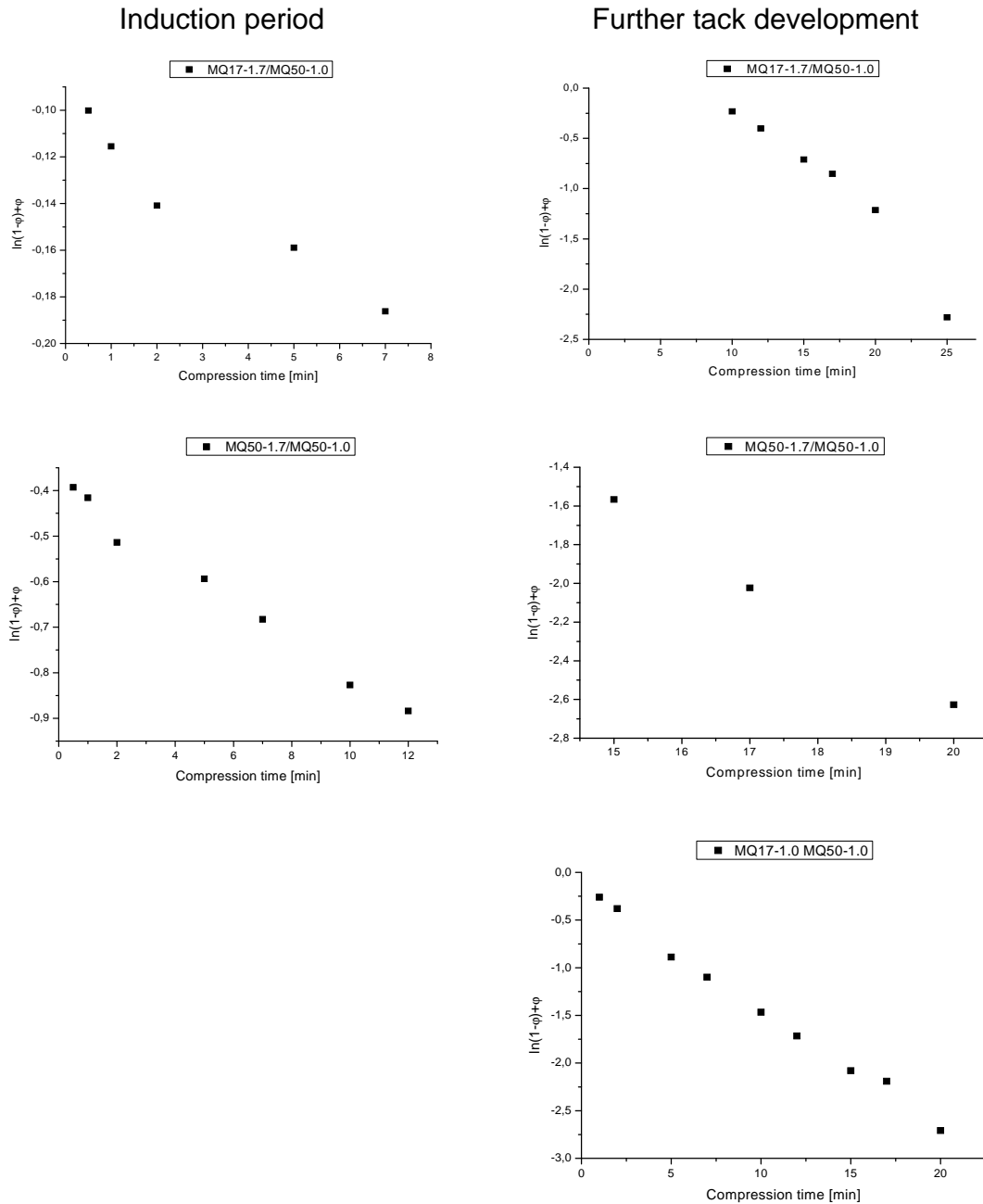


Figure 7-7. The application of first order kinetics of wetting for autohesion description of dissimilar rubber-rubber contacts.

After applying first order kinetics it can be seen, that the autohesion data for contact of MQ17-1.7/MQ50-1.0 do not form a straight line. This may suggest that wetting is not the predominant process here. The MQ50-1.7/MQ50-1.0 and MQ17-1.0/MQ50-1.0 autohesion data do form straight lines: Voyutskii's model can be used to describe the contact formation in these cases. This would

therefore suggest that the contact formation for the aforementioned dissimilar rubber-rubber contacts is driven by viscous wetting.

7.4 DISCUSSION

The difficulty of accurate measurement of adhesion and autohesion was already addressed and discussed in Chapter 6 of this thesis. Even more interpretation problems arise, when dissimilar joints are taken into consideration. The already substantial amount of variables that have to be taken into account increases even further, depending on the type of joint studied.

7.4.1 RUBBER-STEEL TACK

The main difference between rubber-rubber contact and rubber-steel contact is, that there is no interdiffusion possible in the latter case. This effectively eliminates one of the mechanisms of tack formation. In the case of rubber-steel contact, possible tack creation will come from viscous wetting of the interface, and then eventual rearrangement of surface chains and hydrogen bonds formation.

The large difference between rubber-rubber and rubber-steel tack for the trifunctional crosslinker clearly shows, that the main mechanism responsible for rubber-rubber tack is the chain interdiffusion. But, in contrast with the rubber-rubber tack, rubber-steel tack does not disappear completely with increase in crosslink density. However small, a certain measurable interface strength remains. The tack reduction most probably reflects the difficulties in wetting the interface – the more the sample is crosslinked, the stiffer and less compliant it becomes. The remaining tack would then be a result of molecular rearrangement in order to adjust to the polar surface of steel. It was already mentioned in Chapter 3, that due to its extraordinary backbone flexibility, siloxane polymer chains can easily rearrange themselves. Usually, in contact with air, PDMS methyl sidegroups are exposed on the surface in order to reduce surface energy, but in contact with a polar medium mostly polymer backbones will present themselves on the surface.

Increasing the crosslinker functionality from three to four results in the rubber-steel tack being higher than the rubber-rubber tack although the tack values for the rubber-steel are within the same range as for trifunctional crosslinker. It was already mentioned in Chapter 5 of this thesis, that using tetrafunctional crosslinker means a drastic reduction of the amount of free, reptating chain ends. In the case of rubber-steel contact this apparently does not strongly affect the tack formation: the possible rearrangement of polymer chains occurs both in crosslinked as well as in pendent chains. A slight tack reduction, visible especially in the case of MQ50, can be attributed to the higher crosslinking level,

which makes the viscous flow more difficult, as more numerous and longer free chains favor surface wetting¹³.

Further increase in crosslinker functionality results in a substantial reduction of rubber-steel tack, again in contrast to the rubber-rubber tack, which does not change. The question remains, if this phenomenon is only an effect of further reduction in viscous flow, or if it is influenced by reduction in polymer rearrangement capabilities, since the increase in crosslink density affects the rotational freedom of polymer chains as well^{14,15}.

7.4.2 TACK AND TACK TIME-DEPENDENCE FOR DISSIMILAR RUBBER-RUBBER CONTACTS

It is important to note, that in the testing of the dissimilar rubber-rubber joints several additional variables are added. First of all, the contacting sheets differ strongly in crosslink density, and as a result of that in stiffness. In some of the contacts studied, the tested rubbers differed in molecular weight as well, which might result in some degree of thermodynamic incompatibility. The eventual possibility of curative migration from the side with excess of crosslinker to the uncrosslinked side of the interface was eliminated at the stage of samples preparation: post-curing in the oven must have oxidized all remaining possible crosslinking sites at the crosslinker molecules.

The tack of MQ17-1.7/MQ50-1.0 system is much lower than the tack of MQ50, but significantly higher than the tack of MQ17. This is logical; loosely crosslinked MQ50 exhibits a high tack by itself, but is pressed into contact with a tightly crosslinked sheet of low molecular weight rubber. This seriously hampers the possible interdiffusion of polymer chains. In addition, the entanglements can occur only from one side of the interface; MQ17 chains have a molecular weight still too low to form effective entanglements¹⁶. This should significantly lower the possible interfacial strength.

The tack of MQ17-1.0/MQ50-1.0 and MQ50-1.7/MQ50-1.0 contacts is comparable with the MQ50 1.0 tack. In this case the comparison can be made safely, since samples were prepared from the same batch of material. The nature of the tack formation, however, cannot be derived only from looking at the static values. However, it can be seen already that using a less crosslinked, more loose network as a contact, has a huge influence.

The tack-time development curves of dissimilar contacts constitute a very complicated picture. One of the most characteristic observations is the presence of the induction period of some sort, during which the tack is low and develops slowly. This sort of behavior is different from what was observed, for example, by Gent and Kim¹⁷ for dissimilar polymer contacts. It shows in the case of contacts involving highly crosslinked rubber on one side. This would lead to an explanation, that this is a period during which the interdiffusion of chains is hampered by the presence of the tight network – more obstacles on the way to

overcome for the penetrating chains. The further tack development proceeds much faster later on, than in the case of symmetric MQ50 contacts, although the exponents are still lower than the 0.25 postulated by Wool's theory. There is an exception, the MQ17-1.7/MQ50-1.0 contact, which shows an anomalously high time exponent of 0.55. The reason behind this sort of behavior is still unclear.

Application of the viscoelastic wetting model for the autohesion data description (see Figure 7-7) yielded some unexpected results. The data for the MQ17-1.7/MQ50-1.0 contact would suggest that the tack formation is diffusion driven – the data do not form a straight line. However, the data for the other investigated contacts form a straight line on the plot. This is especially surprising for the MQ17-1.0/MQ50-1.0 interface, where more diffusion-driven tack formation would be expected. The diffusion should be much easier for the loosely crosslinked network of MQ17 at the $H/V = 1.0$. It is possible that the numerous low molecular weight free chains, present on the surface of MQ17 1.0 sample do not contribute to the interface strength due to lack of entanglement formation, but they could greatly promote viscous wetting. According to Gent¹⁷, the strength of such contacts is primarily governed by the extent of molecular contact, the contributions from interdiffusion may only appear after very long durations of compression.

7.4 CONCLUDING REMARKS

The problem of dissimilar adhesive joints is very difficult to address, mostly because of its complexity. The rubber-steel tack is already relatively well understood, mainly because of its practical importance. The tack of dissimilar rubber-rubber joints poses more of a problem, since additional factors influencing tack are introduced, and the influence sometimes can be hard to interpret. Especially the problem of a governing mechanism arises: is it still diffusion that controls the tack formation?

Rubber-steel tack is obviously driven by viscous wetting, for the lack of possibility of any sort of interdiffusion. It reacts strongly to changes in crosslink density of the rubber samples used. The influence of crosslinker functionality is a little more pronounced, than in the case of autohesive (similar) rubber-rubber tack; but still the reduction in polymer chains mobility does not affect the bonds formation a lot. PDMS chains are already very mobile. The molecular weight of the polymer does have an influence, although not very much; there is no possibility of entanglement formation.

The time dependence of dissimilar rubber-rubber tack for substrates with different molecular weights and degrees of crosslinking shows some unexpected phenomena. Depending on the specific combination, there can be an induction period of tack development. Its appearance is logical, if the tack formation is diffusion driven, but application of viscous kinetics of wetting also describes the

tack development pretty well. It appears that the contact formation is more controlled by viscous flow than by diffusion, even in cases where interdiffusion would have been expected as based on experience with similar rubber-rubber contacts. The exact mechanism of the dissimilar interface formation requires more in-depth studies, still.

-
- ¹ Vallat M.F, Giami S., Coupard A., *Rubb. Chem Technol.*, 72, 701, 1999.
 - ² Chang R.-J., Gent A.N., *J. Polym. Sci.: Polym. Phys.*, 19, 1619, 1981.
 - ³ Chang R.-J., Gent A.N., *J. Polym. Sci.: Polym. Phys.*, 19, 1635, 1981.
 - ⁴ Kamenskii A.N., Fodiman N.M, Voyutskii S.S., *Vysokomol. soved.*, A11, 2, 394, 1969.
 - ⁵ Wool R.P., *Fundamentals of Adhesion*, L.H. Lee (Ed.), Plenum Press: New York, 1991.
 - ⁶ Gent A.N., Lin C.-W., *J. Adhes.*, 32, 113, 1990.
 - ⁷ Gent A.N., Lai S.-M., *Rubb. Chem Technol.*, 68, 13, 1995.
 - ⁸ van Ooij W.J., *Rubb. Chem Technol.*, 57, 421, 1984.
 - ⁹ Gent A.N., Vondraček P., *J. Appl. Polym. Sci.*, 27, 4357, 1982.
 - ¹⁰ Costin R., Nagel W., Ekwall R., *Rubb. Chem Technol.*, 64, 152 , 1991.
 - ¹¹ Hillborg H., Gedde U.W., *Polymer*, 39, 1991, 1998.
 - ¹² Voyutskii S.S., *Autohesion and Adhesion of High Polymers*, John Wiley & Sons (Ed.), New York, 1963.
 - ¹³ Galliano A., Bistac S., Schultz J., *J. Colloid Interface Sci.*, 265, 372, 2003.
 - ¹⁴ Gillberg G., *J. Adhesion*, 21, 129, 1987.
 - ¹⁵ Yasuda H., Sharma A.K., Yasuda T., *J. Polym. Sci.: Polym. Phys. Ed.*, 19, 1285, 1981.
 - ¹⁶ Dollase T., Wilhelm M., Spiess H.W., Yagen Y., Yerushalmi-Rozen R., Gottlieb M., *Interface Sci.*, 11, 199, 2003.
 - ¹⁷ Gent A.N., Kim A.J., *Rubb. Chem Technol.*, 63, 613, 1990.

Chapter 8

The Influence of Loose and Semi-anchored Siloxane Polymer Chains on the Tack of Crosslinked Silicone Rubber *

“The more I want to get something done, the less I call it work.”
Richard Bach

In this chapter the influence of an addition of non-reactive silicone oil or semi-anchored silicone polymer on PDMS rubber-rubber adhesion is studied. The additive can be considered either a tackifier, or connector molecules, able to cross the interface and entangle. In both cases, it should influence the tack of elastomers. Additional variable is the molecular weight of the additive, which affects the reptation of polymer chains. Polymer-polymer demixing, which is the result of thermodynamic incompatibility of mixed polymers is another factor that influences tack. It causes the free chains to appear at the surface forming a layer of oil, which actually destroys the tack of PDMS samples. The resulting tack phenomena as a function of oil respectively semi-anchored silicone polymer chains, are difficult to interpret due to the transient nature of the polymer reptation: in many cases the polymers have not had sufficient time to obtain equilibrium in interphase crossing, or oil sweats out of the crosslinked polymers, forming a liquid layer between the two phases resulting in a low tack values, due to hydrodynamic wetting alone. This subject needs far more in-depth study to clarify all phenomena.

8.1 INTRODUCTION

As explained in previous chapters, interdiffusion and entanglements of polymer chains are the most important factors responsible for polymer adhesion^{1,2}. Reptating polymer chains may cross the interface and entangle on the other side, thus contributing to the overall interface strength. In the present chapter the

* The work described in this chapter has been presented at Rapra Silicone Elastomers Conference, September 2006, Frankfurt, Germany. This chapter has been submitted for publication to Journal of Applied Polymer Science.

possible role of free, non-attached silicone polymers and of silicone polymer purposely linked to the network on one side only (semi-anchored) on adhesion of crosslinked similar silicone rubber will be highlighted.

8.1.1 POLYMER-POLYMER MISCIBILITY

For most polymers it is thermodynamically unfavorable to form homogenous mixtures with each other³. The necessary requirement for miscibility is:

$$\Delta G = \Delta H - T\Delta S < 0 \quad (8 - 1)$$

where ΔG , ΔH and ΔS are the Gibbs free energy, enthalpy and entropy of mixing, respectively. The contribution of the entropy change for polymers is generally small due to their large molecular weights. On the other hand, the enthalpy change in general is positive for most non-polar polymers; thus the necessary Gibbs energy change is hardly ever negative. The miscibility can be improved by introducing strong interactions between the mixed polymers, which results in a negative specific heat of mixing.

The problem of polymer compatibility on chains interpenetration, and as a result adhesion, was already early investigated by Voyutskii et al.^{4,5}. The adhesion strength of incompatible polymers decreased with the increase in difference in solubility parameters. The polymers were still capable of mutual interdiffusion.

8.1.2 FREE CHAIN DIFFUSION IN PDMS

Due to the common chain structure, PDMS polymer chains can easily penetrate into a crosslinked PDMS matrix. The characterization of the diffusion of different molecular weight PDMS loose chains (oils) into a siloxane matrix led to the following observations:

- the chain penetration is heavily influenced by the network mesh size (crosslink density) and the length of penetrating chains. It is obvious, that the longer the polymer chain, the longer it takes to "crawl" between the obstacles⁶; the penetration depth is lower as well.
- the diffusivity of linear PDMS oil is approximately independent of molecular mass for polymers with molecular weight below the PDMS critical M_e needed to form entanglements⁷.

Silicone oil, due to the very low surface energy of the siloxane liquid, tends to phase separate and diffuse from the bulk to the surface. Depending on the application, this can be a very beneficial or an unwanted phenomenon!

8.1.3 INFLUENCE OF OIL ADDITIVES ON ADHESION OF ELASTOMERS

Depending on the point of view, an oil additive can be considered as a tackifier or as connector molecules. In both cases it promotes adhesion. A tackifier loosens up the entanglement network and so increases the compliance⁸. An excess of additive should be avoided in order not to weaken the rubber. This feature is a function of the molecular weight of the tackifier: if the molecular weight is too high it will act as an incompatible solid, stiffening and strengthening the elastomer but preventing wetting⁹. On the other hand, if it is too low, the tackifier may act as a plasticizer, which to a certain extent promotes tack as well. In addition, tackifiers with bad compatibility with the elastomer or used in large amounts can migrate to the surface, thereby lowering tack¹⁰. Thus, the effect of tackifier addition to a rubber can influence tack either from the side of surface energetics, or by an influence on the bulk viscoelastic properties. The latter is especially important during the bonding stage of a compression test: reduction in modulus (increase in compliance) is reflected in easier viscous flow. That may enable better contact formation in the early stages of the test, and hence increase the rate with which intimate molecular contact is achieved. The influence of a tackifier on the debonding stage is difficult to estimate, since it depends heavily on the type of contact. It was already mentioned, however, that tackifier addition affects the bulk properties, and thus affects energy dissipation processes¹¹.

The effect on surface energy of a tested system is associated with the possibility of migration of the tackifier to the surface of the sample. The effects can vary a lot, since the migrating additive can promote wetting, and thus increase tack, but can also form a layer between the contacting surfaces, effectively lowering tack. Separating the surface energy influence from the bulk effects during tack testing is a very difficult task. The general perception is that a large effect on tack can be expected if the tackifier causes appreciable changes in surface energy. Small changes do not affect the wetting stage, and the change in thermodynamic work of adhesion is too small to influence the debonding force.

The influence of the amount of added tackifier on tack seems to follow a similar trend, not depending on the elastomer and tackifier type: first, tack increases with increasing concentration of tackifier, but after reaching a certain threshold level it starts to go down. Curves of this kind were first noted by Wetzel¹², who interpreted them in terms of a two-phase character of a rubber-tackifier system and the presence of the maximum was attributed to a phase inversion. However, this does not explain similar behaviors noticed in the case of single-phase systems. The effect is there correlated with the influence of the tackifier on the debonding process¹¹.

8.1.4 MOBILE CHAINS BETWEEN TWO RUBBER BLOCKS

The problem of mobile chains connecting two identical rubber blocks and forming a loose bridge has been theoretically investigated by Brochard-Wyart et al.¹³ The single loose bridge is shown in Figure 8-1.

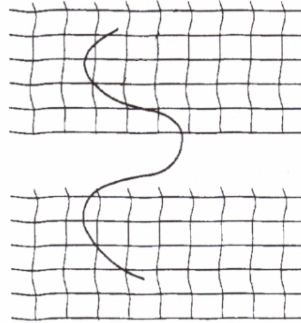


Figure 8-1. The connector molecule between two identical rubber blocks¹³.

Theoretical analysis of such “many stitch” systems shows, that the influence of connector molecules on adhesion or fracture energy can be given:

$$G_f \sim fN_p^{1/2}g \quad (8 - 2)$$

with f being the volume fraction of connectors, N_p their degree of polymerization and g surface tension of a melt of connector molecules. This equation applies only to the regime of very low separation speeds, where the viscoelastic relaxation process near a crack tip is not important.

8.2 EXPERIMENTAL

Materials: The PDMS rubbers MQ17, MQ28 and MQ50 were used for the study. Their specifications are listed in Table 5.1 in Chapter 5 of this thesis. Monovinyl-terminated PDMS, MQ 41, with molecular weight 63 000 g/mol and average vinyl group content 25 mmol/kg was used as an additive. The trifunctional silane was used as crosslinker. The platinum-cyclovinyldimethylsiloxane complex was used as cure reaction catalyst, as described in Chapter 5. Ethyldimethylhydrosilane (monofunctional) was used as end-capping agent. All the above materials were obtained from ABCR, Germany. 1-ethynylcyclohexanol (99%) was used as a temporary reaction inhibitor, as obtained from Aldrich. The solvents used were all of pro analysi quality.

Preparations of unreactive chains: Unreactive siloxane polymer chains with different molecular weights were synthesized through a hydrosilylation reaction of MQ rubbers with monofunctional silane. A 5% excess over a stoichiometric amount of silane was added to a flask containing vinyl-terminated PDMS polymer. Then 10 ppm of catalyst was added and the reaction mixture was heated to 120 °C and allowed to react, while constantly stirred. The extent of hydrosilylation reaction was checked periodically using NMR and IR. The disappearance of NMR vinyl peaks (δ 5.6 – 6.2ppm) was used as an indication of full polymer conversion. The IR silane peak at around 2160 cm^{-1} was used to

check if there was still silane present. If so, the mixture was stirred further, until the leftover silane groups were oxidized, so that they could not interfere with the subsequent crosslinking reaction anymore.

Loose chains samples preparation: Crosslinked samples were based on MQ17 with H/V ratio of 1.7 as a matrix. This composition ensures that the PDMS matrix does not have any detectable tack by itself, and thus does not interfere with measurements, as shown in Chapter 5. Before the curatives, unreactive loose chains were added to the prepolymer in amounts ranging from 5 to 120 phr. It was impossible to make samples with higher quantities of loose chains, because these samples did not cure anymore. Then the curatives were mixed together with the polymer and unreactive chains using a magnetic stirrer. During the preparation it was important, that the inhibitor was added to the reaction mixture before the catalyst. Without the presence of the inhibitor, the cure reaction proceeded quickly even at room temperature. While the amount of crosslinker varied depending on the vinyl group content (VGC) of the polymer used, the amounts of catalyst and inhibitor were kept constant: 10 and 50 ppm, respectively. The mixture was degassed and cured in a compression molding machine (WLP 1600/5x4/3 Wickert laboratory press) at 120°C for 30 min. Clean Teflon foil was placed between the cured mixture and the mold plates to avoid surface contamination and sticking of the material to the mold. The resulting 90x90x2 mm sheets were post-cured in an oven at 120°C for 48 hours.

Preparation of samples with monofunctional chains: Samples with embedded monofunctional chains were prepared in a similar way as samples with embedded unreactive loose chains. The amount of crosslinker was adjusted based on the amount of monofunctional prepolymer added, so the H/V ratio was always kept constant at 1.7.

Tack measurements: Samples were compressed under a load of 2.5 N for 10 minutes. For each sample, several tack measurements were done and the average was taken as the final result. The measurements were always performed at room temperature. The separation speed was constant at 4 mm/sec.

Crosslink density: Crosslink density measurements were made by swelling the rubber samples in toluene for 48 hours; calculations were performed using the well-known Flory-Rehner equation¹⁴:

$$n = \frac{cv_r^2 + \ln(1 - v_r) + v_r}{V_0(0.5v_r - v_r^{1/3})} \text{ [mol/cm}^3\text{]} \quad (8 - 3)$$

where v is the crosslink density, v_r is the equilibrium volume fraction of rubber in the swollen state and V_0 is the molar volume of the solvent. A polymer-solvent interaction parameter χ of 0.456¹⁵ was used for all calculations.

DSC measurements: DSC measurements were performed using a Perkin-Elmer DSC 7 machine with Pyris version 8.0 software. Samples weighing ca 10 mg were put into aluminum pans, cooled rapidly to -170 °C from room temperature and then heated at 10 °C/min.

8.3 RESULTS

8.3.1 THE INFLUENCE OF LOOSE PDMS CHAINS ON TACK

Figure 8-2 shows how the amount of blocked, unreactive chains derived from MQ17 influences the tack and crosslink density of silicone rubber samples. These chains cannot react with the crosslinker and remain loosely embedded in the otherwise crosslinked matrix of MQ17.

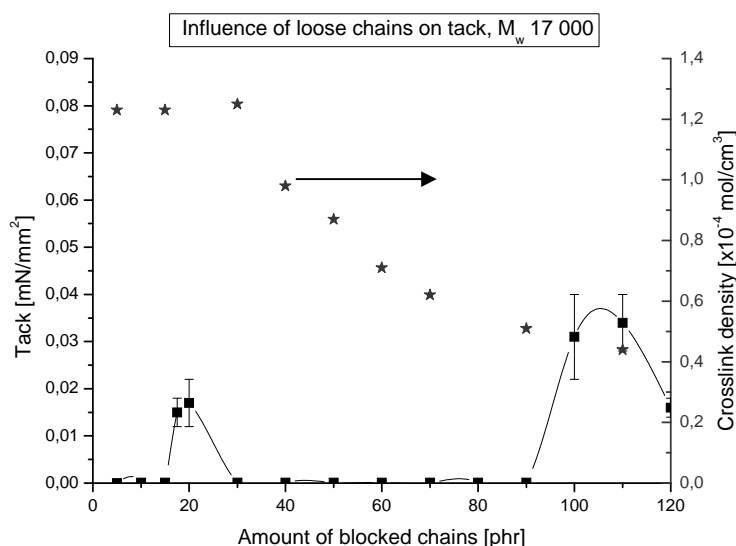


Figure 8-2. The influence of the amount of loose chains on the PDMS rubber tack. M_w of loose chains: 17 000 g/mol. The line is intended to guide the eye.

A small addition of blocked chains does not have any influence on the MQ17 samples tack. When the amount of loose silicone molecules or oil reaches 15 phr, the rubber starts to show some detectable tack, however still very low. If the amount of silicone oil in the samples is further increased, the tack disappears again. When the amount of loose chains reaches 100 phr, i.e. 50 weight % of the sample, the rubber-rubber tack rises again, with values higher than previously measured. Above 110 phr of silicone oil added, the tack starts to decrease again. It is important to note, that samples having more than 100 phr of silicone oil were already gel-like, and the addition of more than 120 phr of oil resulted in complete inability of the samples to crosslink.

The first detectable tack appears in a region, where the crosslink density of the samples is stable and does not change with the increasing amount of oil additive. It starts to decrease only after the amount of loose siloxane chains exceeds 30 phr. The decrease is very pronounced at the beginning, and then crosslink density lowers down slower. Crosslink density of the highest oil-containing sample was impossible to measure, because the sample almost dissolved during swelling.

Figure 8-3 shows the influence of the molecular weight of the loose chains and their amount on the tack of a network based on MQ17.

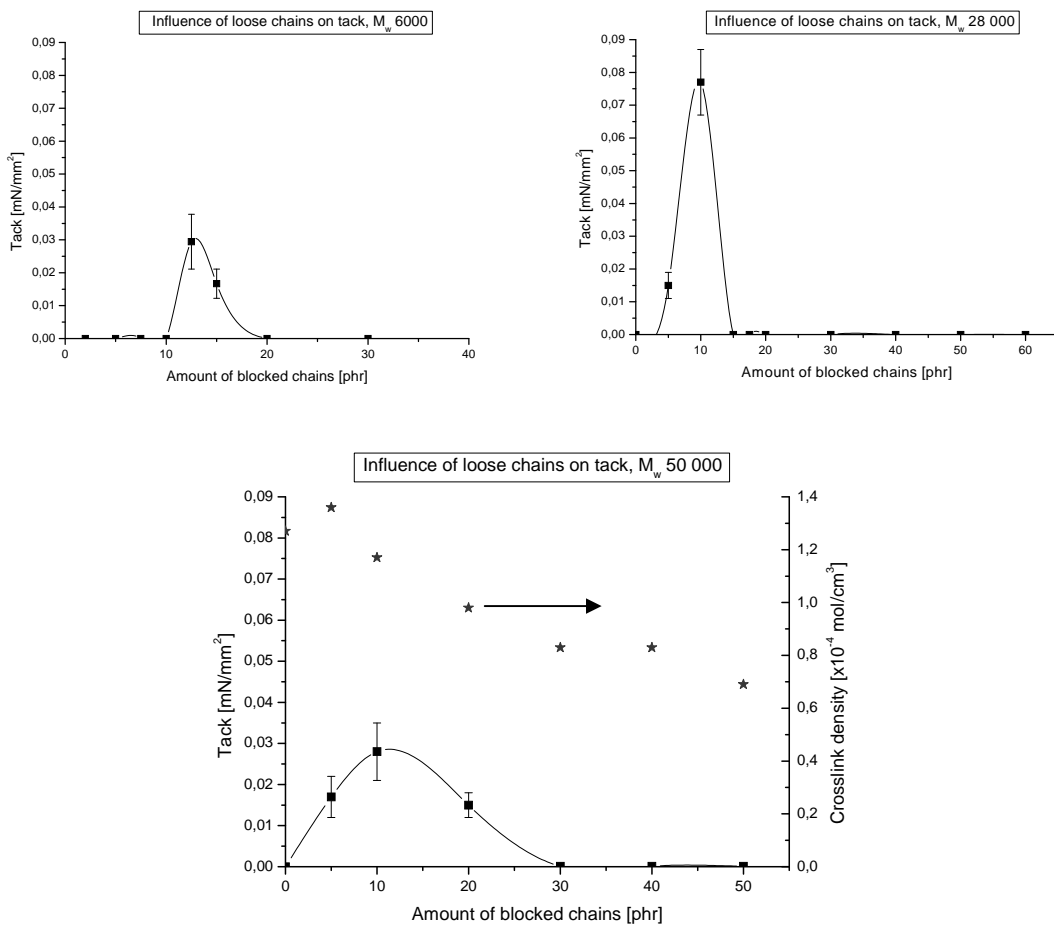


Figure 8-3. The influence of the amount of loose chains and their molecular weight on the PDMS rubber tack. The lines are intended to guide the eye.

As can be seen, the addition of very low molecular weight loose PDMS chains MQ6, also promotes tack, at a similar level as MQ17-based loose chains. However, the tack increase happens at a higher amount of additive than is in case for MQ17-based loose chains. Besides that, the picture is similar: the tack rises at a certain amount of loose silicone oil added and later goes down to zero

again. The addition of blocked loose MQ28-based chains results in much higher absolute levels of tack achieved, as well as in a shift to smaller amounts of oil needed to achieve that tack. After that, like in the two previous cases, tack lowers down to zero after a certain amount of oil is embedded in the samples. It is interesting, that the tack after addition of blocked MQ50-based chains is much lower than after addition of MQ28-based chains. The maximum also spans a broader range of additive amounts.

Crosslink density measurements were also performed for the samples with addition of MQ50-based blocked chains. The trend is the same as in the case of MQ17-based chains: the crosslink density initially stays constant, but this period is much smaller than in the case of MQ17-based loose chains addition. Actually, there is a small increase in crosslink density after some MQ50-based loose chains were added, but most probably this is a reflection of an increased amount of physical entanglements. The increased tack region already coincides with the area of decrease in overall crosslink density of the tested samples.

8.3.2 THE INFLUENCE OF SEMI-ANCHORED PDMS CHAINS ON TACK

Figure 8-4 shows the influence of the addition of semi-anchored, monofunctional PDMS chains of M_w 63 000 on tack of MQ17 samples.

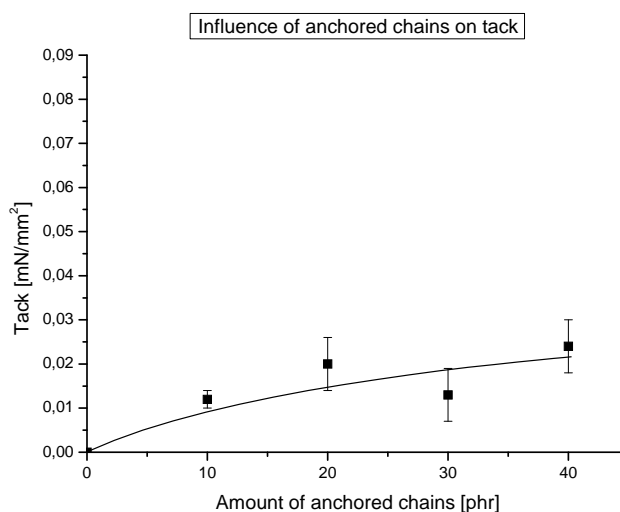


Figure 8-4. The influence of the amount of semi-anchored chains of M_w of 63 000 on the PDMS rubber tack. The line is intended to guide the eye.

The tack of samples with some amount of monofunctional PDMS chains added behaves in a different way than the tack of samples with loose PDMS chains. In the range measured, the tack rises slowly but steadily with the addition of monofunctional chains, and seems to reach a plateau after 30 phr are added.

The values of tack are very low, lower than the tack of samples with MQ6 chains added, however still detectable.

8.3.3 THE INFLUENCE OF LOOSE PDMS CHAINS ON TACK – OVERVIEW

The influence of addition of loose chains is better visible in Figure 8-5, where the amount of loose chains was recalculated from phr to mmol, on basis of the initial average vinyl-group content of the blocked chains.

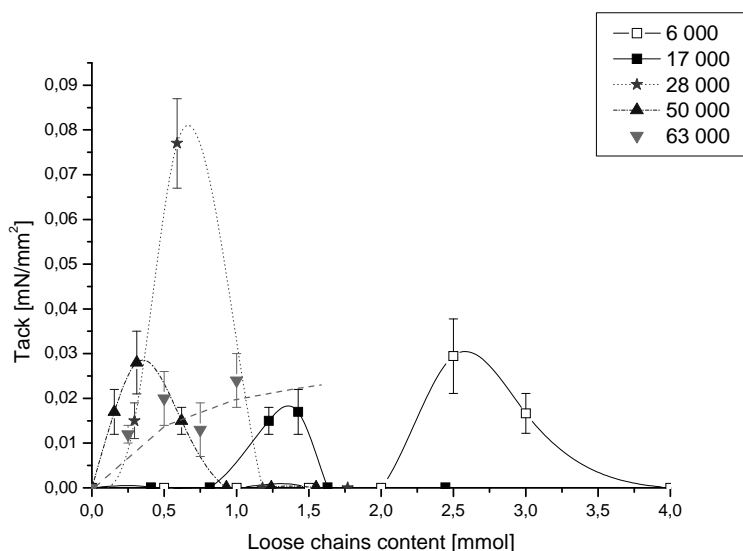


Figure 8-5. The tack as a function of amount of blocked loose chains – an overview. The lines are intended to guide the eye.

The shorter the chains are, the more is needed to induce tack. For $M_w = 6\ 000$ tack starts to appear at around 2.5 mmols addition. This point shifts to 1.3 mmols for the molecular weight of 17 000, 0.7 for 28 000 and 0.4 for 50 000 molecular weight. The semi-anchored, monofunctional chains addition works slightly different: the tack shows up at 0.25 mmols of chains added and then rises slowly with the amount of monofunctional chains in the sample.

Figure 8-5 also clearly shows the differences in tack caused by the addition of different molecular weights of the blocked chains. The effect of MQ6 and MQ17 is similar, even slightly larger for MQ6. MQ28 addition causes a relatively large tack increase, and the tack caused by the addition of MQ50 is again small, on the level of MQ6.

8.3.4 DSC

On the DSC curves of samples with blocked chains two glass transition temperatures are commonly present, at around -150°C and -120°C . The first one

corresponds to the glass transition temperature of a siloxane prepolymer, the second one then should be the glass transition of the cured PDMS matrix¹⁶.

The dependence of the transitions on the amount of blocked MQ17 chains in the polymer matrix is shown in Table 8.1. The dash indicates the spectra, where the presence of a T_g could not be unequivocally detected.

Table 8.1: Glass transition temperatures for the samples with MQ17-based blocked chains added.

Amount of blocked MQ17 chains [phr]	T_{g1}	T_{g2}
0	none	-90
10	-148	-112
20	-148	-120
30	-142	-
50	-148	-120
60	-150	-120
70	-148	-122
80	-145	-122
90	-145	-120
100	-	-120

The lower T_g does not depend on the amount of blocked chains added in the samples, but the higher T_g shifts suddenly upon the addition of loose chains from -90 °C for the fully crosslinked MQ17 sample without any additive, to -112 °C for only 10 phr of blocked chains added, and further to -120 °C for 20 phr of unreactive chains. Further increase in the amount of additive did not cause a substantial T_g shift.

8.4 DISCUSSION

The addition of free, not crosslinkable chains to the PDMS matrix does influence the tack of the crosslinked polymer. Figure 8-2 shows, that this influence can be divided into two regions: the tack rises, disappears and rises again. The second tack maximum appears at more than 50 wt% addition; at this point the non-crosslinkable siloxane oil addition has substantially loosened the polymer network already. It should be noted, that the preparation of samples resembles the preparation of polymer gels, with the unreactive chains acting as a solvent. The tack increase after a large addition of loose chains results in a large decrease in crosslink density, thus decrease in the sample's modulus. The resulting tack is a combined effect of viscoelastic flow and a heavily diluted network.

The first maximum in tack is far more interesting. The addition of uncrosslinked siloxane chains can work in two ways: one is already mentioned as diluting the

crosslinked network, what is usually combined with a decrease in segmental friction⁸, so that the chains can much easier penetrate and entangle. This is the general effect of a tackifier. The second mechanism is an increased amount of free chains, which can diffuse through the interface and entangle on the other side, thus increase tack.

The important factor to take into account is the critical molecular mass of PDMS, above which it can only form entanglements. The borderline for PDMS seems to be a molecular weight of around sixteen thousands¹⁷. Thus MQ6 should be completely unable to form entanglements and MQ17 is a borderline case. It can be seen in Figures 8-2 and 8-3, that both of them still promote tack, when added in small amounts to the crosslinked PDMS samples. Since none or just very few entanglements can be formed, this should be an effect of network loosening.

With the increase of molecular weight of the uncrosslinked chains the tack first increases for MQ28 and then decreases again for MQ50: see Figure 8-5. This may seem contradictory at first glance, but there are several aspects to take into account. First of all, the MQ28 polymer is the first one from the series tested that can form entanglements. This explains the almost threefold increase in tack. Following the same reasoning, addition of MQ50 chains should increase the tack even more. However, their molecular weights differ by a factor of 1.8 in comparison with MQ28. If it is assumed, that a chain reptation is the factor responsible for the tack increase, then MQ50 chains would need 5.8x more time to achieve a similar level of interpenetration, since the reptation time scales with the third power of molecular mass of the polymer¹⁸. Thus, on the timescale of the experiment, the MQ50 chains may not have had sufficient time to reptate and entangle to their full extent.

The addition of monofunctional semi-anchored PDMS chains also promotes tack. Still, the situation here is slightly different from the case of free, uncrosslinked chains. Monofunctional chains are anchored to the polymer matrix at least on one side; the interdiffusion or reptation will therefore be seriously hampered, which is visible in Figure 8-4. The tack detected is very low, lower than the MQ17 addition effect. However, even an addition of a small amount of anchored chains gives a detectable tack as a result, which rises with increasing quantity of the additive. The molecular weight of the monofunctional PDMS can be partially responsible for this effect; the monofunctional chains have a M_w of 63 000, even larger than for MQ50.

The effect is better visible in Figure 8-5, where the amounts of additives were recalculated to milimols of chains, on the basis of the average vinyl group content of the blocked and monofunctional polymer. The amount of MQ6 chains needed to induce tack is far larger than the amount of MQ17 chains. This may actually explain the higher tack after MQ6 addition: the possible network dilution is larger. With the increase in molecular weight of the additive, the tack maximum shifts towards lower amounts of blocked polymer chains. Starting from the MQ17,

PDMS chains are able to entangle; the longer the chain, the more entanglement formation is possible. Figure 8-5 illustrates the difference between anchored chains and loose chains as well. Addition of loose chains causes a sharp increase, and then decrease in tack, whereas tack created by anchored chains rises slowly.

The question remains, why there is a sudden tack decrease after the addition of loose chains. If we consider the mixing of two polymers, as it was described in the introduction, we may see that the enthalpy of mixing, DH , will be most probably close or equal to zero: both polymers are essentially the same poly(dimethyl)siloxane. The change in entropy, however, can be large and negative. The loose chains are restricted in their mobility after being embedded in the crosslinked matrix. Thus, the overall change in Gibb's free energy of mixing will be positive – the system will tend to demix and PDMS uncrosslinked chains will diffuse to the surface of the samples. This phenomenon can be even promoted by the testing procedure, where samples stay under compression for a certain period of time. PDMS oil will then gather on the surface forming a layer of liquid with a very low surface tension. As a result, the tack disappears when more uncrosslinked chains are added. Anchored chains, due to the fact that they are crosslinked to the matrix on one side, cannot demix. They may only be able to partially migrate to the surface.

The DSC data confirm the fact, that the systems containing uncrosslinked PDMS chains embedded in the crosslinked PDMS matrix are immiscible. If they were fully miscible, the presence of only one T_g should be expected. On most of the curves two glass transition temperatures are present, a proof of phase separation¹⁹.

It should be noted, that the tack of systems with free, uncrosslinked chains purposefully added to crosslinked matrix is a complicated phenomenon. The polymer-polymer demixing, and as a result oil gathering on the surface of samples, is an unavoidable factor which is in addition hard to quantify. The molecular weight-tack dependence of these chains needs far more in-depth study to fully understand the mechanism of tack formation.

8.5 CONCLUDING REMARKS

The addition of uncrosslinked and mobile siloxane chains to a crosslinked PDMS matrix influences rubber-rubber tack to a small extent. The increase is quite small and visible only for minor quantities of the additive. Further addition of uncrosslinked chains results in a tack reduction. The tack is influenced by the molecular weight of the loose chains – the higher, the less material is needed to induce tack. This dependence is more complicated: increase in molecular weight causes first a tack increase, then a decrease again. This effect is most probably caused by the timescale needed for the chains to reptate and entangle.

The tack disappearance at large amounts of mobile chains added is caused by migration of the PDMS oil to the samples' surface and the formation of a liquid layer. Because of this layer, two sides of the interface cannot come into direct, molecular contact, and further interface strengthening is then restricted. This problem does not exist if the chains are somehow attached to the matrix. The addition of monofunctional, semi-anchored PDMS polymer that can be vulcanized with the network does not seem to cause such a layer formation.

- ¹ Wool R.P., *Fundamentals of Adhesion*, L.H. Lee (Ed.), Plenum Press: New York, 1991.
- ² Prager S., Tirrell M., *J. Chem Phys.*, 75, 5194, 1981.
- ³ Kammer H.W., *Acta Polym.*, 34, 112, 1983.
- ⁴ Voyutskii S.S., *Autohesion and Adhesion of High Polymers*, John Wiley & Sons (Ed.), New York, 1963.
- ⁵ Kamenskii A.N., Fodiman N.M., Voyutskii S.S., *Vysokomol. Soyed.*, A11, 394, 1969.
- ⁶ Mazan J., Leclerc B., Galandrin N, Couarraze G., *Eur. Polym J.*, 8, 803, 1995.
- ⁷ Gedde U.W., Hellebuych A., Hedenqvist M., *Polym Eng Sci.*, 36, 2077, 1996.
- ⁸ Kraus G., Rollmann K.W., Gray R.A., *J. Adhesion*, 10, 221, 1979.
- ⁹ Gent A.N., Hamed G.R., *Elastomer Technology – Special Topics*, ACS Rubber Division, Akron Ohio, 2003.
- ¹⁰ Hamed G.R., Roberts G.D., *J. Adhesion*, 47, 95, 1994.
- ¹¹ Aubray D.W., *Rubb. Chem Technol.*, 61, 448, 1988.
- ¹² Wetzel F.H., *Rubber Age*, 82, 291 1957.
- ¹³ Brochart-Wyart F., De Gennes P.G., Léger L., Marciano Y., Raphael E., *J. Phys. Chem.*, 98, 9405, 1994.
- ¹⁴ P.J. Flory, J. Rehner, *J. Chem Phys.*, 521, 11, 1943.
- ¹⁵ Hild G., *Prog Polym Sci.*, 23, 1019, 1998.
- ¹⁶ Urayama K., Yokoyama K., Kohjiya S., *Polymer*, 41, 3273, 2000.
- ¹⁷ Orrah D. J., Semlyen J. A., *Polymer*, 29, 1452, 1988.
- ¹⁸ Wool R.P., *Rubber Chem. and Technol.*, 57, 307, 1984.
- ¹⁹ Lorentz G., Blanc D., Odoni L., *Silicone elastomer gels for medical devices: viscoelasticity and performance* Proceedings of RAPRA Silicone Elastomers, Frankfurt, Germany, 19-20 September 2006

Chapter 9

Summary and Final Remarks

"He's beginning to believe"
Morpheus, *Matrix the movie*

This chapter provides a summary of the work done and described in the thesis. Some final remarks, and suggestions for future research are given.

9.1 THE RESEARCH

The objective of this work was to investigate the relationship between different factors characterizing the network structure on the tackiness of silicone rubber (PDMS). A custom tack testing device was constructed, based on the existing Tel-Tak principle. The experimental work involved testing the tack of silicone rubber in relation to crosslink density and type of contact, the development of tack with time of contact in relation to the molecular weight of the polymer, and the influence of loose, uncrosslinked polymer chains embedded in the crosslinked network.

9.2 GENERAL SUMMARY

Chapter 1 gives a general introduction into the problem of elastomer tack, while **Chapter 2** provides the necessary theoretical background, as well as the various descriptions in literature of the mechanisms behind the creation of tack and the models in use for the interpretation of experimental data. Special attention is devoted to the diffusion tack theory of Wool, based on the polymer reptation model of deGennes, as the main model on basis of which the experimental results in this thesis are interpreted. A brief overview of the alternative Hertz and Johnson, respectively Kendall and Roberts (JKR) theories of elastic contact is given at the end of **Chapter 2**.

Chapter 3 gives a description of the synthesis and properties of siloxane polymers, including the methods of crosslinking. Then the NMR methods, which are used for polymer characterization, are described. Every batch of silicone material needs a vinyl-group content determination in order to establish the

required stoichiometric amount of crosslinker, with different functionalities, to obtain well defined telechelic networks. The fastest and simplest method for this is an NMR measurement, with an internal standard.

Chapter 4 provides a general introduction into methods of tack testing, in the first part. The second part describes the design and construction of the custom tack testing device used in this thesis. The main motivation was to build a simple, yet effective tool capable of accurately recording separation forces in the range of millinewtons, which is required since PDMS rubber exhibits inherently very low tack.

Chapter 5 describes the influence of polymer molecular weight, crosslink density and crosslinker functionality on PDMS rubber-rubber tack. The telechelic PDMS, containing crosslinking sites only on the chains ends, is a very good material for preparation of well-defined networks. Crosslink density and crosslinker functionality strongly influence the amount of loose chains that are left uncoupled in a sample, and the molecular weight of the PDMS its ability to form entanglements. The PDMS with very low molecular weight hardly exhibits any detectable tack, no matter the crosslink density. The tack rises very quickly with increase in molecular weight of the PDMS; on the other hand, a high functionality of the crosslinker used favors low tack.

Chapter 6 describes the development in time of the autohesive behavior of loosely crosslinked PDMS rubber networks. The autohesion data are gathered for PDMS with different molecular weights. The influence of molecular weight of the polymer is very pronounced. The data are interpreted on basis of the WooldeGenes reptation theory; the application of first order kinetics of wetting is also tested. PDMS with a molecular weight only partially permitting to form entanglements, exhibits a remarkably different and unusual behavior compared to the high molecular weight polymers. The latter develop tack in the form of logarithmic type curves, while the former show the presence of local maxima in the tack-time curves.

In **Chapter 7** the use of steel and PDMS with varying molecular weight and crosslink density as contacting substrates is described. The tack depends heavily on the type of contact, thus the range of observed behaviors is large. Rubber-steel tack is generally lower than rubber-rubber autohesive tack, due to the inability of polymer chains to interpenetrate the interface. Tack of PDMS against PDMS with dissimilar levels of crosslinking strongly depends on the crosslink levels of the contacting sides. The tack-time dependencies differ from the ones studied in Chapter 6; the behavior is much more complicated, with the presence of induction periods during which tack develops slowly.

In **Chapter 8** the influence of addition of non-reactive silicone oil of various molecular weights on tack is described. These additives can be considered either a tackifier or so-called “connector molecules”, and as such should be able to cross the interface and entangle to promote tack. This turns out to be true only to certain extent, since thermodynamic incompatibility causes the silicone oil to migrate to the surface of the samples, actually causing tack to disappear. The molecular weight of the loose chains influences the tack: the

tack rises with increase in molecular weight of the additive, but then goes down again, which is most probably an effect of the increase in time needed for the high molecular weight polymers to fully reptate.

9.3 FINAL REMARKS AND SUGGESTIONS FOR FURTHER RESEARCH

The tack of elastomers is a very broad subject, especially because of the number of factors that can possibly influence it. Some of them are quite well-known and there was a lot of work devoted to them already, like the development of tack with contact time. Some other areas are still mostly uncovered, however. Chapter 7 contains an investigation into dissimilar rubber-rubber contacts. Although the subject of rubber-steel contacts has been extensively studied, the rubber-rubber joints with dissimilar degrees of crosslinking pose a future challenge, especially the tack-time dependence.

The research described in Chapter 8 only touched a very broad subject as well in a preliminary way. The studies of semi-anchored, monofunctional chains additions could add a lot to the understanding of the mechanisms of tack formation. It would be necessary to prepare monofunctional PDMS chains with different molecular weights, and then study the tack as a function of the network structure of the samples.

The research in this thesis has again demonstrated, that tack of rubber is a complicated phenomenon. Thanks to some theoretical treatments of e.g. Wool, a reasonable understanding of the phenomena can be developed. However, due to the extreme molecular weight dependence of the overall reptation time of polymers, time restrictions do not permit testing after equilibrium in reptation has been reached. Consequently, one measures transient phenomena, catching a certain tack level somewhere in its development in time, particularly for the higher molecular weight polymers. I do express the hope, that with the work described in this thesis the understanding of the underlying mechanisms for tack has been increased. Far more in-depth study will be required to (hopefully) once fully understand the mechanism of tack formation with rubber.

Samenvatting en afsluitende opmerkingen

Dit hoofdstuk geeft een samenvatting van het werk dat beschreven is in dit proefschrift. Enkele afsluitende opmerkingen en suggesties voor toekomstig onderzoek worden gegeven.

HET ONDERZOEK

Het doel van dit werk was het onderzoeken van de relatie tussen verschillende factoren, die de netwerkstructuur en de 'tack' van siliconenrubber (PDMS) karakteriseren. Een speciaal tack test apparaat werd ontworpen, gebaseerd op het bestaande Tel-Tak principe. Het experimentele werk omvatte het testen van de tack van siliconenrubber in relatie tot de crosslink dichtheid en het type contact, de ontwikkeling van tack als functie van de contacttijd en in relatie tot het molecuulgewicht van het polymeer, en de invloed van losse, niet gecrosslinkte polymeerketens ingebed in het gecrosslinkte netwerk.

ALGEMENE SAMENVATTING

Hoofdstuk 1 geeft een algemene introductie in tack van elastomeren, en hoofdstuk 2 geeft de vereiste theoretische achtergrond, als ook de verschillende beschrijvingen in de literatuur van de mechanismen achter de totstandkoming van tack en de modellen die gebruikt worden voor de interpretatie van experimentele gegevens. Speciale aandacht wordt besteed aan de diffusie-theorie van Wool, gebaseerd op het polymeer-reptatie model van deGennes. Op basis van dit model worden de experimentele resultaten van dit proefschrift geïnterpreteerd. Een kort overzicht van de alternatieve Hertz en Johnson, respectievelijk Kendall en Roberts (JKR) theoriën van elastisch contact wordt gegeven aan het einde van hoofdstuk 2.

Hoofdstuk 3 geeft een beschrijving van de synthese en eigenschappen van siloxaan-polymeren, inclusief de methoden om ze te vernetten: crosslinken. Vervolgens worden de NMR-methoden, gebruikt voor polymeerkarakterisering beschreven. Elke batch siliconen vereist bepaling van het vinyl-gehalte om de benodigde stoichiometrische hoeveelheid crosslinker, met verschillende functionaliteiten, te kunnen bepalen, teneinde een goed gedefiniëerd 'telechelic' netwerk te kunnen bereiden. De snelste en simpelste methode hiervoor is een NMR-meting met een interne standaard.

Het eerste deel van hoofdstuk 4 geeft een algemene introductie van de methoden om de tack te meten. Het tweede deel beschrijft het ontwerp en constructie van een speciaal tack test apparaat, dat gebruikt wordt in dit proefschrift. De belangrijkste motivatie was het bouwen van een eenvoudig maar effectief apparaat, dat in staat is om nauwkeurig de scheidingskrachten te meten in de orde grootte van milli-Newtons. Dit is nodig, omdat PDMS rubber een inherent lage tack bezit.

Hoofdstuk 5 beschrijft de invloed van het molecuulgewicht van het PDMS-polymeer, de crosslink dichtheid en de crosslink functionaliteit op de PDMS rubber-rubber tack. De 'telechelic' PDMS, die alleen op de uiteinden van de ketens crosslinking sites bezit, is een erg goed materiaal om goed gedefinieerde netwerken te verkrijgen. De crosslink dichtheid en crosslink functionaliteit beïnvloeden in sterke mate de hoeveelheid losse keteneinden, die niet gekoppeld zijn binnen een monster, en het molecuulgewicht bepaalt de mogelijkheid om verstrengelingen te vormen. PDMS met een heel laag molecuulgewicht laten een nauwelijks waarneembare tack zien, ongeacht de crosslink dichtheid. De tack stijgt zeer snel met het molecuulgewicht van de PDMS; aan de andere kant, een hoge functionaliteit van de gebruikte crosslinker geeft een tendens naar lage tack.

Hoofdstuk 6 beschrijft de ontwikkeling in de tijd van het autohesieve gedrag van licht gecrosslinkte PDMS rubber netwerken. De autohesie gegevens zijn verzameld voor PDMS met verschillende molecuulgewichten. De invloed van molecuulgewicht van het polymeer is weer erg groot. De resultaten worden geïnterpreteerd op basis van de Wool-deGennes reptatie theorie; de toepassing van de eerste orde kinetiek van benetting is ook getest. PDMS met een laag molecuulgewicht, dat alleen gedeeltelijke verstrengeling toestaat, vertoont een opmerkelijk verschillend en ongebruikelijk gedrag vergeleken met de polymeren met een hoog molecuulgewicht. De laatste ontwikkelen tack in de vorm van logaritmische curves, terwijl de eerste lokale maxima bevatte in de tack-tijd curves.

In hoofdstuk 7 wordt het gebruik van staal en PDMS met variërende molecuulgewicht en crosslink dichtheid als contact substraten beschreven. De tack hangt in grote mate af van het type contact, daarom is het scala aan waarnemingen groot. Rubber-staal tack is in het algemeen lager dan rubber-rubber tack, doordat de polymeerketens niet door het grensvlak kunnen diffunderen. De tack van PDMS tegen PDMS met verschillende crosslink niveaus hangt sterk af van de mate van crosslinking van de beide contactoppervlakken. De tack-tijd relaties verschillen van die van hoofdstuk 6; het gedrag is veel gecompliceerder, door de aanwezigheid van inductieperioden, waarin de tack zich langzaam ontwikkelt.

In hoofdstuk 8 wordt de invloed beschreven van de toevoeging van niet-reactieve siliconenolie met verschillende molecuulgewichten op de tack. Deze toevoegingen kunnen opgevat worden als tack-vergroeters of als verbindingsmoleculen, die als zodanig in staat zouden moeten zijn door het grensvlak te diffunderen en zo aan beide kanten verstrengelingen te vormen om zo de tack te verhogen. Dit blijkt maar gedeeltelijk te kloppen, omdat door

de thermodynamische incompatibiliteit de siliconenolie naar het oppervlak van de monsters migreert, en zo de tack verlaagt. Het molecuulgewicht van de losse keteneinden beïnvloedt de tack: de tack neemt toe met toenemend molecuulgewicht van de toevoeging, maar neemt dan weer af, wat waarschijnlijk een gevolg is van de toename in tijd die nodig is voor de polymeren met een hoog molecuulgewicht om volledig te repteren.

AFSLUITENDE OPMERKINGEN EN SUGGESTIES VOOR VERDER ONDERZOEK

Tack van elastomeren is een erg breed onderwerp, vooral door het aantal factoren, die deze kunnen beïnvloeden. Enkele van deze invloeden zijn bekend en veel werk was er al aan gewijd, zoals de ontwikkeling van tack met de contacttijd. Enkele andere gebieden zijn nauwelijks onderzocht. Hoofdstuk 7 bevat een onderzoek naar ongelijk rubber-rubber contact. Hoewel het onderwerp rubber-staal contact uitgebreid onderzocht is, vormen rubber-rubber contacten met ongelijke crosslink niveaus een uitdaging voor de toekomst, vooral de tack-tijd afhankelijkheid.

Het onderzoek beschreven in hoofdstuk 8 stipt ook slechts een breed onderwerp aan. Studies van toevoegingen van half-verankerde, monofunctionele ketens als toevoegingen, zouden een grote bijdrage kunnen leveren aan het begrip van de mechanismen van het ontstaan van tack. Het vereist om monofunctionele PDMS ketens te bereiden met verschillen molecuulgewichten, en vervolgens de tack te bestuderen als functie van het netwerkstructuur van de monsters.

Het onderzoek in dit proefschrift heeft wederom aangetoond, dat de tack van rubber een gecompliceerd verschijnsel is. Dank zij enkele theoretische beschouwingen van bijvoorbeeld Wool, kan een redelijk begrip worden verkregen van deze fenomenen. Echter, door de extreme invloed van het molecuulgewicht op de reptatietijd van polymeren, laten de tijdsrestricties niet toe te testen tot evenwicht in reptatie is bereikt. Daardoor worden slechts overgangsfenomenen gemeten, bij enkele niveaus van tack ergens in de ontwikkeling in de tijd, vooral voor de polymeren met een hoog molecuulgewicht.

Ik druk de hoop uit dat het werk beschreven in dit proefschrift het begrip vergroot heeft van de onderliggende mechanismen van tack. Veel meer studies in de diepte zijn vereist om ooit (hopelijk) een volledig begrip te verkrijgen van het mechanisme van het ontstaan van tack in rubber.

Symbols and definitions

Symbols in Latin alphabet

Symbol	Definition	Unit
ΔG_{12}^a	energy change per unit area	$\text{J}\cdot\text{m}^{-2}$
$\langle X_{cm}^2 \rangle$	mean square center of mass diffusion distance	\AA^2
$E_N^{(0)}$	plateau modulus	MPa
\dot{c}	crack propagation rate	$\text{m}\cdot\text{s}^{-1}$
$\langle l^2 \rangle$	mean square length of escaped chain	\AA^2
$\langle X^2 \rangle$	mean square monomer displacement	\AA^2
a_0	Hertzian contact zone radius	m
a_T	WLF shift factor	-
A_{tot}	total area of contact	m^2
b	monomer length	\AA
D	diffusion coefficient	$\text{m}^2\cdot\text{s}^{-1}$
d	separation distance	m
D_1	curvilinear diffusion coefficient	$\text{m}^2\cdot\text{s}^{-1}$
D-1	Delay after pulse.	sec
DE	-	μsec
DS	Number of dummy scans	-
E	Young's modulus	MPa
e	the tensile strain of the sample after detachment	%
f	force	N
F	peel force	N
f_n	number of elastically effective chains per unit volume	-
G	elastic modulus	MPa
G_f	fracture energy (∞ - in equilibrium state)	$\text{J}\cdot\text{m}^{-2}$
h	peeling strip thickness	m
I_{pyr}	integration of pyrazine ^1H NMR signals	-
I_{vinyl}	integration of vinyl ^1H NMR signals	-
J	compliance	$\text{m}\cdot\text{N}^{-1}$
K	combined elastic modulus	MPa
k_1, k_2	elastic constants	MPa
l	chain segment length	\AA
$l(t)$	average interpenetration depth	\AA
l_∞	average interpenetration depth after reaching equilibrium conditions	\AA
LB	Line broadening	Hz

l_p	average length of a molecular bridge	Å
$l_{p,\infty}$	average length of a molecular bridge after reaching equilibrium conditions	Å
M	molecular mass	g/mol
M_e	molecular mass between the entanglements	g/mol
m_{PMDS}	mass of PDMS in a sample	g
m_{pyr}	mass of pyrazine in a sample	g
n	number of effective chain crossings	-
N	overall number of asperities on a surface	-
$n(t)$	number of chains intersecting the interface	-
n_∞	number of chains intersecting the interface after reaching equilibrium conditions	-
n_c	number of asperities contacts on a surface	-
N_e	number of monomers between entanglements	-
N_p	degree of polymerization	-
NS	Number of scans	-
N_v	number of chains per unit volume	-
$O1p$	Center of spectrum	ppm
P	pressure	Pa
$p(t)$	number of bridges intersecting the interface	-
$P0$	Pulse	deg
p_∞	number of bridges intersecting the interface after reaching equilibrium conditions	-
P_p	pull-out force	N
P_{tot}	total load	N
R	radius of curvature	m
R_c	radius of contact area	m
R_{ct}	rate of contact formation	
R_i	rate of interdiffusion	
R_{s1}, R_{s2}	Herzian radii of spheres	m
R_{sep}	separation rate	
s	standard deviation	
S_0	undeformed area	m ²
SI	Datapoints spectrum domain	K
SWH	Sweep width	Hz
t	time	sec
T	absolute temperature	sec
t_c	contact time	sec
TD	Datapoints time domain	K
t_e	time to equilibrium	s
t_r	reptation time	s
U	strain energy density	J·m ⁻²
U_c	stored strain energy density	J·m ⁻²
U_p	energy needed to pull the chain out of the tube	J
W	work of adhesion	J·m ⁻²
w	strip width	m
W^a	thermodynamic work of adhesion	J·m ⁻²
W^c	thermodynamic work of cohesion	J·m ⁻²
W_c	contact formation probability	-
W_d	work of detachment	J·m ⁻²

$X(t)$	average monomer interpenetration depth	Å
X_{∞}	average monomer interpenetration depth after reaching equilibrium conditions	Å
z	asperity height	m
Z	polymerization index	-
z_0	the smallest distance in which two crystalline bodies can be brought	Å
A	network theory front factor	-
ΔA	change in elastic free energy	$\text{J}\cdot\text{m}^{-2}$
Δc	debonding distance	m
ΔG	Gibb's free energy change	$\text{J}\cdot\text{mol}^{-1}$
ΔH	enthalpy change	$\text{J}\cdot\text{mol}^{-1}$
ΔS	entropy	$\text{J}\cdot(\text{mol}\cdot\text{K})^{-1}$
Δx	the distance, by which the point of application of peeling force moves	m

Symbols in Greek alphabet

Symbol	Definition	Unit
$\varepsilon, \varepsilon_\infty$	deformation; ∞ : at equilibrium conditions	%
Φ	Good-Girifalco parameter	-
γ	surface tension	$\text{J}\cdot\text{m}^{-2}, \text{N}\cdot\text{m}^{-1}$
γ^d	surface tension, dispersive component	$\text{J}\cdot\text{m}^{-2}, \text{N}\cdot\text{m}^{-1}$
γ^n	surface tension, hydrogen bonds component	$\text{J}\cdot\text{m}^{-2}, \text{N}\cdot\text{m}^{-1}$
γ^p	surface tension, polar component	$\text{J}\cdot\text{m}^{-2}, \text{N}\cdot\text{m}^{-1}$
$\gamma_{sl}, \gamma_{lv}, \gamma_{sv}$	interfacial surface energies	$\text{J}\cdot\text{m}^{-2}, \text{N}\cdot\text{m}^{-1}$
η	viscosity	$\text{Pa}\cdot\text{s}$
$\varphi(z)$	distribution of heights	-
$\varphi, \varphi_0, \varphi_\infty$	fractional contact area; 0, ∞ : at contact start and equilibrium, respectively	-
μ	friction coefficient	-
μ_0	monomer friction coefficient	-
μ_e	number of elastically effective junctions	-
ν_P	Poisson ratio	-
ν	crosslink density	mol/cm^3
θ	contact angle	-
Θ	peel angle	-
θ_k	relaxation time of Kelvin-Voigt element	s
ρ	density	$\text{g}\cdot\text{cm}^{-3}$
σ	uniaxial stress	MPa
$\sigma(t_c)$	fracture stress (as a function of contact time)	MPa
σ_∞	fracture stress after reaching equilibrium conditions	MPa
σ_b	tensile stress	Pa
τ_d	disentanglement time	s
τ_e	entanglement time	s
λ	deformation	%
$\lambda_x, \lambda_y, \lambda_z$	deformation along the axis	%
σ_0	force per unit of undeformed area	$\text{N}\cdot\text{m}^{-2}$
ξ	cycle rank of the network	-
ϕ	volume fraction	-

Abbreviations

D ₄	dimethylsiloxane tetramer
IR rubber	Synthetic isoprene rubber
MQ	Synthetic silicone rubber
VGC	vinyl group content

Bibliography

JOURNAL PAPERS AND CONFERENCE PROCEEDINGS

- *Silicone rubber tack in relation to network structure.*
M. Mikrut, J.W.M. Noordermeer, G. Verbeek, J. Adh. (2007). Submitted.
- *The time-dependent autohesion for symmetric contacts of silicone rubber.*
M. Mikrut, J.W.M. Noordermeer, G. Verbeek, J. Adh. (2007). Submitted.
- *The influence of loose and semi-anchored siloxane polymer chains on the tack of crosslinked silicone rubber.*
M. Mikrut, J.W.M. Noordermeer, G. Verbeek, J. App. Polym. Sci. (2007). Submitted.
- *Low surface energy rubber materials: influence of the network structure of silicone rubber on tack.*
M. Mikrut, J.W.M. Noordermeer, G. Verbeek, Elastomery **4**, 12, 2006.
- *Low surface energy rubber materials: influence of the network structure of silicone rubber on tack.*
M. Mikrut, J.W.M. Noordermeer, G. Verbeek, Proceedings of the Elastomery 2005 Conference, October 2005, Warsaw, Poland.
- *Low surface energy rubber materials: influence of the network structure of silicone rubber on tack.*
M. Mikrut, J.W.M. Noordermeer, G. Verbeek, Proceedings of the IRC 2006 Conference, June 2006, Lyon, France.
- *Influence of the network structure of silicone rubber on time-dependent autohesion as mechanism for self-healing.*
M. Mikrut, J.W.M. Noordermeer, G. Verbeek, Proceedings of the Rapra Silicone Elastomers 2006 Conference, September 2006, Frankfurt, Germany.
- *Influence of the network structure of silicone rubber on time-dependent autohesion as mechanism for self-healing.*
M. Mikrut, J.W.M. Noordermeer, G. Verbeek, Proceedings of 1st International Conference on Self Healing Materials, April 2007, Noordwijk, the Netherlands.

EXTERNAL PRESENTATIONS

- M. Mikrut, Elastomery 2005 Conference, October 2005, Warsaw, Poland.
- M. Mikrut, IRC 2006 Conference, June 2006, Lyon, France.
- M. Mikrut, Rapra Silicone Elastomers 2006 Conference, September 2006, Frankfurt, Germany.
- M. Mikrut, 1st International Conference on Self Healing Materials, April 2007, Noordwijk, the Netherlands.

Curriculum Vitae

"Life! Don't talk to me about life."

Marvin (the paranoid android) in Douglas Adams' *The Hitchhiker's Guide to the Galaxy*.

Marek Mikrut was born Szerzyny (Poland) on the 23rd of July, 1976. From 1995 to 2000 he studied organic chemistry at the Jagiellonian University in Krakow. He did his Master's Thesis under a supervision of dr. Helena Borowiec. During his Masters studies he studied the using a b-ketoacids in synthesis of heterocyclic compounds. He graduated in October 2000.

From October 2001 he started work in Rubber Research Institute "Stomil" in Piastow, Poland, as a young researcher.

From February 2003 to July 2007 the author worked as a Ph.D. student under the supervision of prof. dr. ir. J.W.M. Noordermeer at the University of Twente, currently Faculty of Engineering Technology in a project which is a part of the Research Programme of the Dutch Polymer Institute (DPI), project #317. The results of this work are described in this thesis.

Acknowledgements

“So long, and thanks for all the fish.”
Douglas Adams in *“Hitchhiker’s guide to Galaxy”*

Four years seemed like an eternity when they began, and like a blink of an eye when they were over. And all that remains are 140 pages and people that I met during that time. People that I would like to thank.

First of all I would like to acknowledge Dutch Polymer Institute (DPI) for the financial support of my research.

I would like to express my gratitude to Professor Jacques Noordermeer, for being my promoter and the best tutor I ever had. Thank you for the guidance, for giving me the opportunity to study at the Elastomer Technology and Engineering group. I learned a lot from you.

Chcialbym podziekowac moim Rodzicom, za to ze najpierw zachecili mnie do podjecia studiow na Uniwersytecie Twente, a potem za to ze podtrzymywali mnie na duchu, szczegolnie na poczatku kiedy nie raz zwatpilem.

Pragne rowniez serdecznie podziekowac Pani Doktor Parasiewicz. Dziekuje Pani za umozliwienie mi podjecia studiow na UT, jak rowniez za zgode na udzial w obronie i bycie w komisji.

Wilma, thank you very much for your help with all the small things that just kept on popping up. You were always willing to sacrifice some of your time. But I must admit that your laptop still holds its place in my nightmares.

Auke and Rabin, thank you both for your Friday’s advices. There was not much chemistry involved, but I enjoyed our discussions a lot, Auke. A chemist will always understand another chemist. Rabin, your help was more on a physics side, and it was really valuable. But even four years could not impregnate me to your sense of humor.

The industrial contact persons, which were always helpful and willing to sacrifice some of their time. Marcel, Guy, Aurelie: thank you for all the discussions, I always left with a bunch of new ideas.

I acknowledge prof. dr. Eising, dr. Creton, dr. Parasiewicz, prof. dr. Engbersen, prof. dr. Gardeniers, dr. Verbeek, dr. Datta and prof. dr. Schipper for being committee members of my defense.

The secretaries of RBT (later ETE), PBM and MTP have helped me a lot with all the paperwork I got during those four years. Gerda, Aleida, Hillie, Genevieve and Karin: thank you a lot.

It is also time to say thank you to all my colleagues. Boy, I was lucky starting my studies in RBT; no other group had such an atmosphere. First of all I would like to thank my “paranimfen”, Wilco and Tony for all the help they provided with organization. Wilco, my brother in adhesion, fellow administrator and webmaster, and Tony my Mensa team-mate, we had plenty of fun together. Montse: you seemed to be the main source of noise in the office, but now I miss your quacking. Agata: it's a pity that you have joined the group late, since we could have even more fun. I hope the calculator serves you well. Kuno, to your sense of humor I got used quickly, you are a real direct Dutch... sorry, Twents. Ah, and thanks for correcting my English. Geert, I was an administrator after you, and I do not know if I should thank you for that or slip some zinc stearate into your beer. Pratip: there are still many NSO's for me, but I am afraid no more for you, khe khe. You are not allowed anymore. Francesca: you were the only cat-freak in the group, besides me. I miss the morning cats and occasional Sith-joke. Joost, hombre de synthesis, it was nice in the lab, wasn't it? Jan, thank you for all your help in the lab, especially with my always-present degassing. We also had so many discussions about coins, if I find more spare Polish coins lying around, I will not forget about you. Vipin, after you are gone nobody dances on a table anymore! Richard: it was always nice to visit your office in the lab. Jacob, maybe we will have an opportunity to tell nasty jokes again. Shalom, Rabbi. Satoshi, I really enjoyed your company, and the Japanese evenings as well. Domo arigato, Mihara-san. I would like also to thank other members of our group: Mukund, Rui and Hongmei for their help during my time in the group.

Arek, you deserve a special mention. You were the best student I ever had, not only a student but also a friend. You did a great deal of job for me, but that's not all. I hope we can still sit one day and again ponder the nuances of D2 character development.

Clement, Gilbert, Joachim: it is not true what they say: “Do not meddle into the affairs of administrators, for they are subtle and quick to anger”. I did, and I met you. Thank you for all the assistance with computers, and I *did* bother you a lot.

Mark and Martin, with Tony and me we were the Mensa team. I will miss our everyday discussions, which could start with the quality of food in the Mensa and end with the meaning of life. Although I still do not know what the meaning of life is.

And at the end I would like to thank all the people from PBM, STEP and MTP. These were nice coffee breaks, and I miss them too.

If it looks like a duck, and quacks like a duck, we have at least to consider the possibility that we have a small aquatic bird of the family anatidae on our hands.

Douglas Adams, *“Dirk Gently’s Holistic Detectives Agency”*